

**COPY 1**

**REPORT NO. AFO-507-78-2**

4 1 1 0 1 0 0 0

W 7

# **AIRBORNE RADAR APPROACH FAA/NASA GULF OF MEXICO HELICOPTER FLIGHT TEST PROGRAM**



**JANUARY 1980**

Availability is unlimited. Document may be released to the Clearinghouse for Scientific and Technical Information, Springfield, Virginia 22151 for sale to the public.

**DEPARTMENT OF TRANSPORTATION  
FEDERAL AVIATION ADMINISTRATION  
OFFICE OF FLIGHT OPERATIONS  
WASHINGTON, D.C. 20591**

The contents of this report reflect the findings of the Operations Research Staff, Flight Standards National Field Office, Office of Flight Operations, which is responsible for the facts and the accuracy of the data presented herein. The contents do not necessarily reflect the official views or policy of the Department of Transportation. This report does not constitute a standard, specification, or regulation.

1. Report No. AFO-507-78-2		2. Government Accession No.		3. Recipient's Catalog No.	
4. Title and Subtitle Airborne Radar Approach FAA/NASA Gulf of Mexico Helicopter Flight Test Program				5. Report Date January 1980	
				6. Performing Organization Code AFO-507	
7. Author(s) Donald P. Pate James H. Yates, PhD				8. Performing Organization Report No. AFO-507-78-2	
9. Performing Organization Name and Address Operations Research Staff, AFO-507 FSNFO, FAA P. O. Box 25082 Oklahoma City, Oklahoma 73125				10. Work Unit No.	
				11. Contract or Grant No.	
12. Sponsoring Agency Name and Address Office of Flight Operations, DOT 800 Independence Ave. Washington, D.C. 20591				13. Type of Report and Period Covered Final Report	
				14. Sponsoring Agency Code	
15. Supplementary Notes					
16. Abstract  A joint FAA/NASA helicopter flight test was conducted in the Gulf of Mexico to investigate the airborne weather and mapping radar as an approach system for offshore drilling platforms. Approximately 120 Airborne Radar Approaches (ARA) were flown in a Bell 212 by 15 operational pilots. The objectives of the test were to (1) develop ARA procedures, (2) determine weather minimums, (3) determine pilot acceptability, (4) determine obstacle clearance and airspace requirements. Aircraft position data was analyzed at discrete points along the intermediate, final, and missed approach. The radar system error and radar flight technical error were determined in both range and azimuth, and the capability of the radar as an obstacle avoidance system was evaluated.					
17. Key Words Airborne Radar Approach ARA, Helicopter IFR Offshore Helicopter Operations			18. Distribution Statement  Distribution Unlimited		
19. Security Classif. (of this report) Unclassified		20. Security Classif. (of this page) Unclassified		21. No. of Pages 144	22. Price

## TABLE OF CONTENTS

	Page
Introduction	1
Test Description	1
Approach Description	5
Initial Approach	5
Final and Missed Approach	8
Description of Analysis	8
Analysis	13
Approach Azimuth Accuracy	13
Range Accuracy	59
Missed Approach Dispersion	75
Operational Difficulties	90
Summary of Conclusions	95
Approach Tracking Accuracy	95
Range Accuracy	96
Missed Approach	97
General Conclusions	98
Recommendations	101
Approach Tracking Accuracy	101
Range Accuracy	101
Missed Approach	102
General Recommendations	103
Appendix A	105
Collection of Data - Final Approach	105
Extraction of Data - Final Approach	105
Lateral Dispersion Statistics - Intended Course	106
Lateral Dispersion Statistics - Average Course	108
Extraction of Data - Missed Approach	111
Lateral Dispersion - Missed Approach	113
Data Collection - Range Interpretation Error	113
Statistical Analysis - Range Interpretation Error	114
Data Collection - Flight Technical Error	114
Data Collection - Flight Technical Error	115
Statistical Analysis - Flight Technical Error	115
Mann-Whitney U-Test	116
Kruskal-Wallis K-Sample Test	117
Kolmogorov-Smirnov Two-Sample Test	118
Spearman Rank Correlation Test	119
Appendix B	121
The Theoretical Homing Curve	122
Blind Flight Path	124
The Missed Approach Curve	131
Conclusions - Homing Curve	137
Conclusions - Missed Approach Curve	141

## LIST OF ILLUSTRATIONS

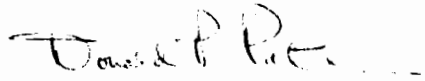
Figure		Page
1	Arcing Entry	6
2	Overhead Entry	7
3	Overhead Entry 15 <sup>0</sup> Offset	9
4	Helicopter Airborne Radar Approach Plate	11
5	Overhead Outbound Turn	21
6	Composite Approach Tracks: Straight-In 1/2 Mile MAP	26
7	Composite Approach Tracks: Offset 1/2 Mile MAP	27
8	Composite Approach Tracks: Straight-In 1/4 Mile MAP	28
9	Composite Approach Tracks: Offset 1/4 Mile MAP	29
10	Approach Envelope: All Approaches Combined	31
11	Approach Envelope: Straight-In	32
12	Approach Envelope: Offset	33
13	Approach Envelope/Average Path: All Approaches Combined	41
14	Approach Envelope/Average Path: Offset Approaches	43
15	Approach Envelope/Average Path: Straight-In	44
16	Error Components	46
17	Aircraft Radar Position CEP	73
18	Composite Missed Approach Tracks: Offset 1/4 Mile MAP	76
19	Composite Missed Approach Tracks: Offset 1/2 Mile MAP	77
20	Composite Missed Approach Tracks: Straight-In 1/4 Mile MAP	80
21	Composite Missed Approach Tracks: Straight-In 1/2 Mile MAP	81
22	Missed Approach Envelope: Offset 1/2 Mile MAP	84
23	Missed Approach Envelope: Straight-In 1/2 Mile MAP	85
24	Missed Approach Track of Aircraft Poorly Positioned at MAP	92
A-1	Lateral Dispersion Error: Intended Path	106
A-2	Lateral Dispersion Error: Average Path	109
A-3	Missed Approach Partitions	112
B-1	Homing Curve Diagram	122
B-2	Blind Flight Path Diagram	124
B-3	Blind Segment Diagram	127
B-4	Intersection of Dynamic Target Path and Blind Path	129
B-5	Wind Effects on Missed Approach Path	131
B-6	Crosswind Diagram 1	133
B-7	Crosswind Diagram 2	133
B-8	Crosswind Blind Segment	134
B-9	Length of Blind Segment vs Degrees of Crosswind 60 kt Airspeed	142
B-10	Distance to Path Intersection with Radar Sweep vs Degrees of Crosswind, 60 kt Airspeed	143
B-11	Length of Blind Segment vs Degrees of Crosswind 70 kt Airspeed	144
B-12	Distance to Path Intersection with Radar Sweep vs Degrees of Crosswinds, 70 kt Airspeed	145
B-13	Length of Blind Segment vs Degrees of Crosswind 80 kt Airspeed	146
B-14	Distance to the Path Intersection with Radar Sweep vs Degrees of Crosswind, 80 kt Airspeed	147

## LIST OF TABLES

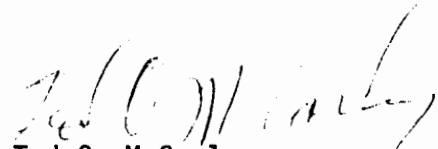
Table		Page
1	Test Pilot Background	2
2	Helicopter Offshore ARA Matrix	10
3	Angular Deviation from Intended Ground Track (All Approaches)	14
4	Angular Deviation from Intended Ground Track (Offset Approaches)	16
5	Angular Deviation from Intended Ground Track (Straight-In Approaches)	18
6	Spearman RHO Correlation of Track Dispersion Compared to Range	24
7	Spearman RHO Correlation of Track Dispersion Compared to Range - 1/2 Mile Intervals	25
8	Angular Deviation from Average Angular Path (All Approaches)	35
9	Angular Deviation from Average Angular Path (Offset Approaches)	37
10	Angular Deviation from Average Angular Path (Straight-In Approaches)	39
11	Components of Error Statistics: All Approaches Combined	48
12	Components of Error Statistics: Primary Approaches	50
13	Components of Error Statistics: Beacon Approaches	51
14	Kolmogorov-Smirnov Comparison of FTE	54
15	Range Error Statistics: Primary Radar Mode	60
16	Range Error Statistics: Beacon Radar Mode	61
17	TSE Range Statistics by Range Scale	63
18	Radar System Error - Range	65
19	Comparison of Advertised 1 Percent and Measured RSE	66
20	Two S.D. Radar Error Components	68
21	Primary Radar Mode Error Comparison	70
22	Beacon Radar Mode Error Comparison	72
23	Partition Statistics About Average Missed Approach Path: Offset 1/2 Mile MAP	83
24	Partition Statistics About Average Missed Approach Path: Straight-In 1/2 Mile MAP	88
B-1	Maximum Speed to Intercept Moving Aircraft, 20 kt Windspeed	148
B-2	Farthest Point of Radar Vision	149

Project Report on Airborne Radar Approach FAA/NASA  
Gulf of Mexico Helicopter Flight Test Program

Project Officer

  
Donald P. Pate  
Operations Research Analyst  
Operations Research Staff

Approved

  
Ted O. McCarley  
Chief,  
Operations Research Staff

Released

  
William D. Crawford  
Chief, Flight Standards  
National Field Office

January 1980



## INTRODUCTION

A joint NASA/FAA helicopter flight test program was carried out between June 1978 and September 1978 in the Gulf of Mexico to investigate airborne weather/mapping radar as an offshore approach system. The objectives of the test were to:

1. Develop airborne radar approach (ARA) procedures.
2. Determine weather minimums.
3. Determine pilot acceptability.
4. Determine obstacle clearance and airspace requirements.

The purpose of this paper is to present the analysis utilized to establish minimums, determine obstacle clearance and airspace requirements, and establish procedures.

## TEST DESCRIPTION

The test, conducted under contract with Air Logistics, was staged from their maintenance center in New Iberia, Louisiana. Fifteen line pilots representing a wide range of helicopter experience (Table 1) participated in the test as subject pilots. A standardized video tape briefing was presented to all crews before participation in the tests. During a flight, one crewmember served as copilot and radar controller providing course corrections to the second pilot controlling the aircraft. Each pilot, hooded during the tests, made eight approaches as a controller and eight as a pilot.

Test Pilot Background

Pilot	Flight Hours				Instrument Hours			Radar Experience	
	Offshore	Helicopter	Fixed Wing	Total	Actual	Hooded	Total	Past Use	Radar Approaches
1	2,002	4,300	186	4,486	33	157	190	Seldom	0-3
2	3,752	4,550	25	4,575	30	100	130	Seldom	0-3
3	2,000	4,000	25	4,025	30	50	80	Seldom	0-3
4	2,500	9,000	300	9,300	500	500	1,000	Seldom	0-3
5	1,500	3,200	50	3,250	140	80	220	Extensive	0-3
6	4,000	10,500	1,500	12,000	170	70	240	Seldom	0-3
7	3,200	5,500	1,200	6,700	80	100	180	Extensive	Over 10
8	NA	NA	NA	NA	NA	NA	NA	Seldom	0-3
9	1,200	6,300	1,800	8,100	250	150	400	Seldom	0-3
10	NA	NA	NA	NA	NA	NA	NA	Seldom	0-3
11	2,929	5,306	2,586	7,892	630	397	1,027	Extensive	Over 10
12	2,000	3,000	350	3,350	15	75	90	Seldom	0-3
13	1,551	6,546	200	6,746	0	113	113	Seldom	0-3
14	1,916	4,148	36	4,184	2	124	126	Seldom	0-3
15	900	2,000	300	2,300	15	200	275	Very little	0-3
<b>Average</b>	<b>2,265</b>	<b>5,258</b>	<b>658</b>	<b>5,916</b>	<b>148</b>	<b>167</b>	<b>315</b>	<b>Seldom</b>	<b>0-3</b>

Table 1

The test aircraft was a twin-turbine Bell 212 helicopter with a two-bladed semirigid rotor, maximum gross weight of 11,200 pounds, and maximum airspeed of 120 knots. The radar was a Bendix RDR-1400 weather/mapping radar, with selectable range scales of 240, 160, 80, 40, 20, 10, 5, 2.5 nautical miles and with a stabilized 12 inch flat plane antenna having a  $7.5^{\circ}$  beam width. The radar could be operated in either the beacon or primary mode with selective scan angle of  $\pm 60^{\circ}$  or  $\pm 20^{\circ}$ . Two different ground beacons, a Motorola model SST-181X-E and a Vegas model 367X, were used.

The approaches were flown to targets in a cluster of seven offshore drilling platforms and oil rigs located in the Gulf of Mexico, Vermillion Block 71 drilling area. Approaches were made to platforms in this cluster, with the target chosen so as to provide an into the wind obstacle free approach and missed approach.

Aircraft tracking was accomplished with a Cubic DM-43 ranging system using three responders positioned on platforms bounding the flight test area. The Cubic system provided a two sigma accuracy of two feet, and including responder location uncertainty, aircraft position was established within a two sigma accuracy of about six feet. Other onboard data collection equipment included a 35mm camera to record the controller's panel, a 35mm camera to record radar display, a Cubic DM-43 interrogator, an interface to multiplex heading, airspeed, radar altitude onto magnetic tape, and an audio cassette recorder to record onboard voice communications. Project logs, meteorological data, chase aircraft film, pilot experience/qualifications forms, and pilot evaluations provided supplemental information to the quantitative data.

## APPROACH DESCRIPTION

### Initial Approach

The initial approach segment was accomplished with either an arcing entry or an overhead entry. The arcing entry was designed to enter the final approach segment for winds within  $\pm 30^{\circ}$  of the en route course by flying direct to the Downwind Final Approach Point (DWFAP) while descending from 1,000' AGL to 500' AGL. At the en route fix, the cluster was identified, approach target chosen, DWFAP determined (for an into the wind approach), and the missed approach turn planned into a clear zone free of obstacles. The approach target was chosen on the downwind edge typically to the right or left side of the cluster to provide final approach and missed segments clear of obstacles. If the approach target was not the destination, it was assumed a visual hover taxi from the Missed Approach Point (MAP) to the destination could be accomplished. (Figure 1)

An overhead entry was used for wind conditions requiring the cluster be overflown to position the aircraft for an into the wind final approach. Approach and missed approach planning was accomplished at the en route fix as in the arcing entry. The target rig was overflown at 1,000' AGL followed by an outbound leg within  $\pm 10^{\circ}$  of the final approach course, descent to 500' AGL, and standard rate turn onto the final approach course. (Figure 2)

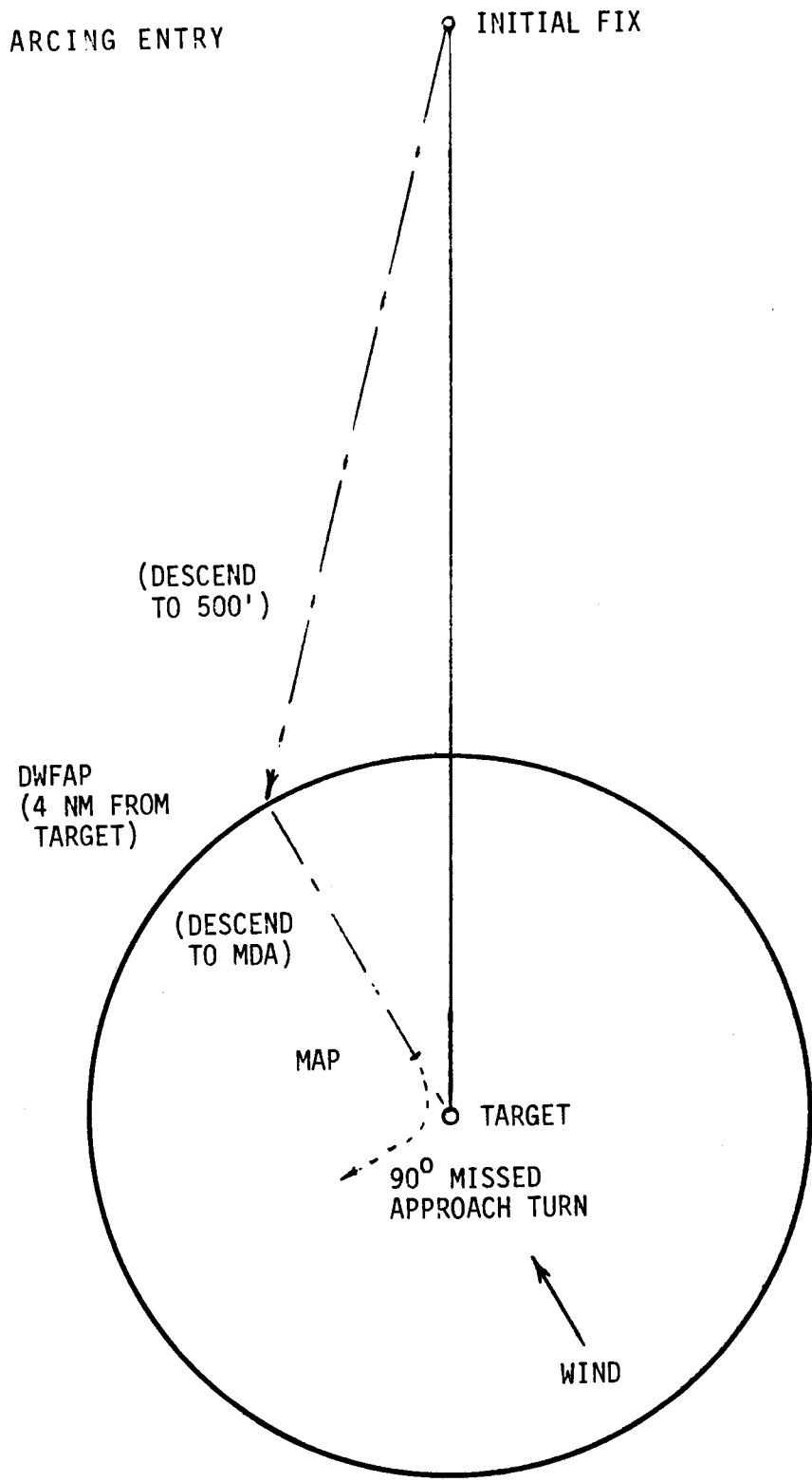


Figure 1

OVERHEAD ENTRY

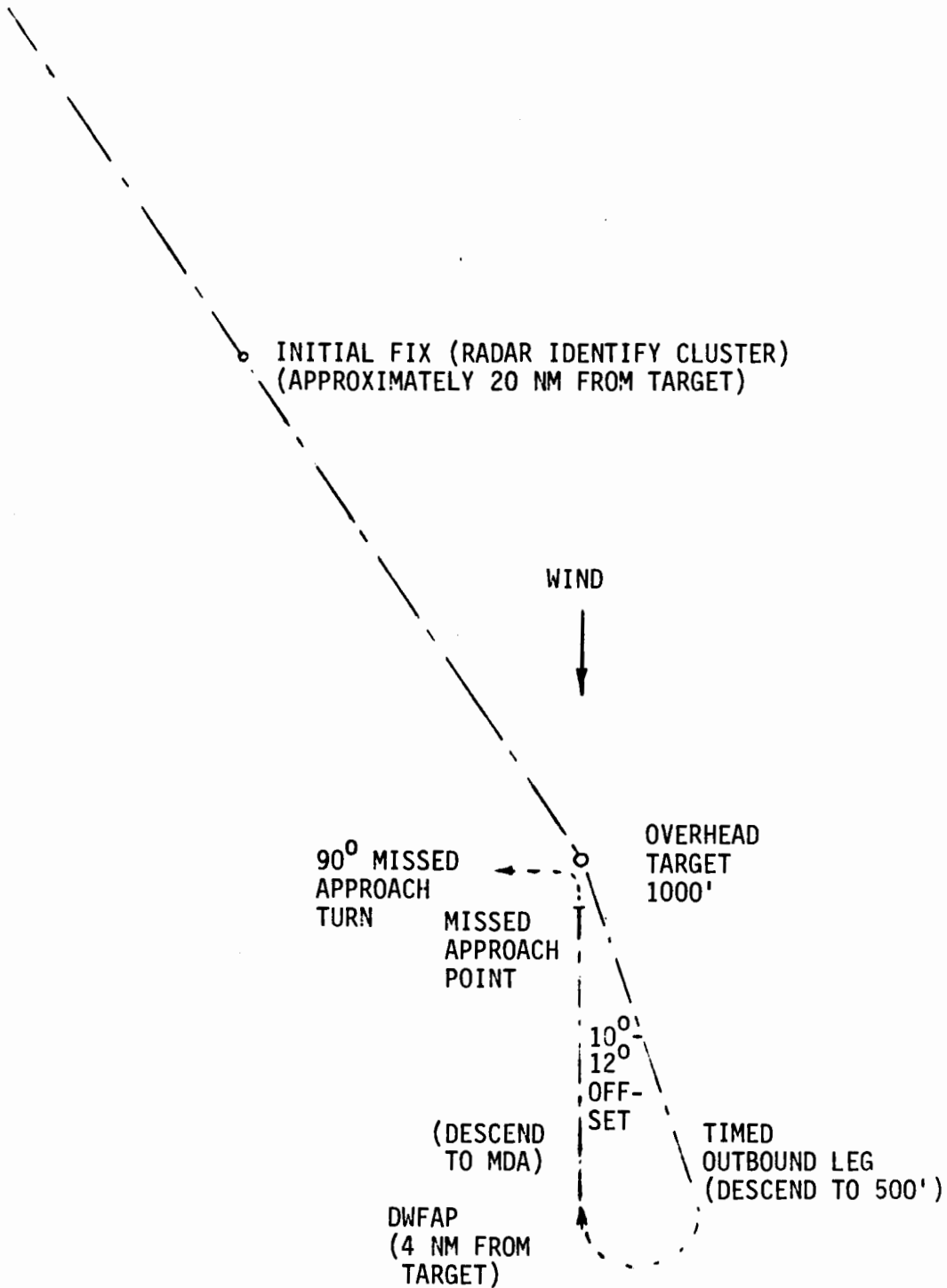


Figure 2

### Final and Missed Approach

The final approach segment began at the DWFAP located 4 nm from the target rig. The aircraft slowed to 60 knots and descended to the MDA during this segment. Two types of approaches were used: straight-in to the MAP and a 15<sup>0</sup> offset accomplished by tracking to within 1 nm of the target then making a 15<sup>0</sup> heading change and continuing to the MAP (Figure 3).

The missed approach in either case was a climbing turn from the MAP into the predetermined clear zone free of obstacles. During the tests, MDAs of 300' and 200' and MAPs of 0.50 nm and 0.25 nm were evaluated. An overall flight test matrix is given in Table 2 and a copy of the approach plate is shown in Figure 4.

### DESCRIPTION OF ANALYSIS

The objectives of the analysis were to:

1. Quantify total system error in azimuth and range,
2. Quantify radar system error in azimuth and range,
3. Quantify radar tracking flight technical error in azimuth and range,
4. Quantify missed approach dispersion,
5. Measure the effects on system performance of test variables:
  - a. Radar mode, beacon or primary
  - b. Final approach profile, straight-in or 15<sup>0</sup> offset and
  - c. Range scale setting,

OVERHEAD ENTRY

15° OFFSET

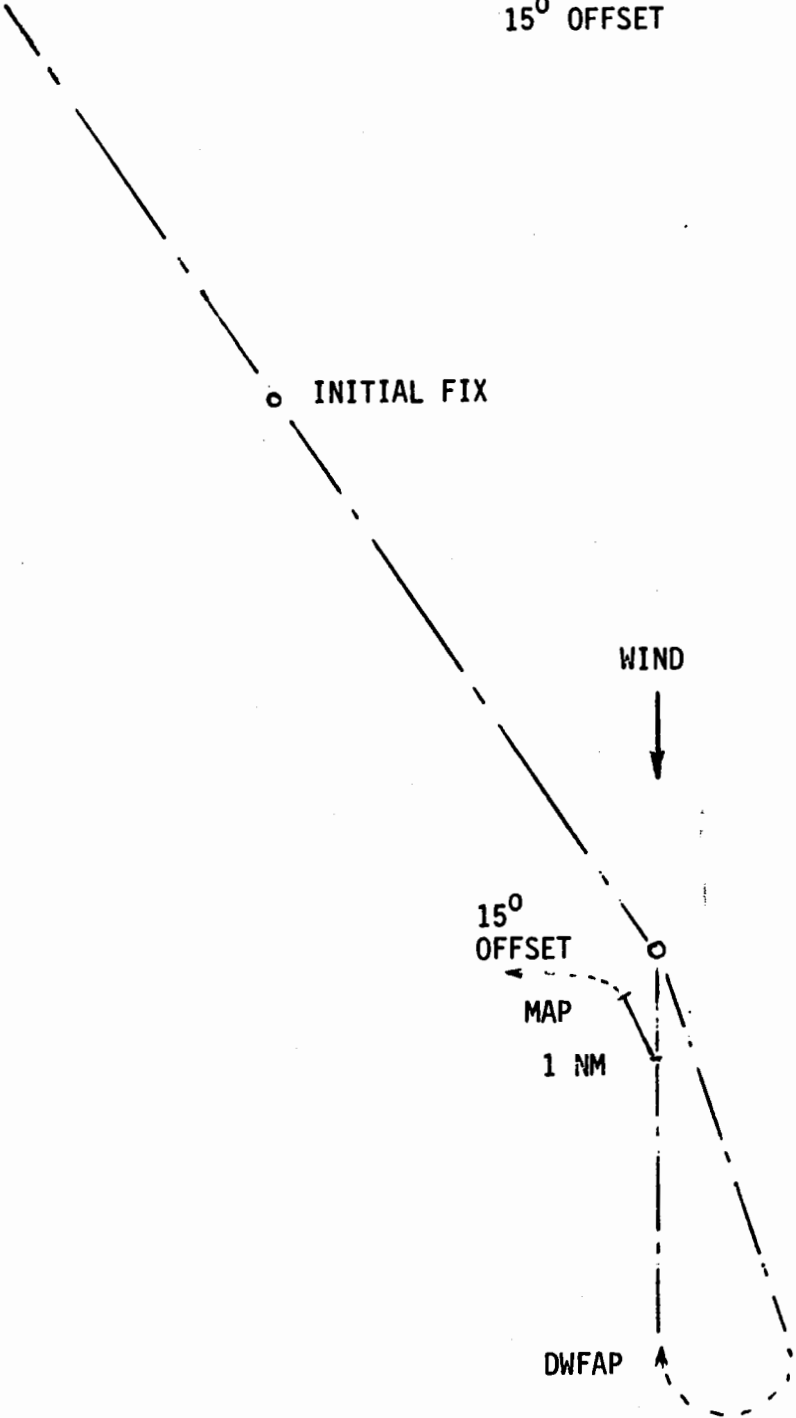
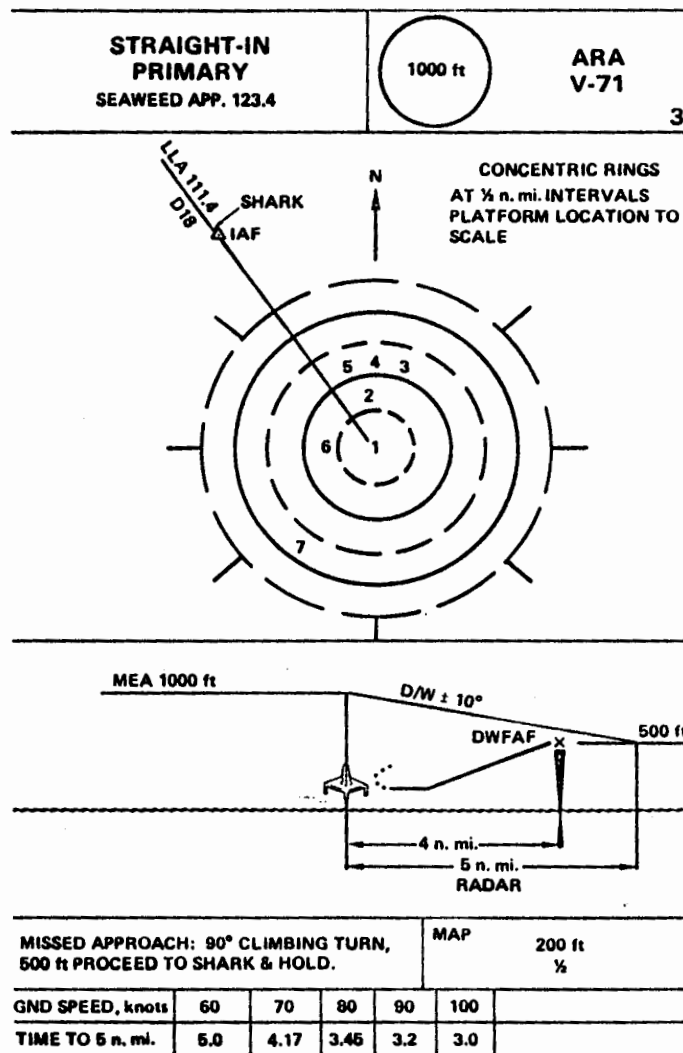


Figure 3

HELICOPTER  
OFFSHORE AIRBORNE RADAR APPROACH  
MATRIX

APPROACH NUMBER	RADAR CONTROLLER	INTERMEDIATE APPROACH	FINAL PROFILE	RADAR MODE	MISSED APPROACH POINT	MDA	MISSED APPROACH PROCEDURE
1	FIRST PILOT	RADAR 30° ARCING ENTRY	STRAIGHT-IN	BEACON	1/4 NM	200'	90° CLIMBING TURN
2	FIRST PILOT	OVERHEAD	15° OFFSET AT 1 NM	PRIMARY	1/2 NM	300'	75° CLIMBING TURN
3	FIRST PILOT	OVERHEAD	STRAIGHT-IN	PRIMARY	1/2 NM	200'	90° CLIMBING TURN
4	FIRST PILOT	OVERHEAD	15° OFFSET AT 1 NM	PRIMARY	1/2 NM	200'	75° CLIMBING TURN
5	SECOND PILOT	OVERHEAD	STRAIGHT-IN	PRIMARY	1/2 NM	300'	90° CLIMBING TURN
6	SECOND PILOT	OVERHEAD	15° OFFSET AT 1 NM	BEACON	1/2 NM	200'	75° CLIMBING TURN
7	SECOND PILOT	OVERHEAD	STRAIGHT-IN	PRIMARY	1/2 NM	300'	90° CLIMBING TURN
8	SECOND PILOT	OVERHEAD	15° OFFSET AT 1 NM	PRIMARY	1/4 NM	200'	75° CLIMBING TURN

Table 2



Helicopter Airborne Radar Approach Plate

Figure 4

6. Establish approach envelopes,
7. Establish missed approach envelopes,
8. Determine minimum radar range to establish the missed approach point (MAP),
9. Determine airborne radar fix error,
10. Determine operational capabilities and limitations of the airborne radar as an offshore obstacle avoidance system.

To achieve these objectives, the analysis was carried out in three parts. Standard statistics were computed for system range error, azimuth error and flight technical error. Secondly, comparative statistics were applied to determine the effects of experimental variables on system accuracy. Thirdly, a mathematical model was developed to evaluate the effects of "homing" tracking, radar scan angle, wind, and the missed approach turn on the radar as an obstacle avoidance system. The following discussion presents details of the analysis and a summary of conclusions.

## APPROACH AZIMUTH ACCURACY

The ability of the subject crewmembers to accurately enter and follow the final approach path was measured from samples of the angular deviation of the aircraft from the intended path at regular intervals from the target (see Appendix A for a full explanation of the sampling procedure). Standard statistics were computed from each sample for all flights, offset flights, and straight-in flights.

It was found that the average angular deviation for all flights at ranges between 5 nm and .588 nm was between  $+5^{\circ}$  and  $+6^{\circ}$  (Table 3). The average angular deviation of the offset approaches at ranges greater than 1.261 nm was found to be between  $+5^{\circ}$  and  $+7.6^{\circ}$  (Table 4). The average angular deviation of the straight-in approaches for all ranges between 2.753 nm and .501 nm was found to be between  $+4^{\circ}$  and  $+5.6^{\circ}$  (Table 5). The mean at 5 nm for the offset approaches was  $+7.352^{\circ}$  while that of the straight-in approaches was only  $+0.099^{\circ}$ . The means for both types of approaches tended to be large within .589 nm since some aircraft had initiated the missed approach turn and most of the turns were toward the right.

A positive angular deviation indicates that the aircraft was right of course when the angle was computed. The average angle of each of the samples is positive, which indicates that on the average, the aircraft flew on the right side of the downwind final approach. It could be reasonably expected that the averages would be near zero with some positive and some negative values.

ANGULAR DEVIATION  
FROM INTENDED GROUND TRACK  
(ALL APPROACHES)

RANGE	SAMPLE SIZE	MEAN ANGULAR ERROR DEGREES	95 PERCENT CONFIDENCE INTERVAL DEGREES	STANDARD DEVIATION DEGREES	MINIMUM DEGREES	MAXIMUM DEGREES	KURTOSIS	SKEWNESS
5.000	76	3.821	1.248 to 6.395	11.262	-27.154	35.850	0.911	-0.045
4.000	99	5.730	3.396 to 8.064	11.703	-29.766	37.775	1.158	-0.285
3.000	106	5.769	3.342 to 8.196	12.601	-30.494	38.504	0.514	-0.217
2.917	107	5.693	3.281 to 8.106	12.587	-30.253	38.310	0.476	-0.201
2.836	106	5.762	3.325 to 8.199	12.654	-30.120	38.206	0.435	-0.219
2.753	107	5.884	3.459 to 8.308	12.649	-30.077	38.203	0.428	-0.241
2.671	107	5.859	3.430 to 8.287	12.671	-30.040	38.265	0.408	-0.244
2.589	107	5.833	3.396 to 8.271	12.717	-30.102	38.410	0.384	-0.244
2.506	107	5.809	3.364 to 8.253	12.756	-30.252	38.600	0.370	-0.243
2.425	107	5.782	3.328 to 8.236	12.805	-30.504	38.977	0.373	-0.242
2.342	107	5.755	3.288 to 8.221	12.869	-30.775	30.445	0.374	-0.243
2.259	107	5.726	3.243 to 8.208	12.954	-31.075	40.070	0.375	-0.242
2.177	107	5.702	3.201 to 8.203	13.048	-31.380	40.615	0.366	-0.237
2.094	107	5.696	3.180 to 8.213	13.129	-31.647	41.266	0.360	-0.227
2.000	107	5.696	3.159 to 8.231	13.233	-32.097	41.886	0.341	-0.219
1.918	103	5.171	2.572 to 7.769	13.297	-32.456	42.542	0.406	-0.156
1.825	103	5.174	2.553 to 7.795	13.413	-32.993	43.253	0.409	-0.149
1.743	103	5.169	2.526 to 7.813	13.526	-33.388	43.681	0.402	-0.138
1.660	103	5.159	2.489 to 7.828	13.658	-33.875	44.423	0.387	-0.127
1.590	103	5.135	2.439 to 7.830	13.793	-34.368	44.793	0.367	-0.120
1.507	103	5.103	2.378 to 7.828	13.941	-34.768	45.302	0.353	-0.111
1.424	103	5.107	2.348 to 7.866	14.119	-35.269	45.887	0.341	-0.098
1.341	102	5.218	2.406 to 8.030	14.315	-35.629	46.547	0.340	-0.098
1.260	103	5.061	2.232 to 7.890	14.474	-35.846	47.084	0.289	-0.062
1.177	103	5.034	2.171 to 7.896	14.651	-36.126	47.700	0.270	-0.052

Table 3



ANGULAR DEVIATION  
FROM INTENDED GROUND TRACK  
(OFFSET APPROACHES)

RANGE	SAMPLE SIZE	MEAN ANGULAR ERROR DEGREES	95 PERCENT CONFIDENCE INTERVAL DEGREES	STANDARD DEVIATION DEGREES	MINIMUM DEGREES	MAXIMUM DEGREES	KURTOSIS	SKEWNESS
5.000	39	7.352	4.002 to 10.702	10.335	-13.335	35.850	0.706	0.749
4.001	51	7.515	4.504 to 10.525	10.704	-13.594	37.775	0.685	0.651
3.002	55	7.457	4.258 to 10.656	11.833	-16.707	38.504	0.102	0.430
2.917	56	7.279	4.115 to 10.444	11.817	-16.872	38.310	0.082	0.447
2.837	55	7.444	4.230 to 10.657	11.889	-17.122	38.206	0.029	0.398
2.752	57	7.419	4.277 to 10.561	11.342	-17.445	39.203	-0.001	0.380
2.671	57	7.356	4.208 to 10.504	11.864	-17.839	38.265	0.002	0.367
2.589	57	7.286	4.121 to 10.452	11.930	-18.499	38.410	0.007	0.350
2.507	57	7.208	4.029 to 10.387	11.982	-19.053	38.600	0.021	0.337
2.424	57	7.132	3.936 to 10.328	12.045	-19.605	38.977	0.059	0.331
2.341	57	7.056	3.840 to 10.272	12.120	-20.318	39.445	0.104	0.323
2.259	57	6.979	3.737 to 10.221	12.219	-20.861	40.070	0.149	0.320
2.177	57	6.915	3.640 to 10.191	12.346	-21.193	40.615	0.166	0.322
2.095	57	6.869	3.562 to 10.176	12.463	-21.282	41.266	0.186	0.331
2.001	57	6.805	3.461 to 10.150	12.604	-21.393	41.886	0.185	0.336
1.917	53	5.806	2.310 to 9.303	12.685	-21.835	42.542	0.516	0.496
1.836	53	5.753	2.212 to 9.294	12.846	-22.190	43.253	0.527	0.503
1.754	53	5.690	2.104 to 9.275	13.009	-22.660	43.881	0.537	0.509
1.669	53	5.618	1.982 to 9.253	13.190	-23.082	44.423	0.531	0.514
1.589	53	5.523	1.841 to 9.204	13.356	-23.571	44.793	0.514	0.514
1.506	53	5.395	1.664 to 9.126	13.534	-24.313	45.302	0.522	0.512
1.424	53	5.293	1.509 to 9.077	13.729	-24.848	45.887	0.524	0.515
1.341	53	5.184	1.344 to 9.023	13.931	-25.372	46.547	0.538	0.520
1.261	53	5.063	1.170 to 8.955	14.123	-25.963	47.084	0.539	0.514
1.178	53	4.942	0.998 to 8.886	14.309	-26.732	47.700	0.567	0.502

Table 4



ANGULAR DEVIATION  
FROM INTENDED GROUND TRACK  
(STRAIGHT-IN APPROACHES)

RANGE	SAMPLE SIZE	MEAN ANGULAR ERROR DEGREES	95 PERCENT CONFIDENCE INTERVAL DEGREES	STANDARD DEVIATION DEGREES	MINIMUM DEGREES	MAXIMUM DEGREES	KURTOSIS	SKEWNESS
5.000	37	0.099	-3.610 to 3.808	11.124	-27.154	19.605	-0.136	-0.590
4.001	48	3.834	0.200 to 7.467	12.513	-29.766	28.132	0.626	-0.801
3.001	51	3.948	0.220 to 7.667	13.256	-30.494	30.023	0.232	-0.640
2.917	51	3.952	0.216 to 7.687	13.280	-30.253	29.931	0.199	-0.628
2.835	51	3.949	0.206 to 7.693	13.310	-30.120	29.785	0.173	-0.620
2.753	50	4.134	0.321 to 7.946	13.416	-30.077	29.635	0.179	-0.652
2.670	50	4.152	0.329 to 7.974	13.450	-30.040	29.502	0.161	-0.646
2.589	50	4.177	0.344 to 8.010	13.487	-30.102	29.399	0.144	-0.640
2.506	50	4.213	0.368 to 8.058	13.529	-30.252	29.285	0.136	-0.635
2.425	50	4.243	0.384 to 8.102	13.578	-30.504	29.180	0.135	-0.633
2.343	50	4.271	0.393 to 8.149	13.645	-30.775	29.017	0.125	-0.632
2.259	50	4.297	0.395 to 8.198	13.728	-31.075	28.731	0.112	-0.634
2.178	50	4.319	0.397 to 8.241	13.800	-31.380	28.514	0.103	-0.639
2.094	50	4.360	0.422 to 8.297	13.855	-31.647	28.277	0.094	-0.641
2.000	50	4.429	0.468 to 8.389	13.936	-32.097	27.989	0.085	-0.643
1.918	50	4.496	0.514 to 8.479	14.015	-32.456	27.766	0.078	-0.644
1.837	50	4.560	0.555 to 8.566	14.094	-32.993	27.885	0.094	-0.651
1.754	50	4.618	0.593 to 8.643	14.164	-33.388	28.290	0.095	-0.652
1.671	50	4.672	0.620 to 8.723	14.256	-33.875	28.713	0.095	-0.652
1.590	50	4.723	0.641 to 8.806	14.366	-34.368	29.222	0.097	-0.650
1.508	50	4.793	0.675 to 8.911	14.490	-34.763	29.902	0.098	-0.641
1.423	50	4.909	0.744 to 9.075	14.657	-35.269	30.848	0.109	-0.628
1.341	49	5.256	0.986 to 9.525	14.865	-35.629	31.487	0.160	-0.650
1.259	50	5.059	0.802 to 9.316	14.980	-35.846	31.673	0.058	-0.575
1.177	50	5.132	0.826 to 9.438	15.150	-36.126	31.966	0.024	-0.549

Table 5



The bias observed in the data may have been caused by a combination of procedure and technique used to reach the downwind final approach point. The overhead procedure required the crew to fly directly over the target rig and then take up a course  $10^{\circ}$  -  $12^{\circ}$  from the reciprocal of the downwind final approach course. Ideally, the helicopter would leave the target rig on the  $10^{\circ}$  -  $12^{\circ}$  offset course as in Figure 2. In practice, the turn to the offset heading, coupled with the inaccuracies of determining when the aircraft was directly above the target rig, resulted in a flight path more like Figure 5. Although no statistical tests were performed to verify this conjecture, evidence does exist which supports it.

Of the 58 offset approaches, 48 turned right during the overhead maneuver while only 5 turned left. The remainder either flew over the target rig already on the outbound course or the overhead portion of the data was missing. Of the 51 straight-in approaches, 31 turned right during the overhead maneuver while only 3 turned left. Eleven of the straight-in approaches used the arcing entry which was always initiated from left of the downwind final approach course. The remainder of the straight-in approaches either flew over the target rig already on the outbound course or the overhead portion of the data was missing.

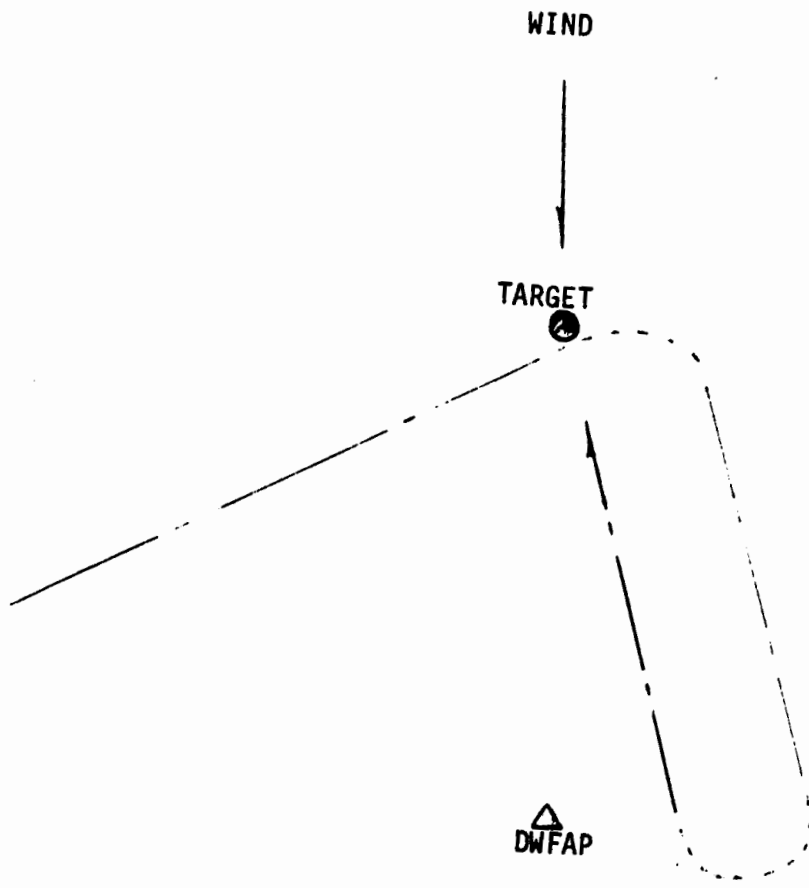


Figure 5

The proportion of right turn entries onto the outbound leg is higher for the offset approaches than for the straight-in approaches. Each of the arcing entries was performed prior to a straight-in approach. The bias of the offset approach data is larger (indicating the flights were on the average farther right of course) than the bias of the straight-in approaches. Therefore, it appears that the overhead turning maneuver tends to adversely affect the accuracy of reaching the Downwind Final Approach Point (DWFAP).

Other factors may also have contributed to the track bias. The offset angle used in the overhead maneuver may have been too large for the speeds and distances flown causing the helicopter to be right of course at the DWFAP. The dead reckoning method of determining the start point of the standard rate turn onto the downwind final approach course could also contribute to the error in reaching the DWFAP. Finally, since the crewmembers were inclined to home toward the target rather than seek the proper approach course, the error in reaching the downwind final approach point was carried through the entire flight. This last point will be discussed in more detail in later paragraphs.

The standard deviations of the angular deviations are also presented in Tables 3, 4, and 5. The standard deviations for All approaches, Offset approaches, and Straight-In approaches are very similar in size, all being about  $10^{\circ}$  -  $12^{\circ}$  at 5 nm and then steadily increasing to  $14^{\circ}$  -  $15^{\circ}$  at 1 nm. This similarity of standard deviations is to be expected since

the Offset approach procedure and the Straight-In approach procedure are identical to the 1 nm point.

It is often possible to combine angular data collected at different ranges into one sample so that a probability density curve may be found which fits the sample data with a high degree of confidence. This procedure requires the samples be statistically from the same population and be formed independently.

The Spearman rank correlation test was used to determine if the samples could be considered to be independent. The Spearman test was chosen because it is a nonparametric test requiring no assumptions about the populations from which the samples are drawn. The test results are shown in Tables 6 and 7. The tables show that correlation between samples at 500 foot intervals, half-mile intervals, and one mile intervals were all highly significant. This means that the aircraft paths, as seen in the composite graphs (Figures 6, 7, 8, and 9), are not crossing one another very much. They are maintaining their relative positions from range to range. When aircraft are attempting to follow a course such as an ILS localizer, the paths cross each other often, and if the range interval width is reasonably chosen, the aircraft position at one range will be independent of its position at another. Thus, the high correlation is an indication that the crewmembers were homing to the target rather than following the predetermined final approach course. Thus the error in reaching the DWFAP is retained throughout the flight.

SPEARMAN RHO CORRELATION OF TRACK DISPERSION  
 COMPARED TO RANGE

RANGE 1	RANGE 2	NUMBER OF CASES	TABLED RHO *	COMPUTED RHO
5.000	4.000	74	0.38512	.92974
4.000	3.000	101	0.32905	.97991
3.000	2.917	107	0.31960	.99946
2.917	2.836	107	0.31960	.99965
2.836	2.753	106	0.32112	.99954
2.753	2.671	108	0.31810	.99971
2.671	2.589	108	0.31810	.99961
2.589	2.506	108	0.31810	.99945
2.506	2.425	108	0.31810	.99919
2.425	2.342	108	0.31810	.99948
2.342	2.259	108	0.31810	.99930
2.259	2.177	108	0.31810	.99947
2.177	2.094	108	0.31810	.99949
2.094	2.000	108	0.31810	.99939
2.000	1.918	104	0.32422	.99941
1.918	1.825	104	0.32422	.99958
1.825	1.743	104	0.32422	.99947
1.743	1.660	104	0.32422	.99931
1.660	1.590	104	0.32422	.99900
1.590	1.507	104	0.32422	.99930
1.507	1.424	104	0.32422	.99926
1.424	1.341	103	0.32581	.99911
1.341	1.260	103	0.32581	.99857
1.260	1.177	104	0.32422	.99829
1.177	1.094	104	0.32422	.99836
1.094	1.000	103	0.32581	.99833

\*Non-correlation may be rejected at the 99.9 significance level if the absolute value of RHO exceeds this value.

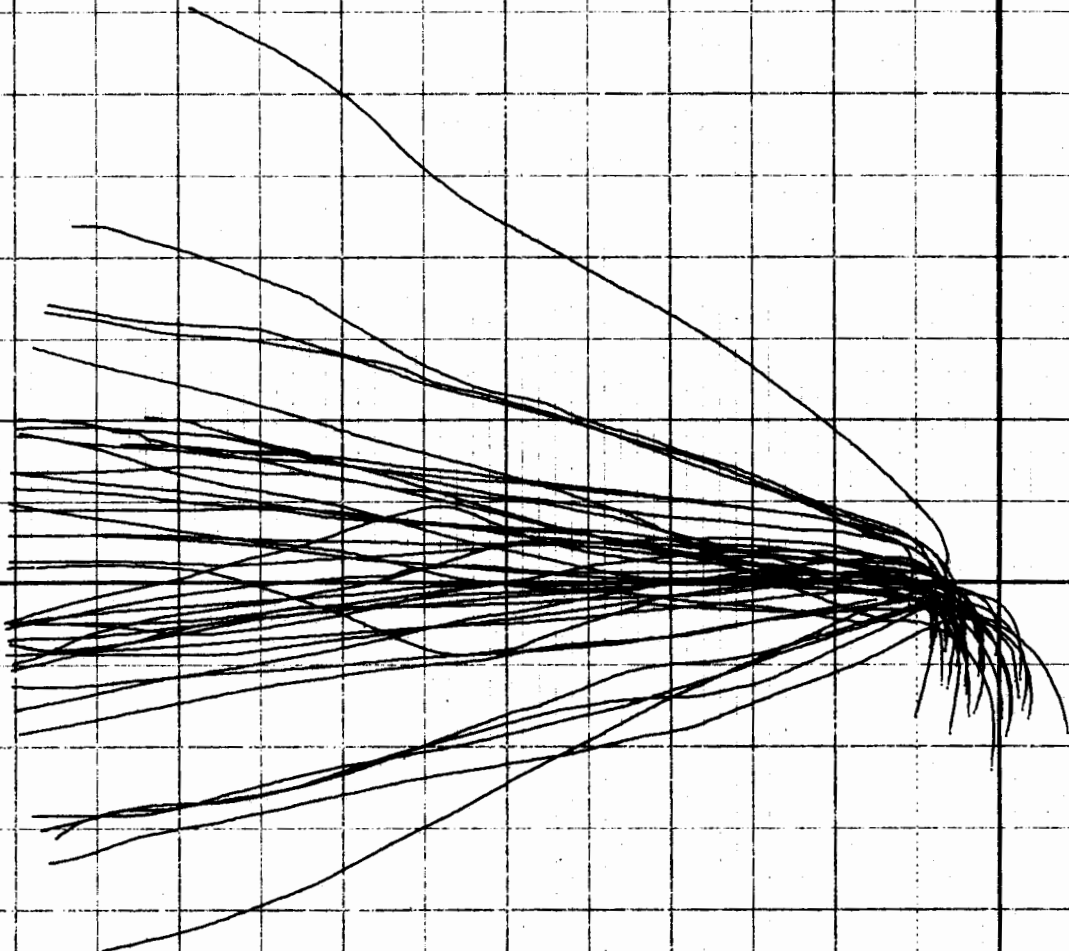
Table 6

SPEARMAN RHO CORRELATION OF TRACK DISPERSION  
 COMPARED TO RANGE - 1/2 MILE INTERVALS

RANGE 1	RANGE 2	NUMBER OF CASES	TABLED RHO *	COMPUTED RHO
3.000	2.506	106	.32112	.99332
2.506	2.000	108	.31810	.99048
2.000	1.507	104	.32422	.98928
1.507	1.000	103	.32581	.97657

\*Non-correlation may be rejected at the 99.9 significance level if the absolute value of RHO exceeds this value.

Table 7



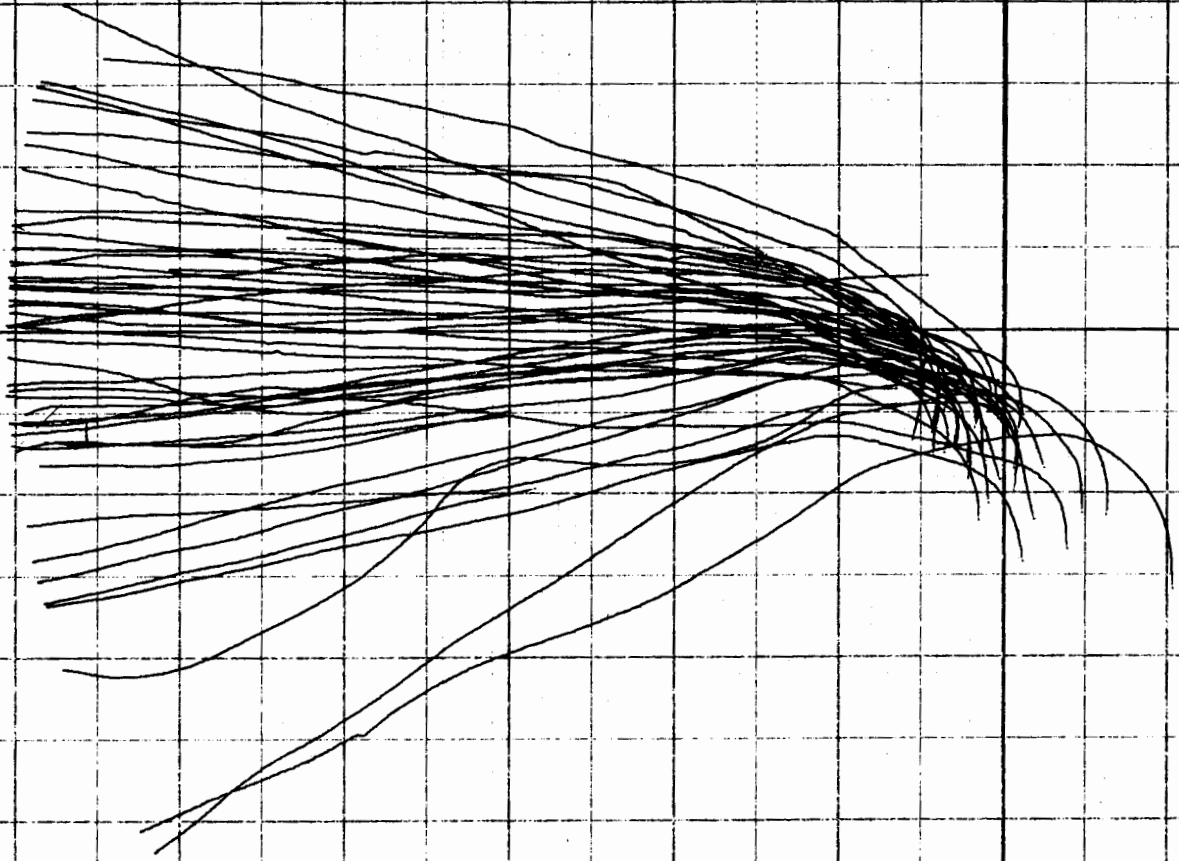
ALL RIGHT TURNS  
ALL STRAIGHT IN APPROACHES      HALF MILE

0.1.2.3.4.

THOUSAND FEET

08/08/79.BORDER03

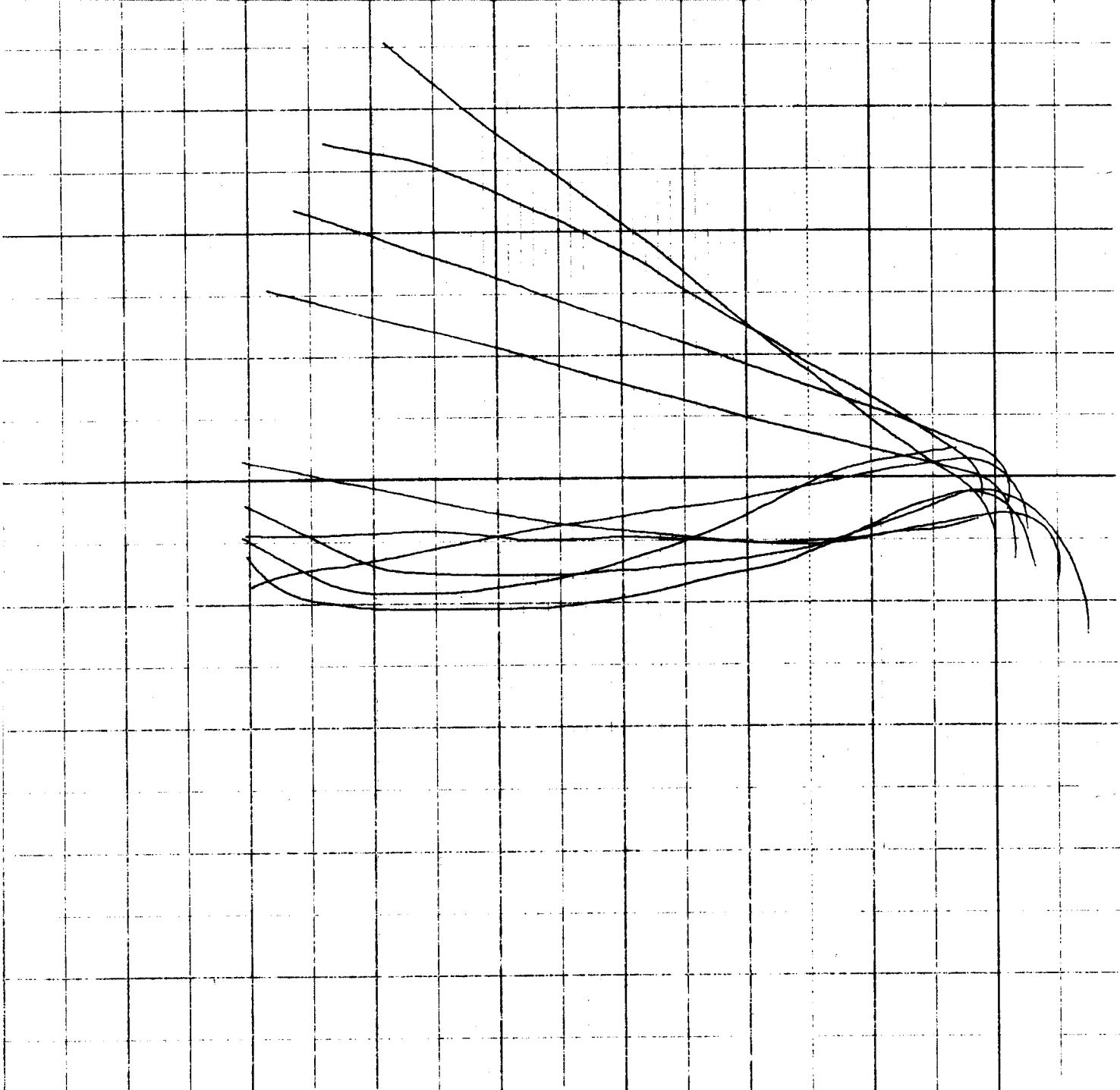
Figure 6  
26



ALL RIGHT TURNS  
ALL OFFSET APPROACHES HALF MILE

0.1.2.3.4.  
THOUSAND FEET  
08/09/79.

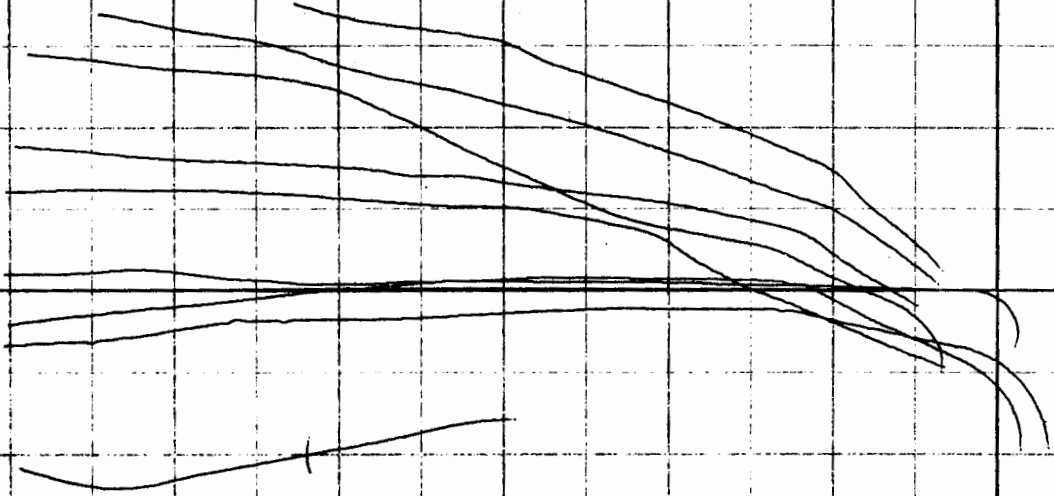
Figure 7  
27



ALL RIGHT TURNS  
ALL STRAIGHT IN APPROACHES      QUARTER MILE

0.1.2.3.4.  
THOUSAND FEET  
08/09/79.

Figure 8  
28



ALL RIGHT TURNS  
ALL OFFSET APPROACHES QUARTER MILE

0. 1. 2. 3. 4.

THOUSAND FEET

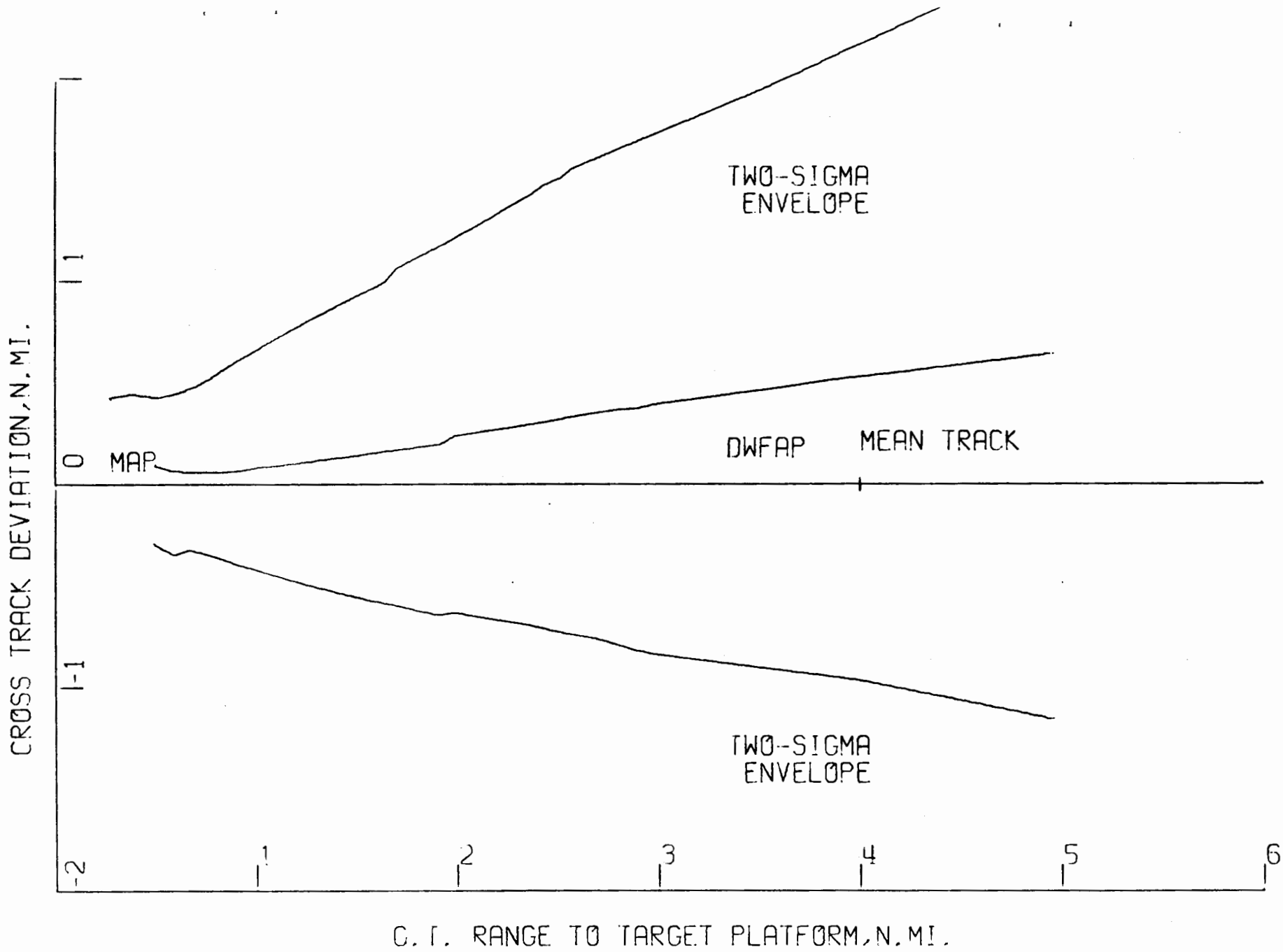
08/09/78.

Figure 9

The samples were not combined, but tests for normality using the sample skewness and kurtosis were conducted. The tests indicate the assumption that samples are from normal populations cannot be rejected at the 5 percent level. The sample means plus or minus two standard deviations were used to prepare Figures 10, 11, and 12. The probability that a number drawn from a normal population is within two standard deviations of the mean is about 0.95; thus at each range the probability of being within the envelopes pictured on the graphs is about 0.95.

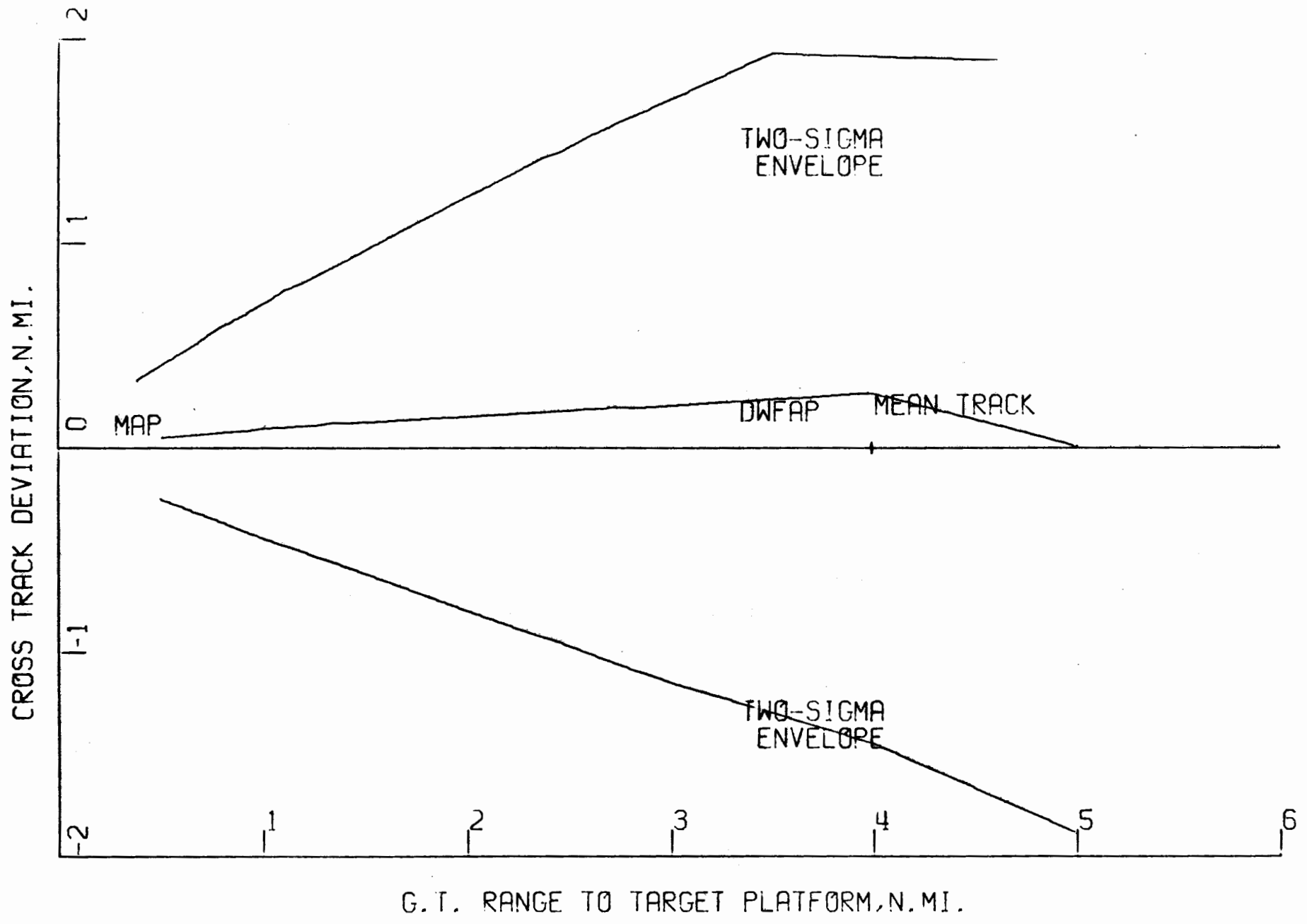
The envelopes are very wide from the 5 nm range to the 1 nm range. At 4 nm, the mean for all approaches is 2,427 feet right of course, and the 95 percent envelope boundary point (including the 5,730<sup>0</sup> mean) is 11,834 feet right of course. The mean at 1 nm is 523 feet right of course. Thus the airspace required for the final approach is funnel shaped, almost 4 nm wide at the 4 nm range, narrowing to about 1 nm at the 1 nm range.

The wide envelope is principally due to wide dispersion at the DWFAP. Once the target was established on the radar centerline, the crewmembers were able to track to the target more accurately than the analysis above would indicate. The tracking accuracy excluding the displacement error at the DWFAP was estimated by comparing track performance to the computed average angle for each approach (see Appendix A).



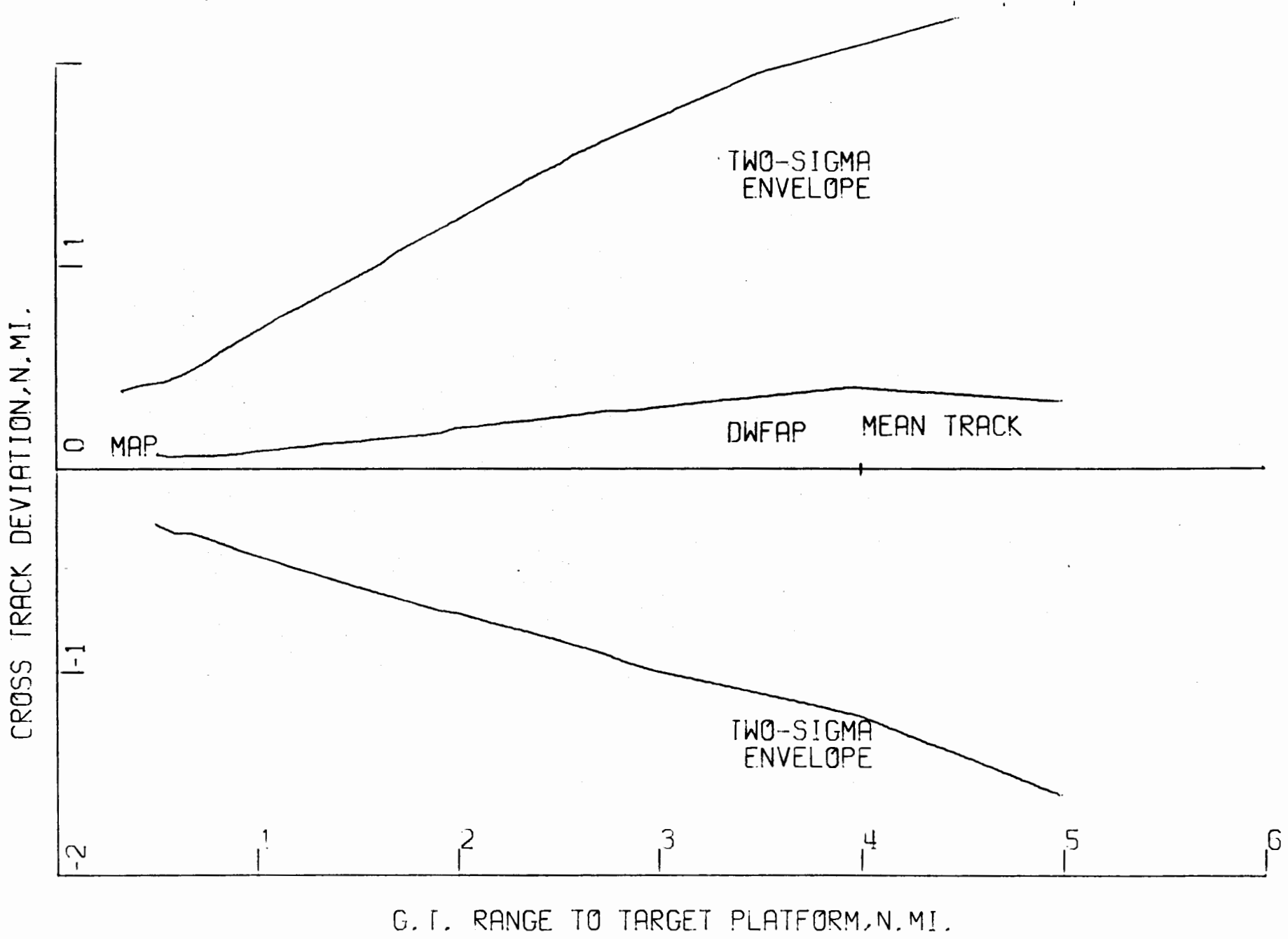
ALL APPROACHES

Figure 10



ALL STRAIGHT-IN APPROACHES

Figure 11



ALL OFFSET APPROACHES

Figure 12

The statistics for the average course are presented in Tables 8, 9, and 10. The mean angular deviation is now much closer to zero.

The means of all approaches are within  $0.4^{\circ}$  of  $0^{\circ}$  for all ranges from 3 nm to 1 nm. The means of the straight-in approaches are within  $0.7^{\circ}$  of  $0^{\circ}$  for all ranges from 3 nm to 1 nm. The means of the offset approaches are within  $1.25^{\circ}$  of  $0^{\circ}$  for all ranges from 3 nm to 1 nm. The means of all approaches and the straight-in approaches are negative at 4 nm and 5 nm while the means of the offset approaches are positive. The means at ranges less than 1 nm increase reflecting the missed approach turns. The means for the offset approaches at ranges less than 1 nm do not approach the  $15^{\circ}$  offset angle since there was a mixture of left and right offsets.

The difference in signs of the means at 4 nm and 5 nm for the offset and straight-in approaches provides further evidence that more right hand procedure turns were used in the offset approaches than in the straight-in approaches. It also shows that many aircraft are still turning at 5 nm and 4 nm but have established a course to the target by 3 nm.

The standard deviations about the average path are much smaller than the standard deviations about the intended path. The standard deviations for all approaches are between  $.724^{\circ}$  and  $4.106^{\circ}$  for the ranges from 1 nm to 3 nm. The standard deviation at 5 nm is only  $6.752^{\circ}$ . A two standard deviation envelope about the mean is shown in Figure 13.

ANGULAR DEVIATION  
FROM AVERAGE ANGULAR  
PATH (ALL APPROACHES)

RANGE	SAMPLE SIZE	MEAN ANGULAR ERROR DEGREES	95 PERCENT CONFIDENCE INTERVAL DEGREES	STANDARD DEVIATION DEGREES	MINIMUM DEGREES	MAXIMUM DEGREES	KURTOSIS	SKEWNESS
5.000	76	-1.252	-2.795 to 0.291	6.752	-28.113	9.183	2.572	-1.271
4.000	99	-0.245	-1.004 to 0.514	3.305	-12.357	7.405	0.332	-0.629
3.000	106	0.160	-0.285 to 0.605	2.312	- 6.608	5.841	0.071	-0.296
2.917	107	0.155	-0.266 to 0.575	2.192	- 6.100	5.656	0.055	-0.307
2.836	106	0.154	-0.248 to 0.556	2.088	- 5.712	5.470	0.014	-0.303
2.753	107	0.199	-0.176 to 0.574	1.959	- 5.306	5.235	0.050	-0.311
2.671	107	0.174	-0.172 to 0.520	1.805	- 4.871	5.056	0.127	-0.314
2.589	107	0.149	-0.166 to 0.464	1.644	- 4.436	4.784	0.179	-0.295
2.506	107	0.124	-0.161 to 0.409	1.488	- 3.879	4.438	0.136	-0.227
2.425	107	0.097	-0.160 to 0.355	1.342	- 3.440	4.153	0.099	-0.156
2.342	107	0.070	-0.163 to 0.302	1.212	- 2.936	3.584	0.151	-0.284
2.259	107	0.041	-0.173 to 0.254	1.113	- 4.149	3.099	1.728	-0.738
2.177	107	0.017	-0.176 to 0.211	1.008	- 4.734	2.481	4.891	-1.399
2.094	107	0.012	-0.162 to 0.185	0.906	- 5.089	2.237	9.859	-2.204
2.000	107	0.010	-0.145 to 0.166	0.811	- 4.867	2.054	13.133	-2.637
1.918	103	-0.020	-0.165 to 0.124	0.738	- 4.184	1.818	10.915	-2.274
1.825	103	-0.017	-0.158 to 0.125	0.724	- 3.062	1.859	3.494	-0.801
1.743	103	-0.021	-0.182 to 0.139	0.821	- 2.175	2.471	0.648	0.091
1.660	103	-0.032	-0.231 to 0.167	1.071	- 2.486	2.993	0.187	0.267
1.590	103	-0.056	-0.300 to 0.187	1.248	- 3.411	2.925	- 0.017	0.151
1.507	103	-0.088	-0.386 to 0.210	1.523	- 4.150	3.884	- 0.099	0.191
1.424	103	-0.084	-0.446 to 0.278	1.852	- 4.856	4.934	- 0.149	0.276
1.341	102	-0.088	-0.522 to 0.345	2.207	- 5.639	6.049	- 0.147	0.356
1.260	103	-0.130	-0.637 to 0.377	2.592	- 6.932	7.366	- 0.049	0.360
1.177	103	-0.157	-0.748 to 0.434	3.023	- 8.409	8.767	0.061	0.377

Table 8



ANGULAR DEVIATION  
FROM AVERAGE ANGULAR PATH  
(OFFSET APPROACHES)

RANGE	SAMPLE SIZE	MEAN ANGULAR ERROR DEGREES	95 PERCENT CONFIDENCE INTERVAL DEGREES	STANDARD DEVIATION DEGREES	MINIMUM DEGREES	MAXIMUM DEGREES	KURTOSIS	SKEWNESS
5.000	39	0.105	-1.475 to 1.685	4.873	-11.163	9.183	- 0.403	-0.351
4.001	51	0.490	-0.406 to 1.385	3.183	- 5.950	7.405	- 0.502	0.062
3.002	55	0.682	0.119 to 1.244	2.082	- 3.640	5.841	- 0.082	0.074
2.917	56	0.659	0.128 to 1.190	1.984	- 3.836	5.656	0.065	0.032
2.837	55	0.668	0.154 to 1.183	1.903	- 3.940	5.470	0.126	-0.013
2.752	57	0.687	0.210 to 1.165	1.799	- 3.941	5.235	0.161	-0.043
2.671	57	0.624	0.184 to 1.064	1.660	- 3.880	5.056	0.449	-0.084
2.589	57	0.555	0.156 to 0.954	1.503	- 3.734	4.784	0.698	-0.086
2.507	57	0.476	0.113 to 0.839	1.369	- 3.545	4.438	0.859	-0.074
2.424	57	0.400	0.073 to 0.727	1.233	- 3.169	4.153	1.008	-0.030
2.341	57	0.324	0.031 to 0.618	1.105	- 2.839	3.584	1.447	-0.335
2.259	57	0.247	-0.026 to 0.520	1.028	- 4.149	3.099	5.155	-1.211
2.177	57	0.184	-0.066 to 0.433	0.940	- 4.734	2.481	11.800	-2.406
2.095	57	0.137	-0.098 to 0.372	0.886	- 5.089	1.932	19.627	-3.587
2.001	57	0.074	-0.146 to 0.293	0.828	- 4.867	1.524	20.709	-3.796
1.917	53	-0.044	-0.254 to 0.165	0.759	- 4.184	1.297	15.427	-3.272
1.836	53	-0.098	-0.306 to 0.110	0.753	- 3.052	1.824	4.040	-1.140
1.754	53	-0.161	-0.402 to 0.800	0.875	- 2.175	2.471	0.887	0.099
1.669	53	-0.233	-0.528 to 0.061	1.069	- 2.486	2.993	0.632	0.356
1.589	53	-0.329	-0.678 to 0.021	1.268	- 3.411	2.925	0.180	0.122
1.506	53	-0.456	-0.867 to -0.045	1.490	- 4.150	3.157	- 0.079	0.076
1.424	53	-0.558	-1.039 to -0.077	1.746	- 4.856	3.741	- 0.175	0.127
1.341	53	-0.667	-1.225 to -0.110	2.023	- 5.639	4.405	- 0.093	0.228
1.261	53	-0.788	-1.442 to -0.135	2.371	- 6.932	4.935	- 0.052	0.160
1.178	53	-0.909	-1.653 to -0.155	2.735	- 8.409	5.557	0.121	0.155
				Table 9				



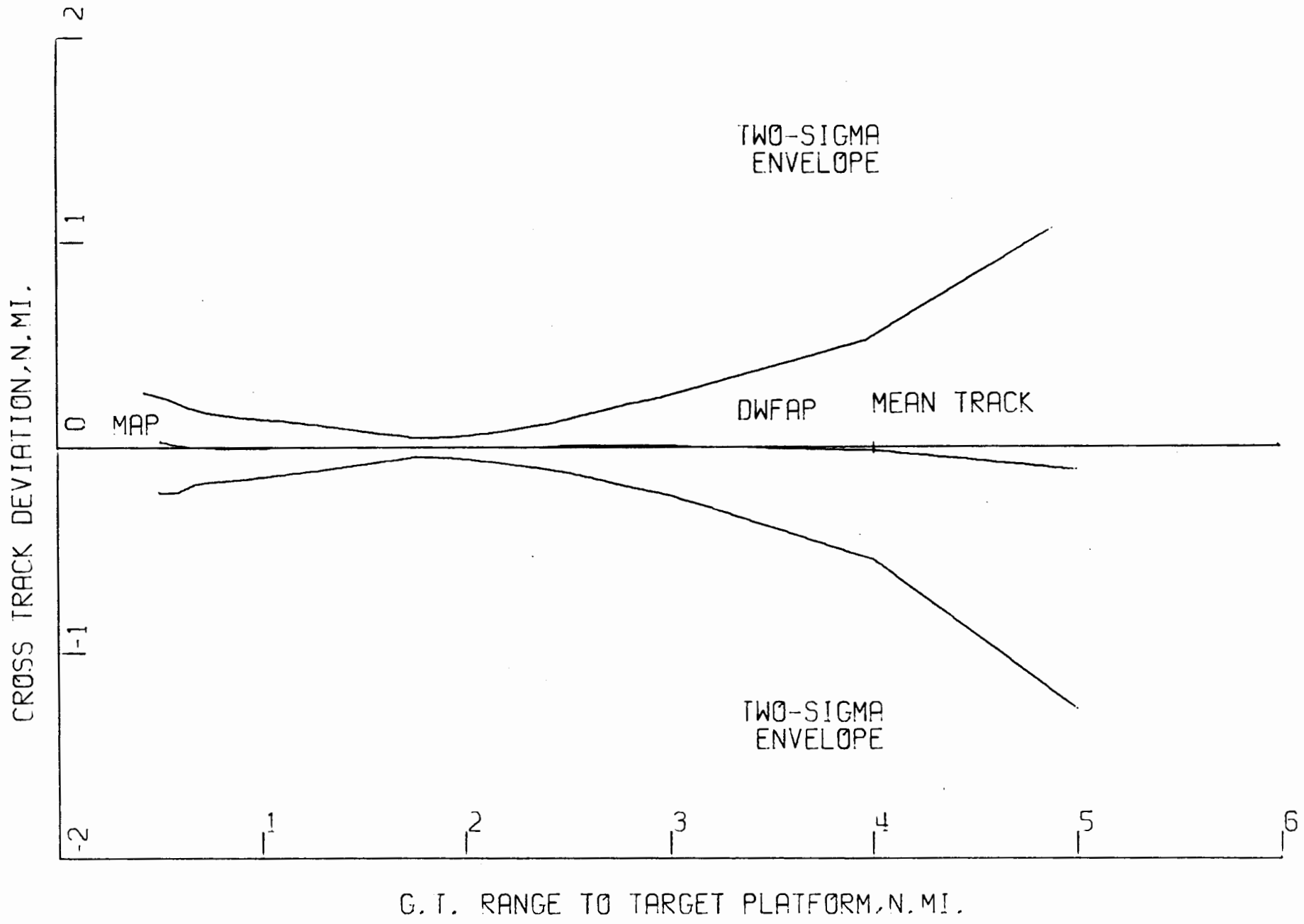
ANGULAR DEVIATION  
FROM AVERAGE ANGULAR PATH  
(STRAIGHT-IN APPROACHES)

RANGE	SAMPLE SIZE	MEAN ANGULAR ERROR DEGREES	95 PERCENT CONFIDENCE INTERVAL DEGREES	STANDARD DEVIATION DEGREES	MINIMUM DEGREES	MAXIMUM DEGREES	KURTOSIS	SKEWNESS
5.000	37	-2.682	-5.386 to 0.023	8.112	-28.113	9.131	1.291	-1.115
4.001	48	-1.026	-2.264 to 0.213	4.266	-12.357	6.862	0.489	-0.718
3.001	51	-0.402	-1.087 to 0.282	2.434	- 6.608	4.537	-0.348	-0.397
2.917	51	-0.399	-1.044 to 0.246	2.293	- 6.100	3.942	-0.456	-0.409
2.835	51	-0.402	-1.007 to 0.204	2.153	- 5.712	3.403	-0.530	-0.402
2.753	50	-0.358	-0.927 to 0.212	2.003	- 5.306	2.895	-0.520	-0.432
2.670	50	-0.339	-0.863 to 0.184	1.842	- 4.871	2.798	-0.520	-0.410
2.589	50	-0.314	-0.794 to 0.166	1.689	- 4.436	2.675	-0.526	-0.346
2.506	50	-0.278	-0.713 to 0.156	1.529	- 3.879	2.451	-0.611	-0.233
2.425	50	-0.248	-0.643 to 0.147	1.390	- 3.440	2.306	-0.690	-0.118
2.343	50	-0.221	-0.582 to 0.141	1.273	- 2.936	2.378	-0.664	-0.110
2.259	50	-0.194	-0.527 to 0.138	1.169	- 3.290	2.431	-0.028	-0.304
2.178	50	-0.172	-0.473 to 0.129	1.059	- 3.274	2.397	1.128	-0.587
2.094	50	-0.132	-0.392 to 0.128	0.915	- 3.188	2.237	2.432	-0.891
2.000	50	-0.062	-0.288 to 0.163	0.794	- 3.198	2.054	4.386	-1.218
1.918	50	0.005	-0.200 to 0.210	0.721	- 2.881	1.818	4.599	-1.030
1.837	50	0.069	-0.127 to 0.265	0.689	- 2.295	1.859	2.174	-0.291
1.754	50	0.127	-0.084 to 0.337	0.740	- 1.651	2.065	-0.140	0.326
1.671	50	0.181	-0.082 to 0.443	0.923	- 1.366	2.322	-0.647	0.399
1.590	50	0.232	-0.101 to 0.565	1.170	- 1.871	2.892	-0.529	0.348
1.508	50	0.302	-0.117 to 0.721	1.474	- 2.342	3.884	-0.446	0.374
1.423	50	0.418	-0.106 to 0.943	1.845	- 2.885	4.934	-0.470	0.382
1.341	49	0.538	-0.107 to 1.183	2.246	- 3.545	6.049	-0.496	0.372
1.259	50	0.568	-0.137 to 1.323	2.657	- 4.204	7.366	-0.430	0.416
1.177	50	0.641	-0.250 to 1.531	3.133	- 5.105	8.767	-0.359	0.414

Table 10



41



ALL APPROACHES - AVERAGE PATH

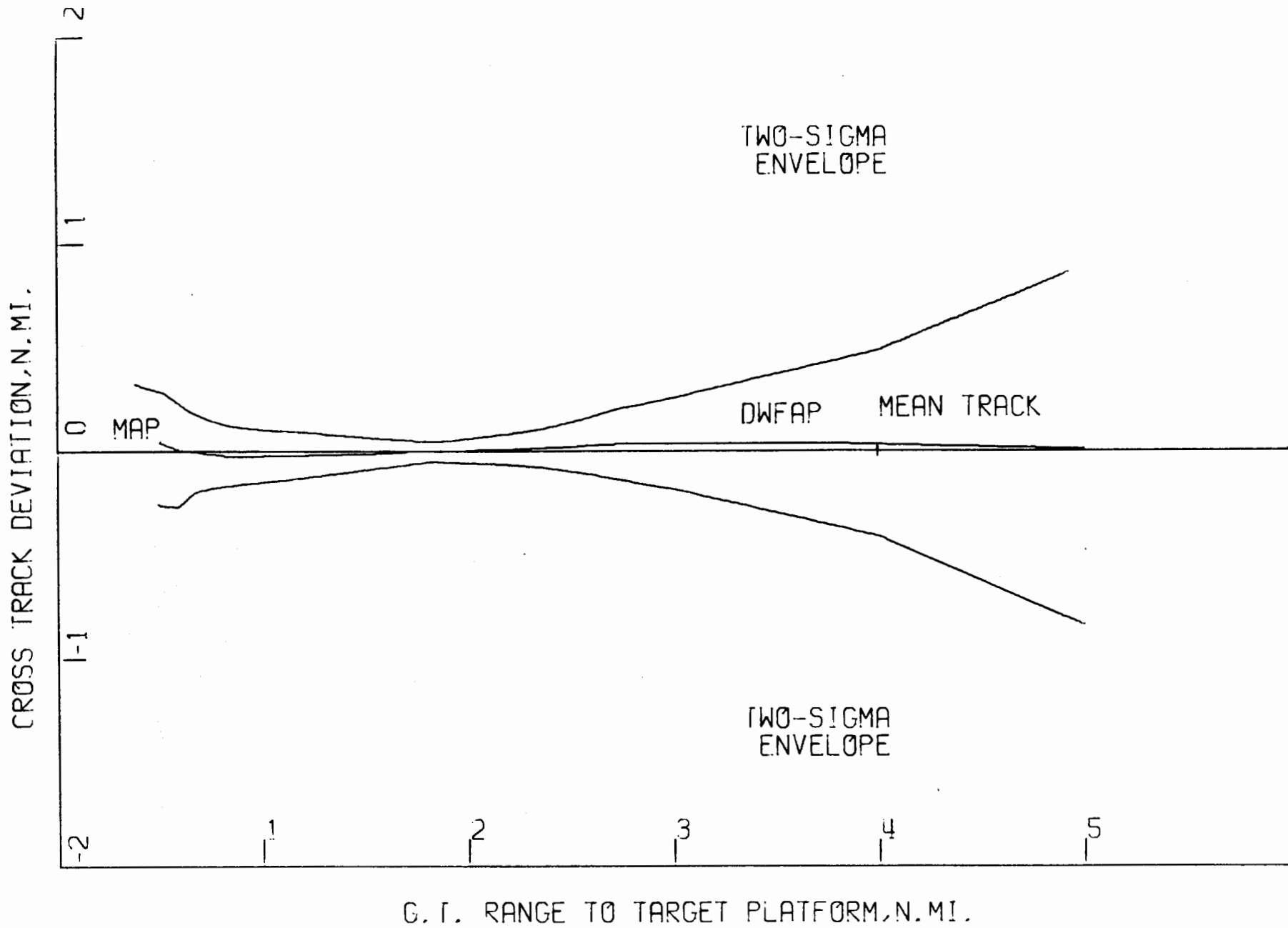
Figure 13

The standard deviations of the Offset approaches and Straight-In approaches are also much smaller than the corresponding standard deviations from the intended path. Two standard deviation envelopes for the offset approaches and the straight-in approaches are shown in Figures 14 and 15.

The small standard deviations from the average angular path indicate that once established on target the pilots flew relatively straight to the target. Thus the wide envelopes found for the intended path are indications of the large inaccuracies associated with reaching the DWFAP. If the DWFAP could be accurately found by the crew, then the lateral airspace requirements could be drastically reduced.

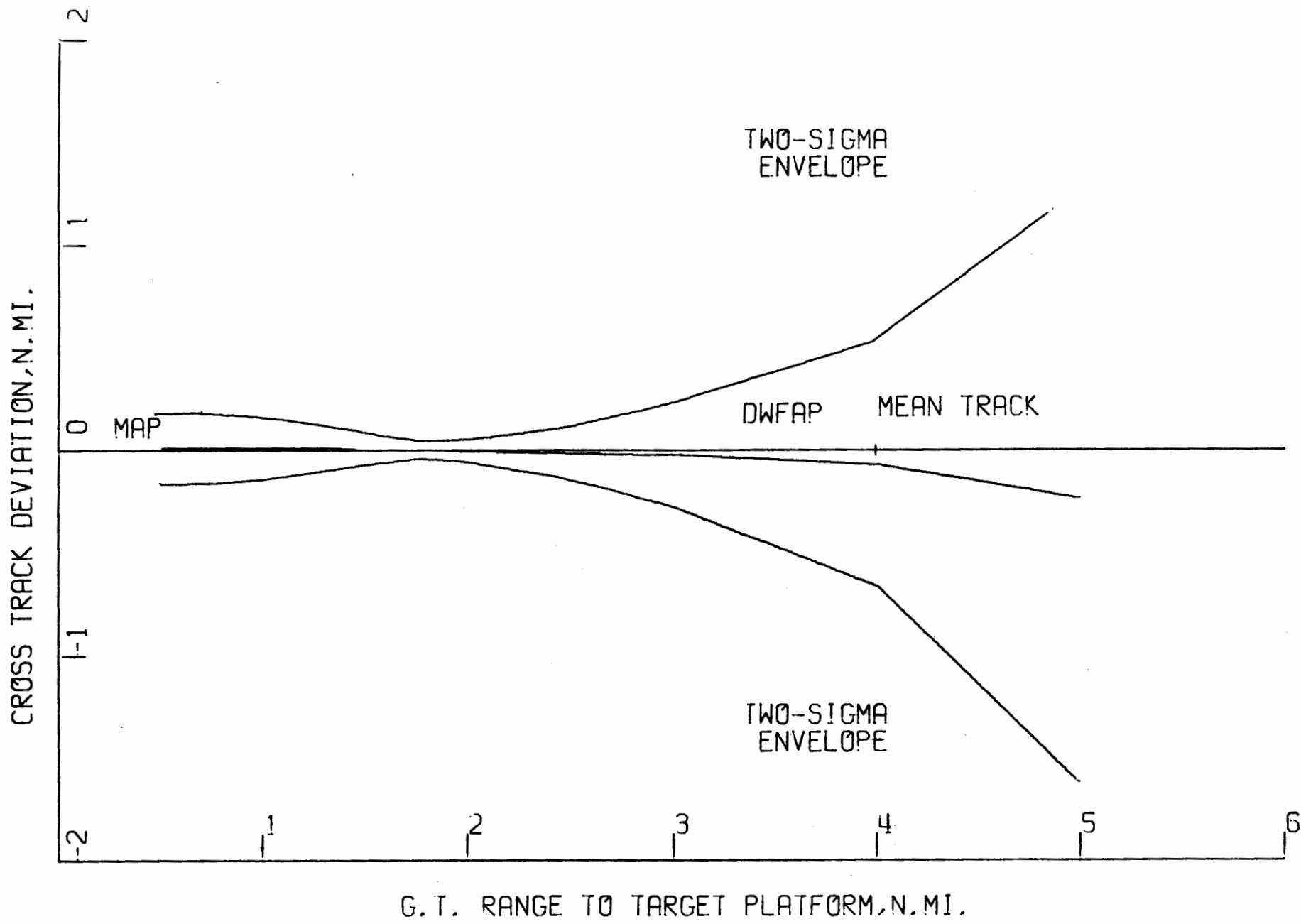
Although the error induced by the dead reckoning method for reaching the DWFAP represents a large portion of the error observed when the aircraft flew the final approach, there are other sources of error which should be considered. Two other primary sources of error are the radar and crew. The radar, because of technological considerations, may induce error, and the crewmember, because of human considerations, may induce error.

Data to establish these two components of error were obtained (see Appendix A) by photographing the radar display at regular intervals. To obtain radar error from these photographs, the aircraft position indicated by radar was compared to the actual position of the aircraft. In addition, the difference in position given by the radar compared to the position where the aircraft should have been was used as the measure of the human error.



ALL OFFSET APPROACHES - AVERAGE PATH

Figure 14



ALL STRAIGHT IN ROACHES - AVERAGE PATH

Figure 15

Referring to Figure 16, the line OD represents the downwind final approach path, O is the target rig, and D is the downwind final approach point. The aircraft's actual position at some time t is the point P, and the position as shown by the radar is R. The point E is the foot of a perpendicular from P to the line OR. The angle POR is the angle formed by the actual aircraft position and the position shown by the radar. The angle POR is called the Radar Bearing Error (RBE). The angle ROD is the angle formed by the radar position of the aircraft with the DWFAP. The angle ROD is called the Flight Technical Error (FTE) and represents the human component of the azimuth error. Flight Technical Error should not be interpreted to be only the error involved in reading the radar scope. It represents all the human errors which cause the aircraft to be off course. The angle POD is the angle formed by the aircraft position and the DWFAP. The angle POD is called the Azimuth Total System Error (ATSE). The length of PR is the distance from the actual aircraft position to the radar position and is called the Radar Position Error (RPE). The length of ER, positive if E is between O and R, is called the Radar Range Error (RRE). The Radar Range Error and the Radar Position Error are measured in nautical miles.

Samples were taken from some of the flights at the same range intervals used for the intended path samples and the average path samples (see Appendix A). Standard statistics were computed from each sample for all flights sampled, flights which used the radar beacon mode, and flights which used the primary radar mode.

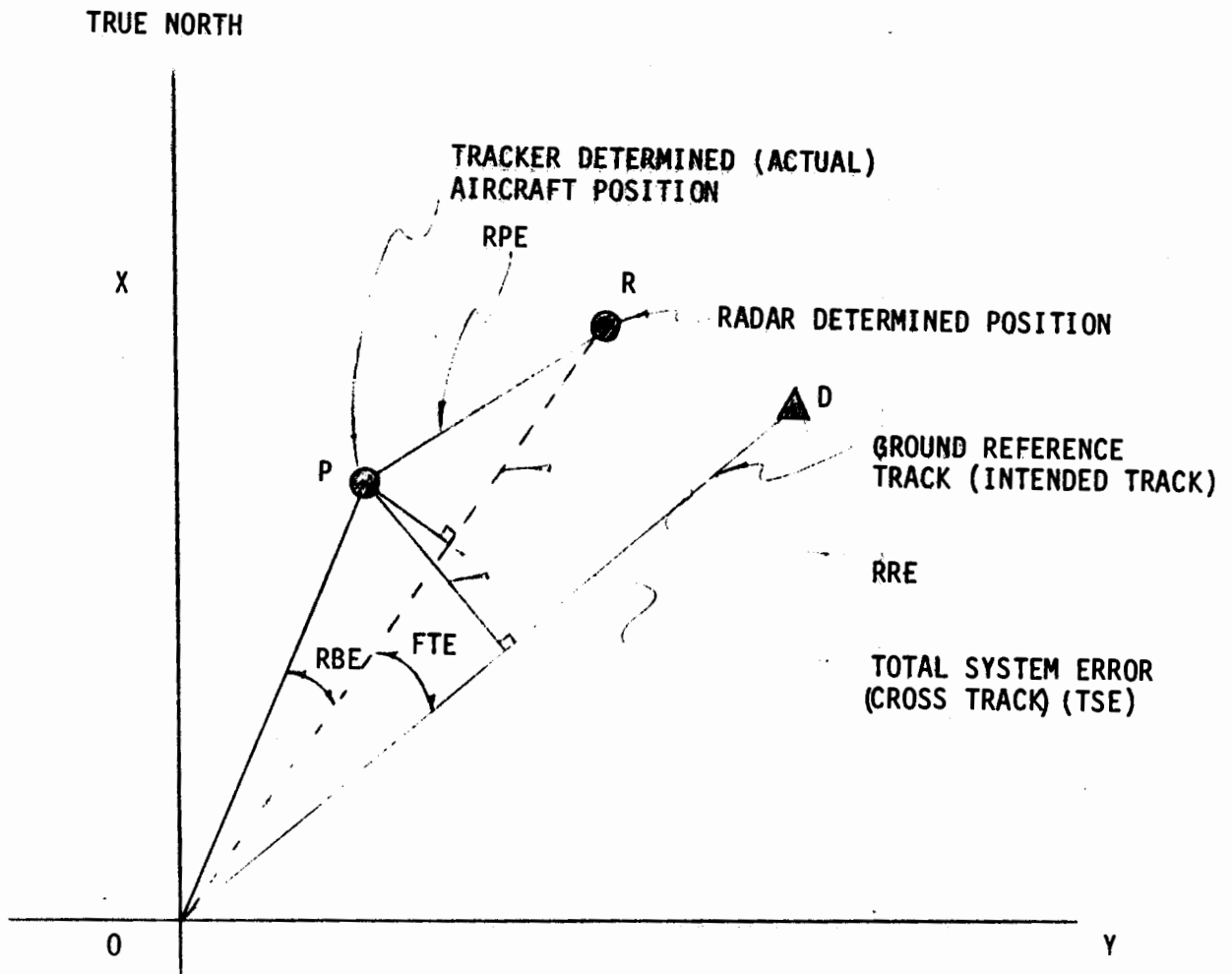


Figure 16

The means and standard deviations of the errors measured for all the flights sampled are given in Table 11. The number of cases at each range is much smaller than the corresponding number of Table 3. The number of cases varies from 30 at 4 nm to 54 at 2 nm, in Table 11 the latter being only one-half the maximum number of cases in Table 3. The column labeled Total System Error represents the same variables as the column labeled Mean Azimuth Error in Table 3. The means of Table 11 are somewhat smaller, but the difference is probably due to the smaller sample sizes. Note that the standard deviations are quite similar.

The means of the Radar Bearing Error for all sampled flights are generally small and negative, varying from  $-1.737^{\circ}$  to  $.053^{\circ}$  at ranges greater than 1 nm. The standard deviations vary from  $2.159^{\circ}$  to  $5.224^{\circ}$  at ranges greater than 1 nm. The mean and standard deviation change drastically at 0.177 nm becoming  $-9.886^{\circ}$  and  $35.012^{\circ}$  respectively, indicating that most of the aircraft have begun the missed approach turn.

The Flight Technical Error means of all the sampled flights are generally larger in absolute value than the means of the Radar Bearing Error, varying from  $1.796^{\circ}$  to  $5.040^{\circ}$  at ranges more than 1 nm. The standard deviations of the Flight Technical Error are much larger, being generally around  $12^{\circ}$  until the missed approach turn is entered. The statistics indicate that Flight Technical Error is the predominant component of Azimuth Total System Error.

COMPONENTS OF ERROR  
(ALL APPROACHES)

RANGE	CASES	RADAR BEARING ERROR		FLIGHT TECHNICAL ERROR		RADAR POSITION ERROR		AZIMUTH TOTAL SYSTEM ERROR	
		MEAN	S.D.	MEAN	S.D.	MEAN	S.D.	MEAN	S.D.
4.000	30	-1.553	3.412	3.153	9.778	.244	.151	1.597	10.519
3.000	43	-1.737	4.659	5.040	11.083	.212	.184	3.302	12.045
2.917	39	-.751	2.995	3.167	13.215	.158	.111	2.413	13.527
2.836	44	-1.105	3.892	2.232	11.444	.171	.137	1.136	11.785
2.753	46	-1.559	3.680	4.826	12.018	.160	.152	3.263	12.793
2.671	46	-.448	3.509	3.963	12.679	.156	.112	3.511	12.925
2.589	46	-.596	3.964	4.237	12.919	.154	.142	3.654	12.423
2.506	46	-.509	3.951	2.628	12.483	.145	.128	2.115	13.278
2.425	44	-.918	2.541	3.082	13.719	.123	.082	2.161	13.364
2.342	45	-.473	3.812	3.669	12.239	.135	.125	3.200	12.957
2.259	46	.030	4.556	2.296	14.010	.140	.156	2.330	12.400
2.177	50	-1.026	4.042	3.504	11.382	.150	.109	2.474	12.041
2.094	51	.053	3.542	1.796	11.190	.122	.102	1.837	12.102
2.000	54	-1.657	4.731	3.633	11.678	.124	.154	1.980	12.103
1.918	53	-.694	3.114	2.708	12.358	.111	.083	2.008	12.333
1.825	54	-.598	2.849	2.907	11.569	.105	.068	2.319	12.012
1.743	54	-1.002	3.147	3.635	11.733	.106	.086	2.624	11.943
1.660	52	-.929	2.849	2.950	11.094	.098	.078	2.021	12.523
1.590	53	-.800	2.159	2.423	12.646	.082	.061	1.640	12.715
1.507	53	-.934	2.852	3.094	12.664	.087	.072	2.164	12.258
1.424	53	-1.091	3.009	2.162	12.191	.092	.064	1.072	12.532
1.341	53	-.970	2.702	1.998	13.000	.081	.063	1.030	12.709
1.260	54	-.767	2.244	1.987	12.691	.075	.061	1.226	12.865
1.177	55	-1.251	3.813	2.840	13.162	.082	.079	1.595	13.336
1.094	56	-.479	5.224	1.950	14.325	.090	.087	1.480	13.438
1.000	54	-.065	8.022	1.467	17.020	.098	.141	1.404	13.985
0.918	52	-1.521	4.463	2.852	14.300	.086	.077	1.335	14.526
0.837	54	-1.083	6.316	2.180	15.602	.095	.096	1.102	14.556
0.754	55	-1.131	4.636	2.116	14.357	.106	.121	.978	14.507
0.671	52	-2.037	9.167	3.446	14.013	.095	.118	1.425	16.079
0.588	52	-2.438	9.975	4.373	14.763	.100	.108	1.929	18.508
0.500	47	-2.151	14.461	5.826	16.535	.116	.126	3.672	22.322
0.416	40	2.123	9.433	6.185	20.333	.137	.149	8.300	22.879
0.335	27	2.370	8.661	3.219	25.685	.094	.077	5.570	29.506
0.254	12	2.175	13.707	-4.042	27.980	.093	.064	-1.892	37.583
0.177	7	-9.886	35.012	-4.186	37.821	.174	.085	-14.071	64.161

Table 11

Table 12 represents error components of the flights which used the primary radar mode tracking. The means of the Azimuth Total System Error vary from  $.986^{\circ}$  to  $2.930^{\circ}$  at ranges greater than 1 nm. The means become larger at the near ranges because of the missed approach turn. The standard deviations of Total System Error are generally near  $10^{\circ}$  varying from  $9.644^{\circ}$  to  $10.931^{\circ}$  at ranges greater than 1 nm. At the close ranges, the standard deviations increase to a maximum of  $46.810^{\circ}$  at 0.177 nm.

The Radar Bearing Error means for flights using the primary mode vary from  $-1.887^{\circ}$  to  $-0.060^{\circ}$  at ranges larger than 1 nm. The means increase in magnitude as the ranges less than 1 nm decrease. The standard deviations vary from  $1.424^{\circ}$  to  $4.431^{\circ}$  at ranges larger than 1 nm. The largest standard deviation is  $29.416^{\circ}$  at .177 nm.

The Flight Technical Error means for flights using the primary mode vary from  $1.869^{\circ}$  to  $4.022^{\circ}$  at ranges larger than 1 nm. The corresponding standards deviations vary from  $8.247^{\circ}$  to  $11.384^{\circ}$ . The standard deviations increase to  $26.187^{\circ}$  at .254 nm.

Table 13 represents components of error of the flights which used beacon mode radar tracking. The sample sizes are very small with the largest sample having only 13 cases. The Azimuth Total System Error means are generally larger than their counterparts taken from the primary mode samples.

COMPONENTS OF ERROR  
(PRIMARY APPROACHES)

RANGE	CASES	RADAR BEARING ERROR		FLIGHT TECHNICAL ERROR		RADAR POSITION ERROR		AZIMUTH SYSTEM	TOTAL ERROR
		MEAN	S.D.	MEAN	S.D.	MEAN	S.D.	MEAN	S.D.
4.000	23	-1.887	3.568	4.022	8.314	.244	.162	2.139	9.776
3.000	33	-1.361	4.431	3.788	8.247	.189	.166	2.430	9.696
2.917	29	-.807	2.657	1.869	9.910	.128	.090	1.055	10.372
2.836	32	-1.525	3.932	2.550	8.441	.154	.149	1.034	9.644
2.753	33	-1.167	3.414	4.100	8.553	.129	.143	2.930	9.842
2.671	33	-.673	2.782	3.048	9.713	.122	.089	2.376	10.420
2.589	35	-1.337	3.536	3.037	10.244	.122	.022	1.711	10.358
2.506	34	-.894	4.050	2.468	9.038	.135	.136	1.574	10.455
2.425	32	-1.345	1.424	2.825	10.029	.096	.044	1.466	10.247
2.342	33	-.552	2.503	2.779	9.933	.098	.076	2.236	10.189
2.259	34	-.679	1.949	3.282	9.607	.090	.057	2.609	10.277
2.177	39	-1.231	3.627	3.492	9.206	.127	.101	2.262	10.256
2.094	40	-.335	3.082	2.328	8.885	.092	.085	1.977	9.881
2.000	42	-1.171	2.813	3.264	9.783	.082	.082	2.090	10.135
1.918	41	-.324	2.759	2.495	10.176	.082	.065	2.161	10.381
1.825	43	-.060	2.372	2.128	9.741	.079	.039	2.074	10.233
1.743	43	-.633	2.494	3.114	10.084	.008	.051	2.472	10.052
1.660	41	-.617	2.500	2.846	9.137	.069	.053	2.239	10.258
1.590	41	-.695	1.512	2.380	10.515	.055	.027	1.700	10.613
1.507	42	-.674	1.942	2.405	10.608	.057	.028	1.731	10.570
1.424	42	-1.214	2.426	2.245	9.499	.068	.042	1.033	9.926
1.341	42	-1.010	1.996	1.993	10.777	.055	.030	.986	10.022
1.260	42	-.983	1.625	2.236	10.257	.048	.029	1.264	10.308
1.177	43	-.756	1.968	2.516	10.889	.049	.027	1.765	10.931
1.094	44	-.241	3.739	1.918	11.384	.062	.055	1.684	10.922
1.000	42	-.707	2.891	2.350	11.534	.065	.081	1.645	11.350
0.918	40	-1.138	2.404	2.762	11.629	.054	.028	1.625	11.711
0.837	42	-1.374	3.740	2.733	11.594	.066	.065	1.360	11.467
0.754	44	-1.505	4.494	3.530	11.292	.096	.132	2.016	11.980
0.671	41	-1.644	6.959	4.327	11.311	.065	.093	2.698	13.392
0.588	41	-1.783	9.167	5.420	10.706	.078	.097	3.629	15.466
0.500	36	-.261	7.048	7.603	12.658	.090	.096	7.336	14.336
0.416	31	2.300	10.522	7.810	16.274	.122	.139	10.100	19.335
0.335	17	3.247	10.046	4.800	16.954	.092	.090	8.035	21.662
0.254	5	5.020	18.348	4.220	26.187	.080	.079	9.220	38.367
0.177	2	-23.700	29.416	23.950	17.466	.086	.086	.200	46.810

Table 12

COMPONENTS OF ERROR  
(BEACON APPROACHES)

RANGE	CASES	RADAR BEARING ERROR		FLIGHT TECHNICAL ERROR		RADAR POSITION ERROR		AZIMUTH SYSTEM	TOTAL ERROR
		MEAN	S.D.	MEAN	S.D.	MEAN	S.D.	MEAN	S.D.
4.000	7	-.457	2.789	.300	14.008	.246	.119	-.186	13.398
3.000	10	-2.980	5.409	9.170	17.511	.288	.229	6.180	18.189
2.917	10	-.590	3.984	6.930	20.266	.246	.123	6.350	20.363
2.836	12	.017	3.708	1.383	17.609	.218	.084	1.408	16.753
2.753	13	-2.554	4.266	6.669	18.502	.237	.154	4.108	18.825
2.671	13	.123	5.003	6.285	18.522	.241	.122	6.392	18.010
2.589	11	1.764	4.490	8.055	19.318	.254	.132	9.836	16.569
2.506	12	.583	3.592	3.083	19.800	.176	.098	3.650	19.744
2.425	12	.250	4.182	3.767	21.250	.193	.115	4.017	19.926
2.342	12	-.258	6.312	6.117	17.413	.236	.176	5.850	18.950
2.259	12	2.042	8.218	-.500	22.683	.284	.243	1.542	17.642
2.177	11	-.300	5.416	3.545	17.686	.230	.102	3.227	17.604
2.094	11	1.464	4.784	-.136	17.690	.232	.087	1.327	18.739
2.000	12	-3.358	8.619	4.925	17.262	.271	.243	1.592	17.963
1.918	12	-1.958	3.989	3.433	18.564	.209	.056	1.483	18.079
1.825	11	-2.700	3.643	5.955	17.263	.204	.067	3.273	17.991
1.743	11	-2.445	4.846	5.673	17.228	.219	.103	3.218	18.196
1.660	11	-2.091	3.810	3.336	17.134	.205	.061	1.209	19.443
1.590	12	-1.158	3.681	2.567	18.811	.176	.051	1.433	18.829
1.507	11	-1.927	5.048	5.727	19.052	.201	.074	3.818	17.874
1.424	11	-.618	4.758	1.845	20.070	.183	.054	1.218	20.316
1.341	11	-.818	4.646	2.018	20.065	.179	.056	1.200	20.690
1.260	12	-.008	3.689	1.117	19.567	.167	.054	1.092	20.035
1.177	12	-3.025	7.225	4.000	19.896	.199	.094	.983	20.404
1.094	12	-1.350	8.984	2.067	22.791	.192	.108	.733	20.876
1.000	12	2.183	16.486	-1.625	29.774	.215	.229	.558	21.475
0.918	12	-2.800	8.338	3.150	21.646	.191	.093	.367	22.150
0.837	12	-.067	11.774	.242	25.817	.196	.118	.200	23.014
0.754	11	.364	5.115	-3.536	22.821	.146	.040	-3.173	22.264
0.671	11	-3.500	15.228	.164	21.787	.205	.138	-3.318	23.869
0.588	11	-4.882	12.765	.473	25.136	.184	.110	-4.409	27.093
0.500	11	-8.336	27.078	.009	25.461	.202	.174	-8.318	36.964
0.416	9	1.511	4.247	.589	31.254	.189	.179	2.100	33.077
0.335	10	.880	5.776	.530	37.177	.098	.052	1.380	40.620
0.254	7	.143	10.414	-9.943	29.676	.102	.056	-9.829	37.840
0.177	5	-4.360	38.585	-15.440	38.926	.209	.060	-19.780	74.057

Table 13

The means vary from  $-0.186^{\circ}$  to  $9.836^{\circ}$  at ranges larger than 1 nm and reach a maximum magnitude at 0.177 nm of  $-19.780^{\circ}$ . The standard deviations of Azimuth Total System Error, are with one exception, much larger than their counterparts taken from the primary mode samples. In some instances, the standard deviations are double those from the primary mode samples. The standard deviations vary from  $13.398^{\circ}$  to  $20.876^{\circ}$  at ranges greater than 1 nm. Note that  $13.398^{\circ}$  is larger than any of the standard deviations for the primary mode samples at ranges larger than 1 nm.

The Radar Bearing Error means for the beacon mode flights appear to be about the same as those for the primary mode flights. The means vary from  $-3.358^{\circ}$  to  $1.764^{\circ}$  for ranges larger than 1 nm. The standard deviations, however, appear to be generally somewhat larger. The standard deviations vary from  $2.789^{\circ}$  to  $8.984^{\circ}$  for ranges larger than 1 nm.

The Flight Technical Error means and standard deviations for the beacon mode flights also appear larger than those of the primary mode flights. The means vary from  $-0.500^{\circ}$  to  $9.170^{\circ}$  at ranges larger than 1 nm while the standard deviations vary from  $14.008^{\circ}$  to  $22.791^{\circ}$ . The smallest,  $14.008^{\circ}$  is larger than all of the primary mode standard deviations at ranges of 0.500 nm and larger.

The Radar Position Error means of the beacon mode flights also appear to be larger than those of the primary mode flights. This is especially evident since none of the beacon mode means are less than 1 nm while 23 of the primary mode means are less than 1 nm. The means for the beacon

mode vary from 0.146 nm to 0.288 nm or 877 ft. to 1,750 ft. The standard deviations appear to be quite similar in size to those of the primary mode flights and vary from 0.040 nm to 0.243 nm, or 243 ft. to 1,477 ft.

Since the means and standard deviations of the components of error appear to be different for the beacon mode flights and primary mode flights, further statistical tests were conducted. The Kolmogorov-Smirnov two sample test was used to compare the Flight Technical Error of the primary mode flights to that of the beacon mode flights at the 4 nm, 3 nm, 2 nm, and 1 nm ranges (see Appendix A). Likewise, comparisons of the Radar Bearing Error and the Azimuth Total System Error were also conducted for the same ranges. The null hypothesis  $H_0$  is that the samples are drawn from the same population while the alternate hypothesis  $H_1$  is that the samples were drawn from different populations.

The Kolmogorov-Smirnov test (Table 14) indicates that the differences between primary and beacon radar range error samples at 4 nm, 3 nm, 2 nm, and 1 nm were highly significant. The Radar Position Error samples at 2 nm and 1 nm were highly significant. However, the azimuth components of error did not show significant differences except for the 3 nm Flight Technical Error samples, but the range errors appear to be significantly different.

The statistical analysis of the data indicates that the largest component of azimuth error present in the final approach segment is Flight Technical

Kolmogorov - Smirnov Comparison  
of Flight Technical Error

Range NM	Primary Cases	Beacon Cases	Probability associated with the sample				
			RRE	RBE	RPE	FTE	ATSE
4	23	7	.0006*	.2938	.3838	.7734	.9112
3	33	10	.0001*	.7443	.0839	.0452*	.5077
2	42	12	.0000*	.1848	.0001*	.6653	.6041
1	42	12	.0000*	.7261	.0001*	.6041	.3329

\*Significant at 5% level

Table 14

Error. Flight Technical Error represents error introduced by the flight crew through technique and judgment.

The analysis indicates that the error in reaching DWFAP is very large. If the dead reckoning procedure used to enter the final approach could be replaced with a procedure which would rely on a system such as a highly accurate RNAV, then the dispersion of the flight paths could be significantly reduced. If a radio-navigational aid cannot be provided, then the present procedure should be studied for possible improvements. The procedure could be improved by a careful study of the overhead maneuver to determine the most appropriate type of turn to use to enter the outbound leg of the flight toward the DWFAP. A variety of turns, such as those used for holding pattern entries, might be necessary depending on the direction taken to enter the overhead maneuver. The offset angle between the outbound leg and the downwind final approach course should also be studied to determine the best angle for the airspeed and windspeed combinations which would be expected. The amount of error which could be eliminated by improvements in the procedure is unfortunately unknown.

The analysis also indicates that the crews homed to the target even though they were specifically instructed to correct their course to the downwind final approach course. When the aircraft homes to the target, the wide lateral dispersion at the DWFAP is maintained and other significant problems emerge.

Since the final approach heading is chosen so that the approach is directly into the wind, a large error at the DWFAP will cause the aircraft to fly with a crosswind instead.

The homing path, under crosswind conditions, is a curve instead of a straight line (see Appendix B). Under some rather ordinary combinations of windspeed and crosswind angle, the curvature of such a path is large enough that significant segments of the flight path are not visible when using the  $40^{\circ}$  ( $\pm 20^{\circ}$ ) radar sweep. Since the approach procedure is based upon using the radar for obstacle clearance during the final approach and initial part of the missed approach, the possibility of the aircraft flying somewhat sideways, i.e., flying a homing path under crosswind conditions, should be minimized.

The homing tendency, together with the wide dispersion at the DWFAP, also creates problems in the missed approach maneuver. This problem will be discussed in the section of this paper entitled "Missed Approach Dispersion".

An effective way to eliminate the homing curve problems would be to provide the crew with accurate wind information with which to determine the DWFAP and a radio navigational aid with which to accurately find it. In addition, a device such as a cursor might be added to the radar equipment to enable the crew to more systematically correct their course to the final approach course. The cursor would have the added benefit

of enabling the crew to maintain a stable crab and hold a ground track heading where necessary.

Another measure which may be taken to minimize the possibility of a blind flight path due to a homing path is to simply maintain an airspeed in excess of three times the current windspeed when using the 40° radar sweep.

As shown in Appendix B, the windspeeds which can cause a blind flight are greater than one-third the airspeed of the helicopter. This would also serve to minimize the possibility that a ship could move behind the radar sweep of the aircraft and yet intersect the path of the aircraft. This possibility is also discussed in Appendix B where it is shown that the speeds required of the ship would be well within the operational capabilities of many types of vessels.

Finally, the analysis shows that the largest component of error is produced by the dead reckoning method of reaching the DWFAP. The crewmembers do fly relatively straight, tight courses to the target once established on a heading. Thus the lateral dispersion could be drastically reduced by improving the method of reaching the DWFAP.

## RANGE ACCURACY

A remote handheld push button device was provided the radar controller to identify range "calls", specified in Tables 15 and 16. The controller was instructed to depress the button when he determined the target was at a given range. Depressing the button caused an event mark to be written on the data tape at the same time as the tracker determined aircraft position. Range Total System Error (RTSE), defined as the difference between controller determined range and Cubic tracker range, was computed from the information during post flight analysis. RTSE includes both Range Flight Technical Error (RFTE) and Radar System Error (RSE).

Range calls for overhead, 0.25 nm, 0.50 nm, 1.25 nm, and 2.00 nm were made with the radar range scale selector set on 2.5 nm. The range calls made at 2.50 nm, 3.00 nm, 4.00 nm were made with the 5.00 nm range scale selection. Range calls for 5.00 nm to overhead, 5.00 nm from target on approach, and 6.00 nm to overhead target were made on the 10.00 nm range scale selection. Range calls 0.50 nm, 2.00 nm, 3.00 nm, 4.00 nm, and 6.00 nm occurred on marked range rings, whereas calls at 0.25 nm, 1.25 nm, 2.50 nm, and 5.00 nm occurred between range rings requiring visual interpolation.

The data was separated into two groups; approaches using only the primary radar return and approaches made with the radar beacon (or transponder). Standard statistics were computed for each group and are included in Tables 15 and 16. The data was also combined by range scale selection and the

RANGE ERROR STATISTICS  
 PRIMARY RADAR MODE  
 (STRAIGHT-IN AND 15° OFFSET COMBINED)

SCALE (NM)	RANGE CALLS (NM)	SAMPLE SIZE	MEAN (NM)	95% CONFIDENCE INTERVAL (NM)	S.D. (NM)	MIN (NM)	MAX (NM)	KURTOSIS	SKEWNESS
2.50	0.50	66	-0.078	-0.102 to -.053	0.101	-0.412	0.088	1.357	-1.299
	1.25	9	-0.011	-0.093 to 0.072	0.107	-0.216	0.136	0.781	-0.495
	2.00	56	-0.025	-0.054 to 0.004	0.109	-0.527	0.188	9.242	-2.122
5.00	2.50	68	0.012	-0.041 to 0.065	0.220	-0.644	1.336	20.992	3.335
	3.00	9	-0.001	-0.096 to 0.095	0.124	-0.096	0.095	5.296	-2.170
	4.00	60	-0.100	-0.167 to -0.032	0.261	-0.962	0.718	2.948	-0.475
	(Absolute error overhead)	69	0.187	0.156 to 0.217	0.126	0.019	0.715	3.511	1.503
10.00	5.00 (Approach)	35	-0.187	-0.307 to 0.067	0.349	-0.921	0.399	-0.135	-0.631
	5.00 (TO OH)	9	-0.002	-0.303 to 0.299	0.392	-0.488	0.738	0.289	0.806
	6.00 (TO OH)	7	-0.133	-0.471 to 0.206	0.366	-0.773	0.373	0.861	-0.653

Table 15

RANGE ERROR STATISTICS  
 BEACON RADAR MODE  
 (STRAIGHT-IN AND 15° OFFSET COMBINED)

SCALE (NM)	RANGE CALLS (NM)	SAMPLE SIZE	MEAN (NM)	95% CONFIDENCE INTERVAL (NM)	S.D. (NM)	MIN (NM)	MAX (NM)	KURTOSIS	SKEWNESS
2.50	0.50	13	-0.102	-0.233 to 0.076	0.086	-0.233	0.076	0.349	0.611
	1.25	2	-0.193	-0.353 to -0.033	0.226	-0.353	-0.033	0	0
	2.00	20	-0.150	-0.180 to -0.121	0.064	-	-	2.230	0.644
5.00	2.50	20	-0.131	-0.158 to -0.104	0.054	-0.281	-0.046	1.724	-1.234
	3.00	4	0.081	-0.782 to -0.944	0.543	-0.365	0.871	3.080	1.642
	4.00	20	-0.092	-0.185 to .000	0.198	-0.357	0.669	12.487	3.169
	(Absolute error overhead)	12	0.172	0.080 to 0.264	0.145	0.046	0.559	4.468	2.029
10.00	5.00 (Approach)	15	-0.183	-0.293 to -0.072	0.200	-0.633	0.048	0.278	-1.074
	5.00 (TO OH)	3	-0.042	-0.740 to 0.656	0.281	-0.278	0.269	0	1.123
	6.00 (TO OH)	13	-0.189	-0.274 to -0.104	0.141	-0.375	0.059	-0.875	0.303

Table 16

statistics are presented in Table 17. A negative mean indicates that on the average the aircraft was closer to the target than pilot and/or radar indicated. For example, inside 2.50 nm of the target, it can be seen from Table 16 (beacon radar mode) that the means, ranging from -0.193 to -0.102, are negative indicating that on the average the aircraft was 0.193 nm to 0.102 nm closer to the target than the pilot assumed. From Table 15 (primary radar mode), it can be seen the mean range errors ranging from -0.078 nm to -0.011 nm, were also negative. It was not possible to identify and quantify all the causal factors of the observed range bias.

As can be seen from Table 17, the standard deviation for primary radar mode was approximately 0.11 nm for the 2.50 range scale selection, 0.24 nm for the 5.00 nm selection, and 0.36 nm for the 10 nm range scale selection. Over the ranges considered, the standard deviation increased by about 0.12 nm as the range scale was doubled. Similarly, the standard deviation estimates for beacon radar mode ranged from 0.08 nm to 0.21 nm. These values represent RTSE and include RSE, RFTE, screen resolution, and update on scan rate error.

Data was acquired which provided an estimate of the RSE component. Discrete timed photographs of the radar screen were made, distinct from the controller actuated photographs, and time correlated to the tracker established aircraft position. This photographic information was digitized and merged with aircraft position data to establish Radar Bearing Error (RBE),

TSE RANGE STATISTICS BY RANGE SCALE SELECTION

SCALE	PRIMARY RADAR MODE			BEACON RADAR MODE		
	N	$\bar{x}$ (NM)	s (NM)	N	$\bar{x}$ (NM)	s (NM)
2.5 NM (0.5, 1.25, 2.0 NM)	131	-0.0504	0.1076	35	-0.1350	0.0845
5.0 NM (2.5, 3.0, 4.0 NM)	137	-0.0378	0.2395	44	-0.0940	0.2070
10.0 NM (5.0, 6.0 NM)	51	-0.1471	0.3584	31	-0.1717	0.1835

Table 17

Radar Position Error (RPE), and Azimuth FTE (AFTE). These error quantities were illustrated in Figure 16. The RSE statistics are presented in Table 18 and RBE, FTE, RPE statistics were previously presented in Tables 11, 12, and 13. These statistics reflect the errors from the total radar system and include such errors as radar timing and processing errors, screen resolution, and update or scan error.

The Bendix RDR 1400 radar has been advertised to have at most a one percent RSE with no mention of a negative range bias. Assuming the advertised one percent value represents a two S.D. error, the one percent values have been compared to the observed two S.D. RSE in Table 19. The comparison (Table 19) shows a much larger measured RSE than the advertised one percent RSE. However, the advertised error may not include screen resolution and/or scan rate error. Based on the Bendix RDR 1400 CRT display matrix, radar screen resolution is approximately 119 ft. (0.02 nm) on the 2.50 nm scale, 237 ft. (0.04 nm) on the 5.00 nm scale, and 475 ft. (0.08 nm) on the 10.00 nm scale. Assuming the screen display dot moves forward each time the target is midway between two consecutive dots, the average screen resolution error would be zero (no expected bias) with maximum errors of  $\pm 0.01$  nm,  $\pm 0.02$  nm, or  $\pm 0.04$  nm for range selections of 2.50 nm, 5.00 nm, and 10.00 nm respectively.

RADAR SYSTEM ERROR - RANGE

RANGES	PRIMARY					BEACON				
	CASES	MEAN NM	S. D.	MIN	MAX	CASES	MEAN NM	S. D.	MIN	MAX
4.000	23	-.062	.051	-.037	.158	7	-.185	.068	.115	.302
3.000	33	-.038	.060	-.042	.179	10	-.161	.054	.095	.280
2.917	29	-.033	.060	-.106	.183	10	-.174	.064	.088	.286
2.836	32	-.020	.042	-.069	.103	12	-.138	.053	.063	.251
2.753	33	-.030	.082	-.088	.353	13	-.138	.053	.063	.230
2.671	33	-.032	.063	-.113	.161	13	-.131	.045	.072	.250
2.589	35	-.024	.050	-.101	.107	11	-.158	.097	.074	.412
2.506	34	-.037	.051	-.075	.119	12	-.112	.053	.034	.232
2.425	32	-.031	.059	-.134	.179	12	-.128	.057	.035	.241
2.342	33	-.031	.059	-.046	.231	12	-.129	.050	.061	.215
2.259	34	-.025	.064	-.195	.171	12	-.146	.049	.075	.241
2.177	39	-.036	.061	-.185	.147	11	-.141	.043	.084	.213
2.094	40	-.022	.048	-.091	.147	11	-.164	.028	.122	.202
2.000	42	-.023	.039	-.066	.136	12	-.151	.043	.095	.253
1.918	41	-.025	.040	-.046	.118	12	-.152	.038	.095	.217
1.825	43	-.013	.044	-.080	.124	11	-.147	.054	.073	.231
1.743	43	-.018	.044	-.081	.127	11	-.160	.066	.087	.333
1.660	41	-.016	.040	-.065	.093	11	-.164	.048	.115	.269
1.590	41	-.006	.041	-.081	.097	12	-.141	.048	.075	.219
1.507	42	-.002	.035	-.068	.082	11	-.156	.024	.124	.195
1.424	42	-.004	.043	-.087	.175	11	-.143	.039	.073	.195
1.341	42	-.005	.035	-.106	.083	11	-.146	.045	.093	.244
1.260	42	-.001	.039	-.071	.127	12	-.149	.043	.082	.230
1.177	43	-.003	.036	-.095	.119	12	-.135	.054	.052	.274
1.094	44	-.005	.041	-.068	.128	12	-.127	.045	.038	.238
1.000	42	-.027	.085	-.064	.518	12	-.111	.039	.055	.173
0.918	40	-.014	.042	-.067	.122	12	-.151	.044	.099	.247
0.837	42	-.023	.067	-.082	.333	12	-.137	.039	.066	.218
0.754	44	-.059	.138	-.071	.767	11	-.129	.042	.060	.195
0.671	41	-.029	.056	-.039	.290	11	-.146	.031	.100	.191
0.588	41	-.036	.055	-.053	.203	11	-.144	.041	.084	.223
0.500	36	-.059	.098	-.077	.409	11	-.128	.088	-.072	.298

Table 18

COMPARISON OF ONE PERCENT AND MEASURED RSE

RANGE (NM)	ONE PERCENT ERROR (ASSUMED 2 S.D. VALUES) (NM)	PRIMARY RSE 2 S.D. VALUES (NM)	BEACON RSE 2 S.D. VALUES (NM)
0.50	0.005	0.196	0.176
1.25	0.013	0.078	0.086
2.00	0.020	0.078	0.086
2.50	0.025	0.102	0.106
3.00	0.030	0.120	0.108
4.00	0.040	0.102	0.136

Table 19

The antenna scan rate introduces an error in range due to the update delay. For the 120° scan, a target on the +60° or -60° radial is updated once every 5 seconds. Whereas a target on the centerline is updated once every 2.5 seconds. Assuming a zero wind and an aircraft speed of 60 knots, the centerline target range would have a maximum delay error of 253 ft. (0.04 nm) by the next update. For the same conditions with a ±20° scan angle, an error of 84 ft. (0.014 nm) would occur. This error condition would produce a negative bias since it results in a delay of new position information; i.e., the aircraft is closer to the target than indicated. The target display moving in discrete steps also tends to induce the radar controller to anticipate the target return precisely on a range ring before making a range call resulting in a high frequency of late calls.

Utilizing these estimates of delay, screen resolution and process errors, and assuming the RSS statistical combination method is applicable, a theoretical estimate of  $SD_{RSE}$  can be computed by the formula:

$$SD_{RSE} = \sqrt{SD_R^2 + SD_D^2 + SD_D^2}$$

where,

$SD_{RSE}$  = 2 S.D. Radar System Error

$SD_R$  = 2 S.D. Screen Resolution Error

$SD_D$  = 2 S.D. Scan Rate Delay Error

$SD_P$  = 2 S.D. Signal Processing Error

Values have been computed and are given in Table 20.

TWO S.D. RADAR ERROR COMPONENTS

RANGE	$SD_R$	$SD_D$ (A/C speed 60 kts $\pm 60^\circ$ sweep)	$SD_P$ (1%)	$SD_{RSE}$ (By RSS)
0.50	.04	.08	.005	.090
1.25	.04	.08	.013	.090
2.00	.04	.08	.020	.092
2.50	.08	.08	.025	.116
3.00	.08	.08	.030	.117
4.00	.08	.08	.040	.120
5.00	.16	.08	.050	.186
6.00	.16	.08	.060	.189

Table 20

Comparing Table 19 to Table 20, it can be seen that with the exception of 0.50 nm, the error theoretically predicted by combining  $SD_R$ ,  $SD_D$ ,  $SD_P$ , and the observed  $SD_{RSE}$  agree very well.

In regard to the beacon mode, information provided by Motorola indicated the ground beacon contained an inherent timing delay resulting in approximately a 500 ft. (0.082 nm) negative bias error in range. This delay would account for approximately one-half of the range bias observed in the beacon mode.

In the cases considered, clearly the RSE standard deviations are much smaller than the respective RTSE (Tables 15, 16), and the balance of Range Total System Error must be provided by RFTE. Assuming the RSS technique applicable to RTSE:

$$SD_{RTSE} = \sqrt{SD_{RFTE}^2 + SD_{RSE}^2}$$

or solving for  $SD_{RFTE}$ ,

$$SD_{RFTE} = \sqrt{SD_{RTSE}^2 - SD_{RSE}^2}$$

Based on this last equation, estimates of  $SD_{RFTE}$  for primary radar mode at selected ranges were computed and are presented in Table 21. It should be pointed out that the data set and sample sizes are not identical for the two sets of data, but for the primary radar mode with reasonable sample

PRIMARY RADAR MODE

RANGE (NM)	1 S.D. RSE	1 S.D. RTSE	1 S.D. RFTE
0.50	0.098 (36)	0.101 (66)	0.024
1.25	0.039 (42)	0.107 (9)	0.100
2.00	0.039 (42)	0.109 (56)	0.102
2.50	0.051 (34)	0.220 (68)	0.214
3.00	0.060 (33)	0.124 (9)	0.109
4.00	0.051 (23)	0.261 (60)	0.256

Note: Number in parenthesis is sample size.

Table 21

size, a comparison of RSE, RTSE, RFTE was made. Because of the limited sample sizes, no  $SD_{RFTE}$  values were computed for beacon radar mode, but a comparison of RSE and RTSE is given in Table 22. It is apparent that RFTE is the major error component of RTSE, at all ranges except 0.5 nm.

Range accuracy plays a significant role in the selection of a Missed Approach Point (MAP) and on the concept of using radar to provide clearance from surface targets. Assuming a 60 kt. approach speed, 500 fpm descent rate and a 1,000 ft. altitude at the 4 nm DWFAP, an aircraft would be at a 200 ft. MDA approximately 2.5 nm from the target. During tracking to the target over this 2.5 nm, it would be necessary for the aircraft to maintain lateral clearance of surface obstacles, 200 ft. AGL or higher, by previously planning an approach course sufficiently clear of obstacles or maneuvering around them by reference to the radar. The radar avoidance capability is a function of such factors as system accuracy, pilot/aircraft performance, and system limitations. The system accuracy necessary for obstacle avoidance is a function of both range error and bearing error. Bearing or azimuth error was discussed previously. The combination of range and bearing error is defined to be Radar Position Error (RPE) illustrated in Figure 16. RPE statistics at selected ranges are given in Tables 11, 12, and 13. Essentially, RPE identifies the radius of error associated with aircraft position established by radar but does not include AFTE or RFTE. Figure 17 illustrates this concept.

BEACON RADAR MODE

RANGE (NM)	RSE 1 S.D.	RTSE 1 S.D.
0.50	0.088 (11)	0.086 (13)
1.25	0.043 (12)	0.226 (2)
2.00	0.043 (12)	0.064 (20)
2.50	0.053 (12)	0.054 (20)
3.00	0.054 (10)	0.543 (4)
4.00	0.068 (7)	0.198 (20)

Table 22

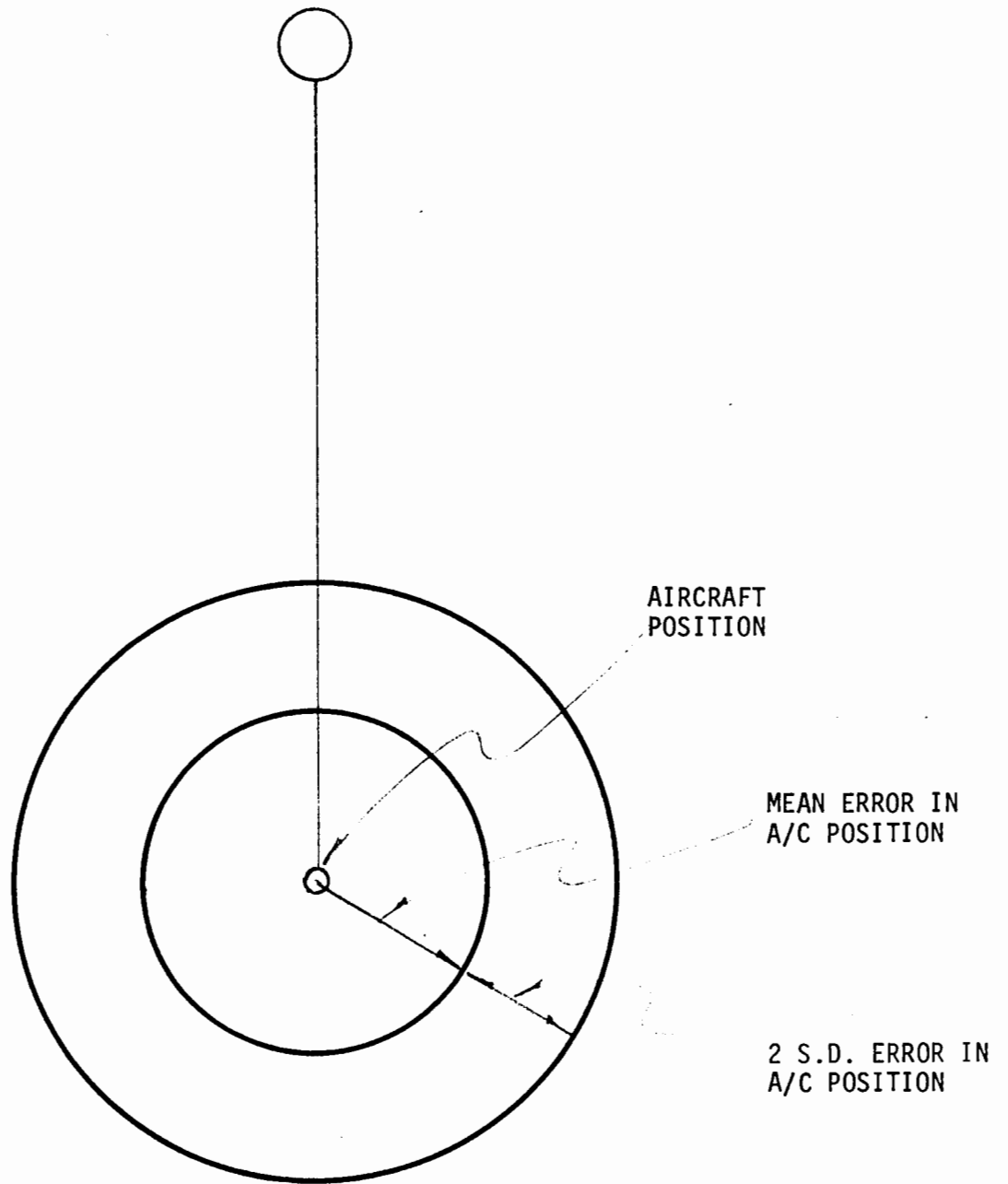


Figure 17

AIRCRAFT RADAR POSITION ERROR

With reference to Tables 11, 12, and 13, the two S.D. circular error varied from 0.197 nm to 0.432 nm over the ranges 2.50 nm to 0.50 nm from the target. Expressing the second case in terms of probability, aircraft position established by radar was within a circle of radius 0.432 nm with center at the actual position 95 percent of the time.

Tables 15 and 16 summarize range error at the 0.5 nm Missed Approach Point (MAP) for primary and beacon radar modes. At 0.5 nm, the mean error is -0.078 nm with a 0.101 nm S.D. for primary and the mean error is -0.102 nm with a 0.086 nm S.D. for the beacon radar mode. The two S.D. point (approximately 95 percent probability) of the MAP identification was 0.28 nm and 0.27 nm beyond the actual 0.5 nm MAP for primary and beacon radar mode respectively. Stated in another way, 95 percent of the aircraft had identified the 0.5 nm MAP within 0.22 nm and 0.23 nm of the target for primary and beacon radar mode respectively. As can be noted from Tables 21 and 22, Radar System Error (RSE) is the dominant error at the 0.5 nm MAP; i.e., the radar itself is responsible for most of the range error observed at the 0.5 nm MAP. These values clearly indicate that with the existing system, the MAP should not be 0.25 nm or less. However, to establish MAP minimums, the pilot/aircraft performance during the turning missed approach maneuver must also be considered. This is discussed in a later paragraph.

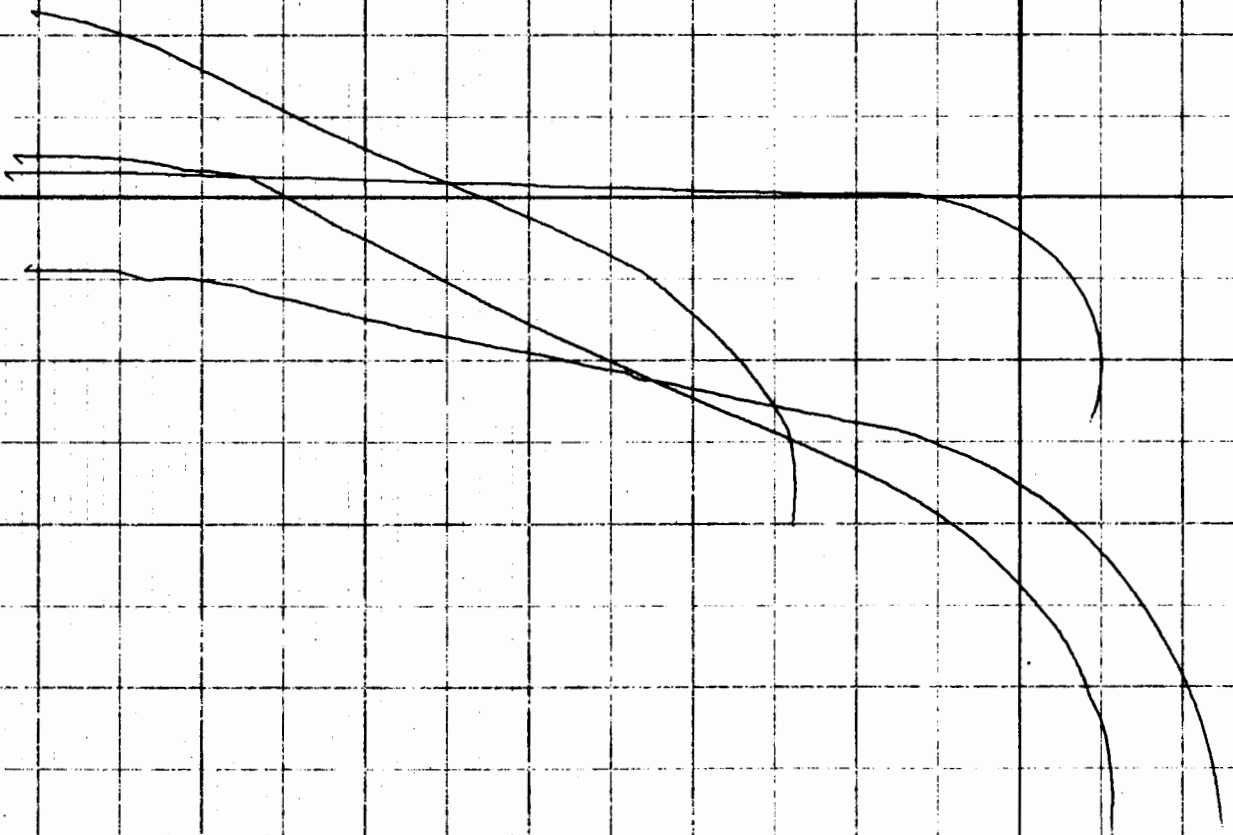
### MISSED APPROACH DISPERSION

Prior to the statistical analysis of the missed approach segment of the maneuver, the graph and log of each flight was carefully examined to eliminate data which was not representative of the intended flight operation due to either a crew blunder or an equipment malfunction. The portion of the graph which lay between the point where the aircraft was one mile from the target and the point where the aircraft had completed a 90<sup>0</sup> heading change was used in the analysis.

The graph of each flight in which the crew turned to the left was mathematically transformed so that the turn could be treated as a right turn. The graphs were then grouped into four categories - offset approaches with a one-half mile missed approach point, offset approaches with a one quarter mile missed approach point, straight-in approaches with a one-half mile missed approach point, and straight-in approaches with a one-quarter mile missed approach point.

Figure 18 is a composite graph of the offset approaches with a one-quarter mile missed approach point. Four graphs were used in the analysis. Three of the graphs ended outside the intended clear zone which is bounded by the negative x-axis and negative y-axis. One of the graphs came within 200 feet of the target rig. Low altitude flights outside the clear zone are not guaranteed lateral separation from surface obstacles.

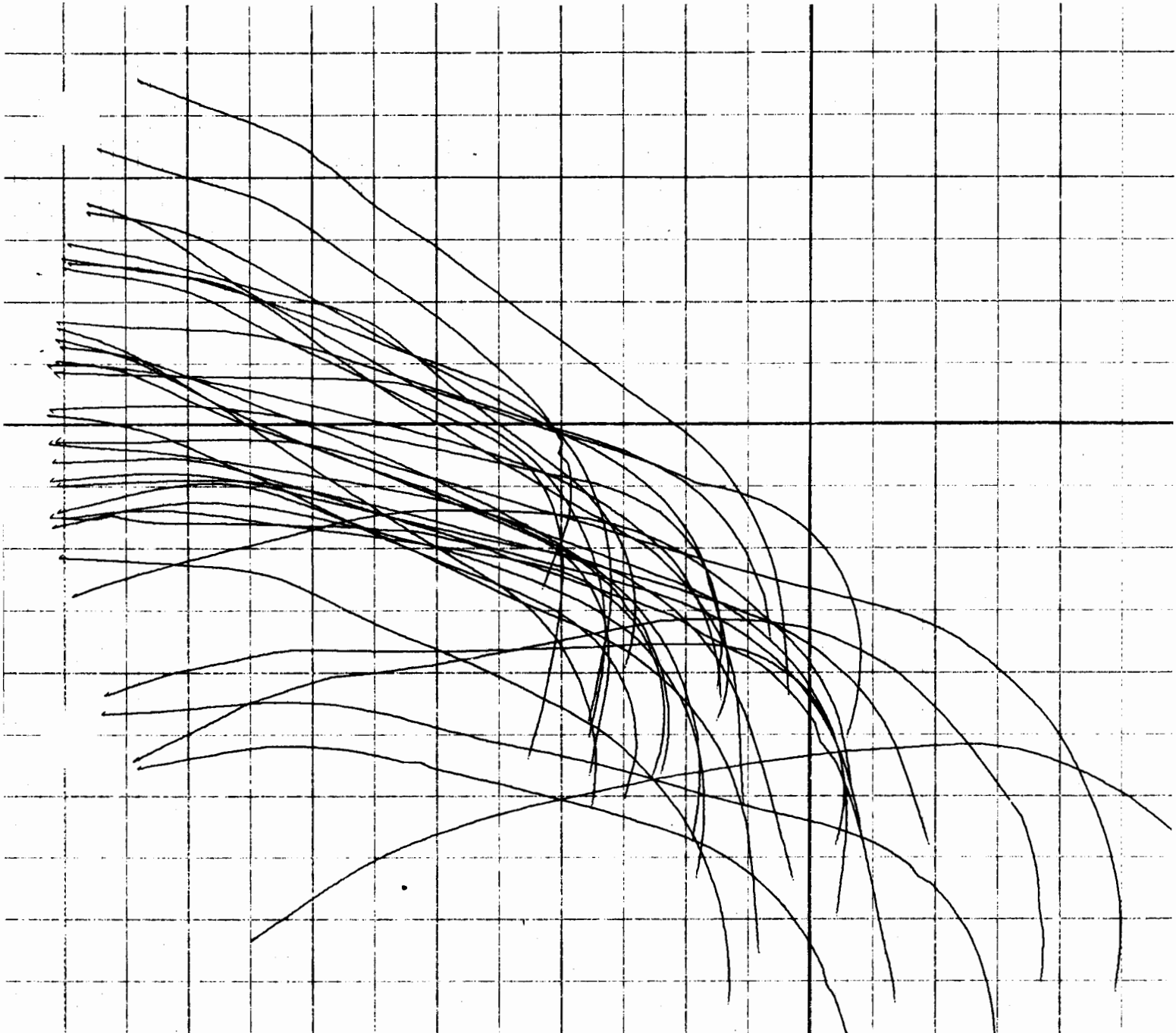
Figure 19 is a composite graph of the offset approaches with a one-half mile missed approach point. Twelve of these graphs ended outside the clear zone.



ALL RIGHT TURNS  
ALL OFFSET APPROACHES QUARTER MILE

0. 1. 2. 3. 4.  
THOUSAND FEET

Figure 18  
76



ALL RIGHT TURNS  
ALL OFFSET APPROACHES HALF MILE

0. 1. 2. 3. 4.  
THOUSAND FEET  
08/09/79.

Figure 19

Two of the flights passed within 750 feet of the target rig. The composite graph clearly shows the wide dispersion of the flights at one nautical mile from the target. This wide dispersion is the result of the wide dispersion at the DWFAP combined with the homing track flown by the crew.

Note that some of the flights such as the one labeled A in the figure would not have flown outside the clear zone if the aircraft had been on the intended final approach path.

The arc in Figure 19 is of radius one-half nautical mile with center at the target rig. Several of the flights initiated the missed approach turn well within the one-half mile missed approach distance. One flight continued about 3,900 feet after crossing the one-half mile MAP before initiating the missed approach turn.

The crewmembers occasionally continued the offset portion of the flight after radar contact with the target had been lost. The flights labeled B and C began the missed approach turn with the target rig well behind the aircraft.

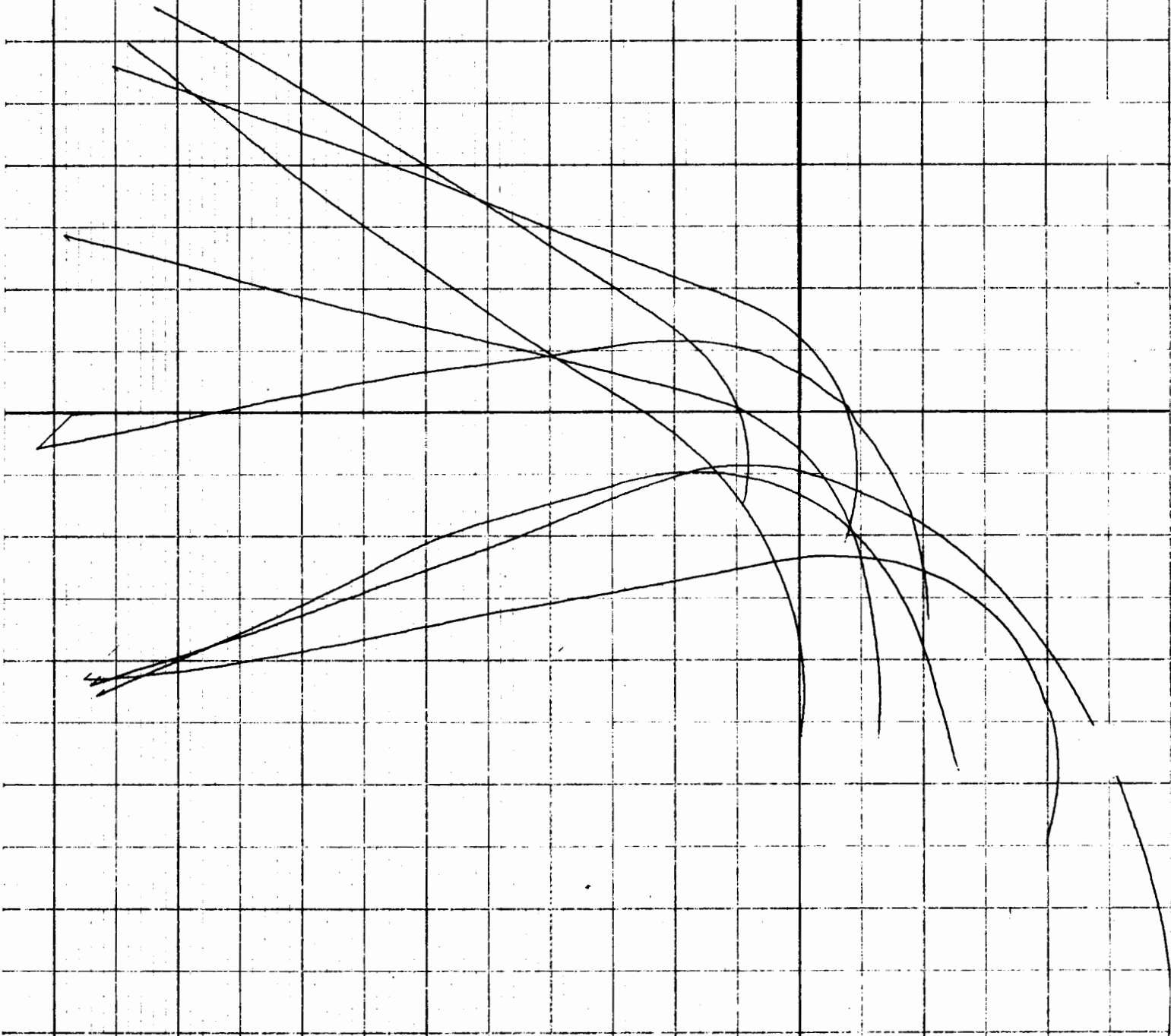
The turns also exhibit a wide variety of turn radii. Some aircraft turned with a radius of about 3,000 feet while others turned with a radius of about 1,400 feet.

Figure 20 is a composite graph of the straight-in approaches with a one quarter mile missed approach point. Eight graphs were used to construct this composite graph. Seven of the graphs terminated outside the intended clear zone, the area in the lower left quadrant bounded by the negative x-axis and negative y-axis. Two of the flights penetrated the cluster region, the upper right area bounded by the positive x-axis and the positive y-axis. The graph indicates that the quarter mile missed approach turn is likely to be made within the cluster region.

Figure 21 is a composite graph of the straight-in approaches with a one-half mile missed approach point. Eight of the graphs ended outside the clear zone. One of the graphs passed within 500 feet of the target rig. These graphs are also widely dispersed at one nautical mile from the target. This wide dispersion is the result of the wide dispersion at the DWFAP combined with the homing track flown by the crew.

Several of the flights, such as the one labeled A, would not have flown outside the clear zone if the aircraft had been on the intended DWFAP.

The arc in Figure 21 has a radius of one-half mile with center at the target rig. All of the graphs initiate the missed approach turn inside the one-half mile MAP.



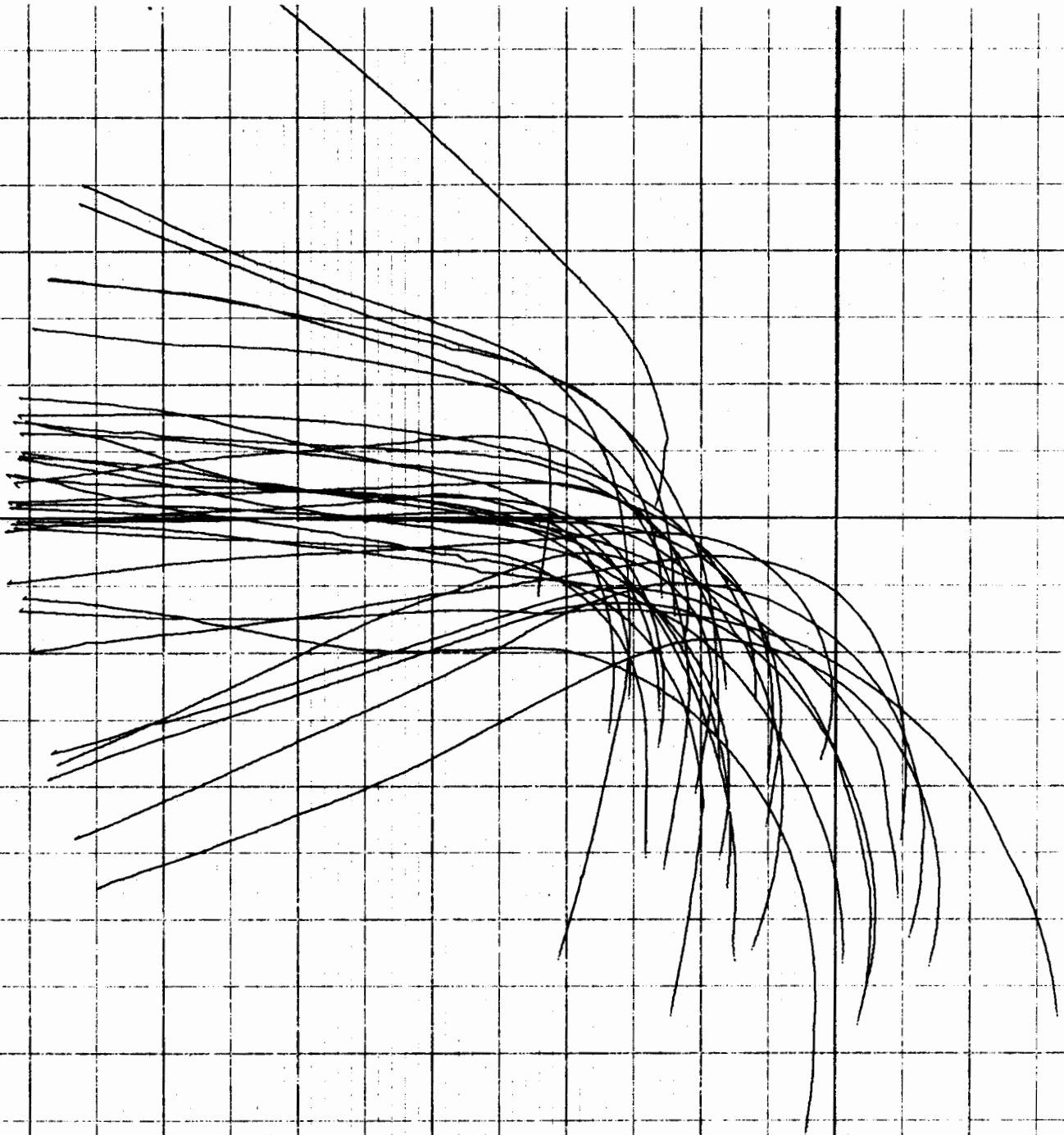
ALL RIGHT TURNS  
ALL STRAIGHT IN APPROACHES      QUARTER MILE

0.      1.      2.      3.      4.

THOUSAND FEET

08/09/79.

Figure 20



ALL RIGHT TURNS  
ALL STRAIGHT IN APPROACHES HALF MILE

0. 1. 2. 3. 4.

THOUSAND FEET

08/09/79.

Figure 21

The graphs also exhibit a wide variety of turn radii. Some of the graphs would not have ended outside the clear zone if the turn had been expedited. The offset approaches with a one-half mile MAP and the straight-in approaches with a one-half mile MAP were statistically analyzed. The approaches having one-quarter mile missed approach point were not statistically analyzed due to the small sample sizes.

The statistical analysis was accomplished by first determining circles which best fit the apparent center of the composite graphs of each type of missed approach maneuver. Then standard statistics were computed on the points where the graphs cross rays emanating from the centers of the circles of best fit (see Appendix A for a detailed explanation). The means and standard deviations thus found were used to determine mean paths and two standard deviation envelopes for each type of missed approach maneuver.

The statistics for the offset approaches are found in Table 23 while the graphical representation of the mean path with its envelope is found in Figure 22. The means found in Table 23 represent the average distance from the center of the best fitting circle at which the graphs cross the rays emanating from the center. The center for the offset approaches is located at  $x = 5,000$  feet,  $y = 6,800$  feet. The ray labeled  $0^\circ$  passes through the center perpendicular to the x-axis while the ray labeled  $90^\circ$  passes through the center perpendicular to the y-axis.

PARTITION STATISTICS ABOUT MISSED APPROACH "AVERAGE" PATH AT 10<sup>0</sup>  
 INCREMENTS  
 FIFTEEN DEGREE OFFSET APPROACHES  
 ONE-HALF NM MISSED APPROACH

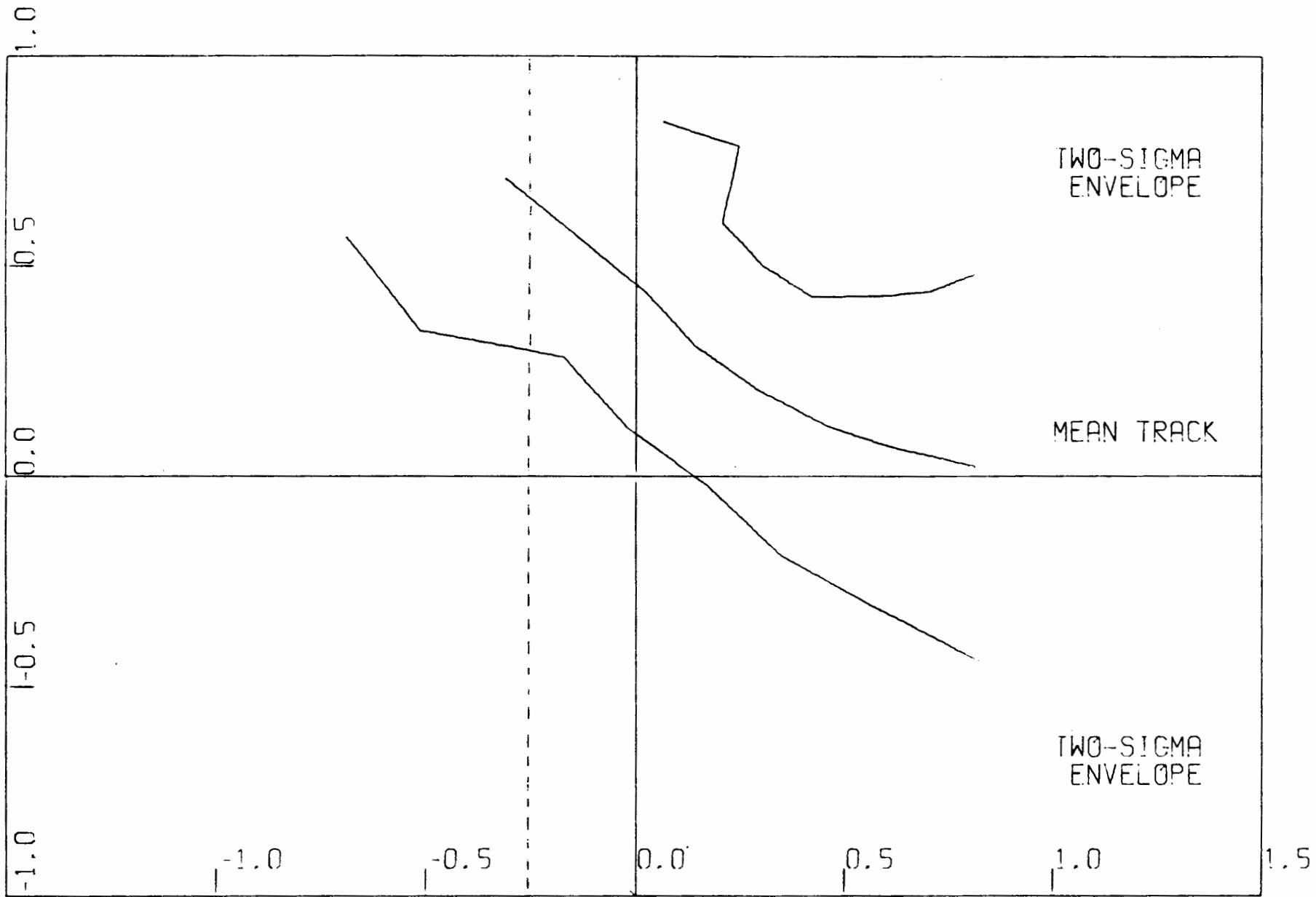
Center Coordinates - x = -5,000 feet, y = -6,800 feet

SECTOR PARTITION	SAMPLE SIZE	MEAN (SLANT RANGE TO CENTER) (FT)	95% CONFIDENCE INTERVAL (FT)	S.D. (FT)	MIN (FT)	MAX (FT)	KURTOSIS	SKEWNESS
0 <sup>0</sup>	42	6670.8	6233.5 to 7108.1	1403.4	2243.2	9404.1	1.061	-0.839
10 <sup>0</sup>	42	6510.7	6150.7 to 6870.8	1155.5	2667.6	8682.2	1.555	-0.915
20 <sup>0</sup>	42	6463.8	6153.1 to 6774.6	997.2	3173.1	8649.5	1.775	-0.836
30 <sup>0</sup>	38	6423.6	6166.8 to 6680.4	781.2	4006.1	7840.9	1.564	-1.064
40 <sup>0</sup>	29	6437.7	6142.1 to 6723.3	764.1	4861.7	7751.5	-0.522	-0.560
50 <sup>0</sup>	18	6395.3	6020.1 to 6770.4	754.4	5332.4	7946.5	-0.767	0.216
60 <sup>0</sup>	12	6721.9	5871.8 to 7572.0	1116.6	5025.4	9295.1	-0.853	0.513
70 <sup>0</sup>	5	7340.0	5820.1 to 8859.9	1224.1	5629.8	8881.1	-0.988	-0.180
80 <sup>0</sup>	1	9152.4	9152.4 to 9152.4	0	9152.4	9152.4	0	0
90 <sup>0</sup>	0	---	---	---	---	---	---	---

83

Table 23

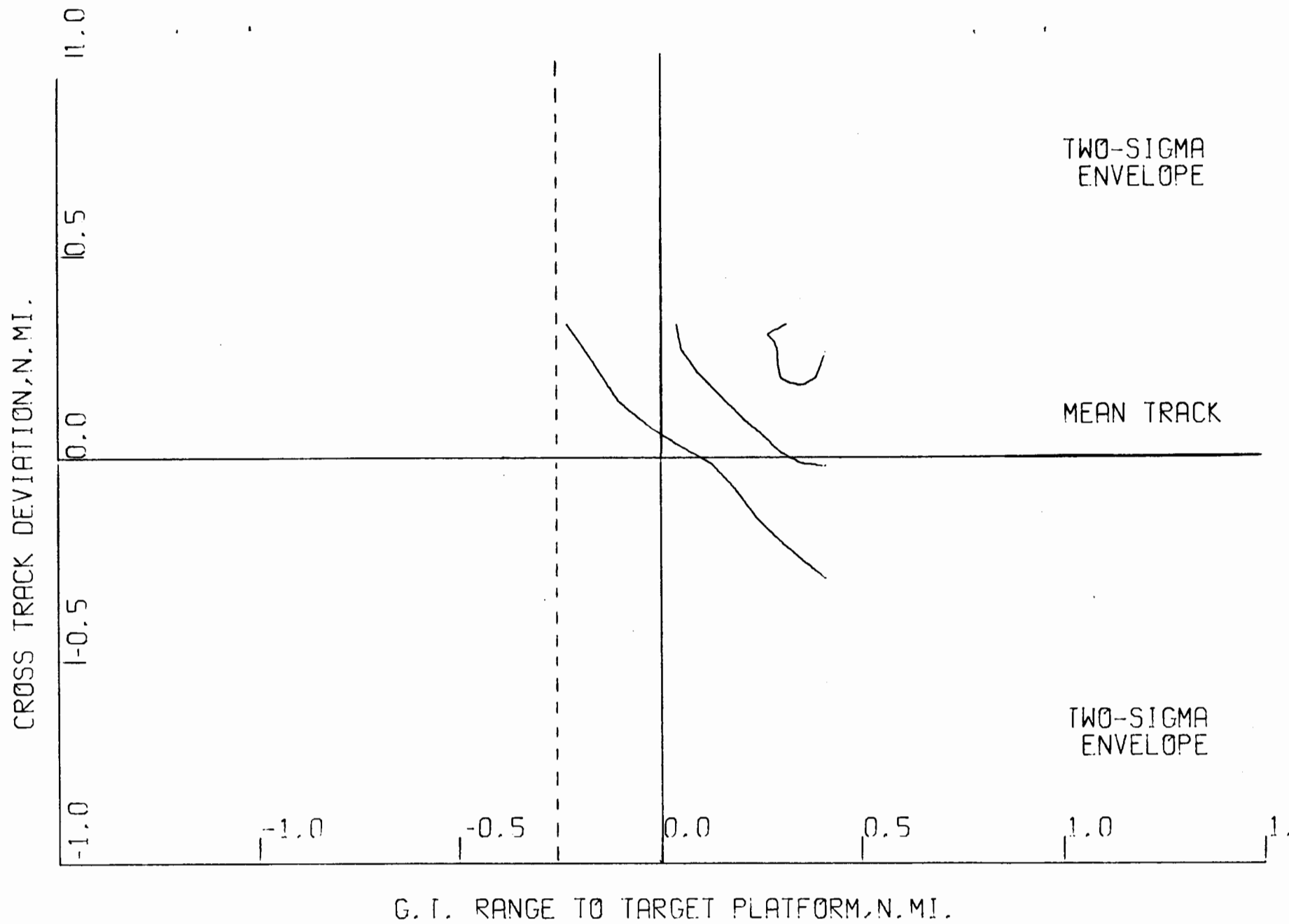
94  
CROSS TRACK DEVIATION, N. MI.



G. T. RANGE TO TARGET PLATFORM, N. MI.

MISSED APPROACH - OFFSET - 1/2 MILE MINIMUM

Figure 22



MISSED APPROACH - STRAIGHT-IN - 1/2 MILE MINIMUM

Figure 23

The graph of the mean path of the offset approaches with the two standard deviation envelope (Figure 22) is oriented differently due to the  $15^{\circ}$  offset path taken at 1 nm. The MAP is located to the right of the target rig. The envelope is 4,456 feet wide at the MAP and narrows to 3,017 feet at the  $50^{\circ}$  radial. The envelope then widens considerably, but sample sizes of the remaining radials are much smaller. The reduction in sample size is due to the fact that most of the aircraft have completed a  $90^{\circ}$  heading change.

The mean path of the offset approaches is 2,066 feet from the target at its closest point while the two standard deviation envelope is 506 feet away at nearest point from the target. The mean path and its envelope extend outside the clear zone, but the samples sizes for the portion of the path outside the clear zone are small. The sample sizes are adequate at the  $40^{\circ}$  radial to support the proximity of the mean path and 95 percent envelope to the target.

If the missed approach distance had been three-quarters mile instead of one-half mile and if the flight crews flew with the same proficiency, then the y-axis could be moved one-quarter mile to the left to the position of the dashed line of Figure 22. The target rig would then be located at the intersection of the x-axis and the dashed line. The mean path would then be no closer than 0.5 nm of the target rig while the envelope would be no closer than 1,500 feet. The mean path still extends beyond the clear zone, but it does so at a radial with a sample size of only one.

The statistics for a straight-in approach are found in Table 24 while the graphical representation of the mean path with its envelope is found in Figure 23. The means found in Table 24 represent the average distance from the center of the best fitting circle at which the graphs cross rays emanating from the center. The center of the best fitting circle of the straight-in approaches is located at  $x = -2,500$  feet,  $y = -2,000$  feet. The ray labeled  $0^{\circ}$  passes through the center perpendicular to the x-axis while the ray labeled  $90^{\circ}$  passes through the center perpendicular to the y-axis.

The graph of the mean path of the straight-in approaches with the two standard deviation envelope (Figure 23) is oriented the same as the mean path graph of the offset approaches (Figure 22). The missed approach point is located to the right of the target rig with the direction of flight being to the left and then upward as the aircraft completes the right turn. The envelope is 3,380 feet wide at the  $0^{\circ}$  radial and narrows to 1,660 feet at the  $40^{\circ}$  radial. The envelope then widens to 3,344 feet at the  $90^{\circ}$  radial. The sample sizes decline after the  $40^{\circ}$  radial, decreasing from 31 to 19 sample points.

The mean path of the straight-in approaches is 1,316 feet from the target at its closest point while the two standard deviation envelope is 409 feet away at its nearest point from the target. The mean path stays within the clear zone through the maneuver, but the two standard deviation envelope does leave the clear zone.

PARTITION DISPERSION STATISTICS ABOUT MISSED APPROACH "AVERAGE" PATH AT 10<sup>0</sup> INCREMENTS  
 STRAIGHT-IN APPROACHES, ONE-HALF NM MISSED APPROACH

Center Coordinates - x = -2,500 feet, y = -2,000 feet

SECTOR PARTITION	SAMPLE SIZE	MEAN (SLANT RANGE TO CENTER) (FT)	95% CONFIDENCE INTERVAL (FT)	S.D. (FT)	MIN (FT)	MAX (FT)	KURTOSIS	SKEWNESS
0 <sup>0</sup>	33	2123.5	1823.9 to 2423.1	845.0	505.8	4419.0	0.529	0.725
10 <sup>0</sup>	31	2108.4	1872.2 to 2344.5	643.8	1054.5	3780.9	0.383	0.821
20 <sup>0</sup>	31	2030.0	1836.9 to 2223.0	526.3	1098.1	3297.5	0.078	0.667
30 <sup>0</sup>	31	1915.0	1751.0 to 2079.0	447.2	782.7	3176.9	1.288	0.191
40 <sup>0</sup>	31	1891.4	1738.9 to 2043.8	415.6	1120.9	3181.4	1.352	0.637
50 <sup>0</sup>	29	1900.0	1717.0 to 2082.8	480.9	1140.1	3261.5	0.521	0.589
60 <sup>0</sup>	27	1961.7	1738.4 to 2185.1	564.6	981.1	3417.3	0.168	0.374
70 <sup>0</sup>	23	2091.7	1816.7 to 2336.8	636.1	1108.0	3582.6	-0.176	0.241
80 <sup>0</sup>	21	2225.7	1922.2 to 2529.2	666.7	789.3	3811.2	-0.882	0.154
90 <sup>0</sup>	19	2262.4	1859.2 to 2665.6	836.6	789.3	3811.2	-0.882	0.154

88

If the missed approach distance had been three-quarters mile instead of one-half mile and if the flight crews flew with the same proficiency, the y-axis could be moved one-quarter mile to the left to the position of the dashed line in Figure 23. The target rig would then be located at the intersection of the x-axis and the dashed line. The mean path would then be within 2,090 feet of the target rig while the two standard deviation envelope would be within 1,275 feet of the target rig. Both the mean path and the two standard deviation envelope would remain within the clear zone.

In summary, the dispersion of the offset approaches is wider than the dispersion of the straight-in approaches. The mean path of the straight-in approaches stays within the clear zone while the mean path of the offset approaches does not. The envelopes of both types of approaches depart from the clear zone. The mean path and envelope of the straight-in approaches come nearer to the target rig than the corresponding curves of the offset approaches. If the missed approach distance were increased to three-quarters mile, then the mean path and envelope of the straight-in approaches would remain within the clear zones.

## OPERATIONAL DIFFICULTIES

During the course of the test, some difficulties arose which could not be quantified and included in the statistical analysis. These difficulties are important and steps should be taken to minimize their occurrence.

It was found that the identification of the desired target from a group of targets is very difficult when using the primary mode and not completely certain when using the beacon mode. In the statistical analysis, it appears that the tracking is possibly better using the primary mode, but the beacon mode is desirable for identification purposes.

This problem is easily understood when using the primary mode since the helicopter is often approaching the cluster of rigs from a direction other than the one based on the preplanned DWFAP. In addition, the radar presents a view of the cluster from an oblique angle rather than from straight above as on the approach plate. The radar also presents the targets on the screen as rather long, indistinct images which are indistinguishable from one another and from ships operating in the area.

The crewmembers incorrectly identified the target 19 times during the test. The overhead approach was made to a correct target, but the final approach was to an incorrect target, 8 times. The overhead approach was made to an incorrect target, but the final approach was made to the correct target, 6 times. The overhead approach was made to the correct target, but the final approach was made to a ship, 5 times. This means that the crew incorrectly

identified the target almost 16 percent of the time and even homed on ships 4 percent of the time. These incorrect identifications all occurred when the primary mode was in use; however, on one occasion the crew was forced to switch from beacon mode to primary mode, due to equipment malfunction, during the approach and then incorrectly identified the target.

The incorrect identification of the target could lead to an undesirable situation when approaching a cluster of rigs, especially if a missed approach turn is necessary.

The missed approach turn is a blind maneuver and an incorrect identification may position the aircraft at the missed approach point such that a turn might be made into an area which is not necessarily clear of obstacles. Figure 24 is a graph of a flight in which an incorrect identification resulted in a turn toward an obstacle. The approach was planned to rig 5 but was actually conducted to rig 6.

Even during the final approach, an incorrect identification coupled with a crosswind could cause a blind flight into an area with obstacles (see Appendix B).

The beacon mode eliminated the identification problem but created some additional problems. Both the radar and the surface based beacon malfunctioned occasionally. The surface based beacon was intended for use

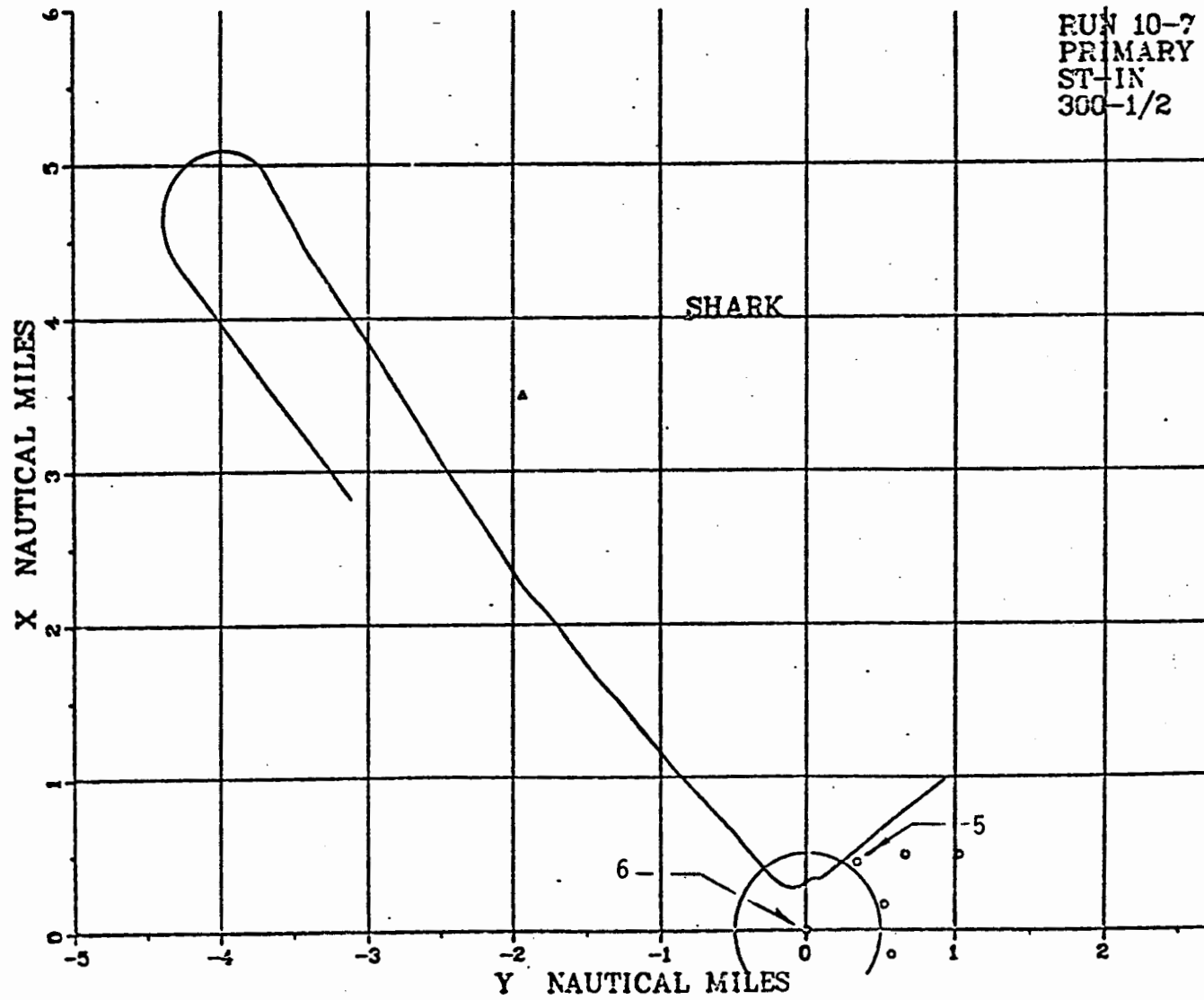


Figure 24

at long distance and occasionally at close range, it caused the return image on the radar screen to break up creating tracking difficulties. During six of the flights, the crew reported that the beacon image was breaking up. Before two other flights, the beacon equipment failed completely which caused the flight to be conducted in primary mode. During one flight, the crew was forced to switch from beacon mode to primary mode while on the final approach. Thus, problems with the beacon occurred during at least nine flights from a total number of only thirty flights or 30 percent of the time while conducting approaches in the beacon mode. In addition, the use of the beacon does not permit a radar return of surface obstacles that must be avoided during the final approach. Hence, the radar "see-and-avoid" concept would not be applicable.

The crewmembers turned the wrong direction seven times during the outbound procedure turn. This resulted in a large deviation from the DWFAP. The large deviation from the DWFAP and the tendency to home caused the aircraft to track toward the target along a path different from the final approach path and resulted in a missed approach track different from the one planned.

Occasionally the target disappeared from the screen or, in the case of the beacon mode, broke up near the missed approach point. This may have been caused by an insufficient adjustment of the tilt angle for the horizontal distances involved. The crew sometimes delayed the missed approach turn when this happened allowing the helicopter to approach the rig closer than

the planned minimum range. This delay usually resulted from the crew attempt to reestablish contact with the target. This problem occurred at least twice.

## CONCLUSIONS

### APPROACH TRACKING ACCURACY

1. The final approach flight track dispersions can be described by normal distributions. The 95 percent approach envelope is funnel shaped, about 4 nm wide at the DWFAP narrowing to approximately 1 nm at 1 nm from the target.
2. A significant portion of the final approach azimuth error was introduced at the DWFAP by the dead reckoning procedure and retained throughout the approach by the tendency to home to the target.
3. Once established on target, tracking was accomplished with a reasonably small lateral dispersion and little effort was made to regain the intended final approach course.
4. The mean final approach path contained approximately a  $5^{\circ}$  positive bias error, introduced most likely by the inaccuracies of the outbound procedure and the direction of turn onto the outbound leg.
5. The largest component of azimuth error was Flight Technical Error.
6. Homing tracking flown under some crosswind conditions can produce a curved ground track with segments not visible by the radar set on the  $\pm 20^{\circ}$  sweep.

7. The current radar system does not provide a reasonable procedure to establish and maintain a crosswind crab.

#### RANGE

1. A negative bias (closer to the target than assumed) was present in both primary and beacon mode range determinations.

2. The beacon mode negative bias tended to be larger than the primary mode for ranges inside 5 nm.

3. The standard deviation for primary radar mode was 0.11 nm for 2.50 nm scale, 0.24 nm for 5.00 nm scale, and 0.36 nm for 10.00 nm scale. The standard deviation increased by approximately 0.12 nm as the range scale was doubled.

4. The observed Radar System Error (RSE) was approximately the same as that predicted by combining the advertised 1 percent error (assumed to be processing error), delay or scan rate error, and screen resolution error at all ranges except 0.50 nm.

5. Approximately 50 percent of the negative bias error observed in the beacon mode was due to a timing delay present in the design of the ground beacon used in the test.

6. With the exception of the 0.50 nm range, Range Flight Technical Error (RFTE) is the dominant source of range error.
7. The radius of the 95 percent Circular Error Probability (CEP) varied from 0.197 nm to 0.432 nm over the ranges 0.50 nm to 2.50 nm.
8. The Radar System Error was the dominant source of error at the 0.50 nm Missed Approach Point (MAP).
9. The 95 percent point for the 0.50 MAP was 0.22 nm and 0.23 nm from the target rig for primary and beacon mode respectively.

#### MISSED APPROACH

1. Based on the dispersion of missed approach tracks, the one-fourth mile Missed Approach Point (MAP) is unacceptable.
2. The missed approach mean track of the straight-in approaches is closer to the target rig than the mean track of the offset approaches.
3. The missed approach dispersion of the offset approaches is greater than the dispersion of the straight-in approaches.
4. A greater proportion of the missed approaches initiated by aircraft from offset approaches completed their turn outside the intended clear zone than those initiated from a straight-in approach. (Aircraft must complete their

missed approach turn inside the clear zone to be guaranteed lateral obstacle clearance.)

5. The point on the 95 percent envelope nearest the approach target for the offset approach is only 97 feet greater than that for the straight-in approach. That is, the minimum distance from the offset 95 percent envelope (506 ft.) is not substantially greater than that of the straight-in approach (409 ft.).

6. The missed approach dispersion is primarily due to MAP range accuracy, performance in execution of the turn, and the large crosstrack dispersion at the MAP. The most significant factor appears to be the large crosstrack dispersion at the MAP.

7. If the MAP was three-fourths mile from the target, the mean path and 95 percent envelope of the straight-in approaches would remain within the clear zone.

#### GENERAL CONCLUSIONS

1. Crew coordination is critical; well developed training procedure should be developed to prepare the crew for this task.

2. Difference in instruments such as the directional gyro can produce confusion. For example, if the controller and pilot DGs differ significantly, commands such as "steer 175<sup>0</sup>" are inappropriate.

3. In using the radar in primary mode to avoid obstacles:
- a. Forty degrees is unacceptable for peripheral information.
  - b. One hundred twenty degrees is acceptable for peripheral information, but update and target resolution is a problem.
  - c. Assuming a homing technique, certain crosswind/airspeed combinations can produce conditions in which the ground track traverses a region not presented on radar. This condition can only occur if  $\text{windspeed/airspeed} > \sin \left[ \frac{\text{sweep angle}}{2} \right]$ ; the blind condition is most likely to occur when homing at low airspeed on  $40^\circ$  sweep.
  - d. Manual tilt and gain controls caused some difficulties; inadvertent or improper adjustments can result in lost target or significant changes in target illumination.
  - e. The present radar system displays do not give a sufficient indication of the magnitude of lateral separation between the aircraft and a surface obstacle.
  - f. Considerable variability exists on establishing target position, such as referencing centerline of near edge, centerline or leading edge.

g. Large delays are inherent in interpretation, announcement, and pilot action.

h. The workload (tilt, gain, interpretation, announcement, etc.) is very high when the aircraft is close in to a cluster of targets. A busy "dynamic" obstacle environment enhances the problem. Single platform approaches with low density dynamic obstacle environment produce a relatively low workload.

## RECOMMENDATIONS

### APPROACH TRACKING ACCURACY

1. Where sufficiently accurate RNAV systems are available, the DWFAP should be identified as a positive fix. To achieve improvement over the present DR/RADAR method, the 95 percent error must be substantially less than  $\pm 2$  nm at the 4 nm DWFAP.
2. If the DWFAP can't be established by a positive fix, the DR/RADAR procedure should be investigated for improvements.
3. The present radar system should be modified to provide a more positive means to intercept and maintain a chosen ground track.
4. The present radar system should be modified to provide a more positive means of maintaining a ground track under crosswind conditions.

### RANGE

1. The current radar systems should be investigated to determine methods for eliminating negative range bias.
2. Ground beacons with known design timing delays should not be used in Airborne Radar Approaches.
3. Investigations should be carried out with existing radar range displays to determine methods for reducing Range FTE.

4. Due to range error, the Missed Approach Point should not be less than 0.50 nm.
5. Due to the combinations of azimuth and range error, the radar should not be used to provide lateral clearance of surface obstacles within 0.5 nm or less.

#### MISSED APPROACH

1. To increase the probability of remaining in the missed approach clear zone, the straight-in approach should be used during approaches to clusters.
2. To reduce the missed approach dispersion, the accuracy of acquiring the DWAP should be improved and homing tracking should not be used.
3. To increase probability of lateral clearance of cluster and/or target, the crew should be trained to expedite the missed approach turn.
4. The crew should be trained to immediately initiate a missed approach when the radar target is lost.
5. The range system accuracy (crew and radar) for establishing the MAP range should be improved.
6. The crew should be trained to initiate the minimum radius missed approach turn deemed acceptable for IFR maneuvering in the aircraft used.

## GENERAL RECOMMENDATIONS

1. This type approach requires high crew coordination; all flight crews making this type approach should be provided extensive training before approaches under actual instrument conditions are made.
2. Instruments frequently referenced by controller and pilot should be closely calibrated to each other and any differences clearly noted by the crew, e.g., directional gyro.
3. If the radar is used for obstacle avoidance, it should be set in primary mode or a combination primary/beacon mode, with  $120^{\circ}$  sweep, and the aircraft should not "home" to the target, and the approach should not be flown under conditions where  
windspeed/airspeed  $> \sin \left[ \frac{\text{sweep angle}}{2} \right]$ .
4. The radar display should be modified to improve ground tracking reference, holding a crab, indication of lateral clearance, target identification.
5. If technically and economically feasible, it would be desirable to have a system that would "lock" on the target, thus substantially reducing controller workload.

## Appendix A

### COLLECTION OF DATA - FINAL APPROACH

During each helicopter flight, the position of the helicopter relative to the target was computed at one second intervals. The position of the aircraft was recorded in cartesian coordinates with the origin set at the target, the positive x-axis in the direction of true north, the positive y-axis in the direction of true east, and the positive z-axis upward. In addition to the position, the horizontal distance from the aircraft to the target as well as several other variables such as aircraft heading and airspeed were recorded each second. Since the approach was to be made into the wind, the wind direction (the intended approach heading) for each flight was recorded.

### EXTRACTION OF DATA - FINAL APPROACH

In order to analyze the lateral and vertical dispersion of the flights on the downwind final approach, the position, range from target, ground-speed, ground heading, airspeed, and aircraft heading of each aircraft when at 5 nm from the target on final approach was recorded to form one sample. In a similar manner, the position and the other data described above, for each aircraft, was recorded when the aircraft reached 4 nm, 3 nm, and then in decreasing 500 foot intervals to the missed approach point for the particular flight, to form 35 other samples. Each sample contains the data from all the flights at a particular distance from the target rig. The samples vary in number of cases since not all flights reached a distance of 5 nm from the target and occasionally, due to

technical difficulties at the time of a flight, data at a particular range was missing.

#### LATERAL DISPERSION STATISTICS - INTENDED COURSE

The lateral dispersion statistics were computed on each sample by finding the angle formed by the intended approach course line and the line joining the aircraft position and the target rig. This was done by first finding the perpendicular distance  $D$  from the aircraft position to the intended course line. The distance was recorded as positive if the aircraft was located on the right side of the intended course looking toward the target, and negative if the aircraft was located on the left side of the intended course. The angle  $A$  was then computed by the formula  $A = \text{Arcsin}(D/R)$  where  $R$  is the distance to the target.

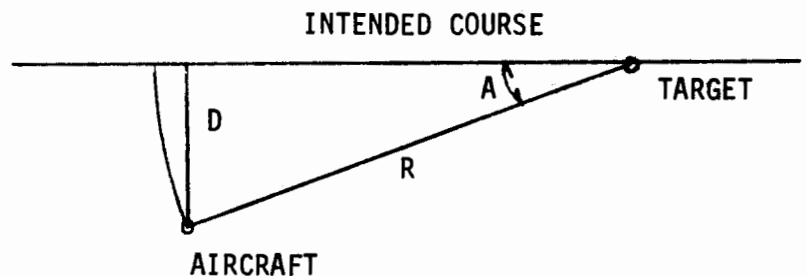


Figure A-1

Standard statistics of this angle such as the mean, variance, skewness, and kurtosis were computed for each sample on all flights, the offset

flights, and the straight-in flights. These statistics may be found in Tables 3, 4, and 5. Graphs of the mean paths with two-standard-deviation envelopes may be found in Figures 10, 11, and 12.

The sample sizes of the experiment are small, so in order to fit probability density curves to the lateral dispersion data with high confidence, larger samples are required. A large sample may be formed by combining smaller samples when the samples are statistically from the same population and the samples were formed independently.

The lateral position of the aircraft at a particular distance is given in terms of the angle of displacement. Inspection of the standard statistics of this angle for the various samples indicate that the samples may possibly be considered to come from the same population although no statistical tests were performed to support this conclusion. Inspection of the data also indicates that the aircraft lateral position in one sample may be correlated to its lateral position in another. To test for correlation between samples, the Spearman rank correlation test was employed.

The Spearman rank correlation test was performed for each pair of adjacent samples and for each pair of samples located at half-mile intervals (Tables 6 and 7). The test indicates that the null hypothesis should be rejected in every case. Therefore, the samples of lateral deviation were not combined.

Although sample sizes are small, each sample was analyzed to determine if the samples could be considered to be from normal populations. If samples are drawn from a population then the sample kurtosis and skewness are random variables. The distributions of the skewness and kurtosis of samples drawn from a normal population are known (reference 1).

If a sample is drawn from a normal population then it would be unlikely that the absolute value of either the skewness or kurtosis would be large. Thus the null hypothesis  $H_0$  is that the sample is drawn from a normal population and the alternate hypothesis  $H_1$  is that the sample was drawn from a population which was not normal. From tables of critical values of skewness and kurtosis, it was determined that the null hypothesis could not be rejected for any of the samples.

#### LATERAL DISPERSION STATISTICS - AVERAGE COURSE

The lateral dispersion statistics described above are indications of the dispersion from the intended course given by the wind direction. These statistics do not measure how well the pilot homed to the target rig, but instead measure how well the pilot followed the intended course. In order to measure lateral dispersion independently of the intended course, the average course for each flight was computed and then statistics of dispersion from these average courses were computed. The average course for a flight was computed while the data for the intended course was being extracted. The average  $\bar{A}$  of the angles of the dispersion corresponding to 4 nm through 1 nm was found for the flight. Then  $\bar{A}$  was subtracted from the intended course heading to establish the average course.

Using the same sample points, the lateral dispersion angle formed by the average approach course line and the line joining the aircraft position to the target rig was found. The perpendicular distance D from the aircraft position to the average course line was found. The angle  $A_a$  was then computed by the formula

$$A_a = \text{Arcsin} (D/R)$$

where R is the distance to the target.

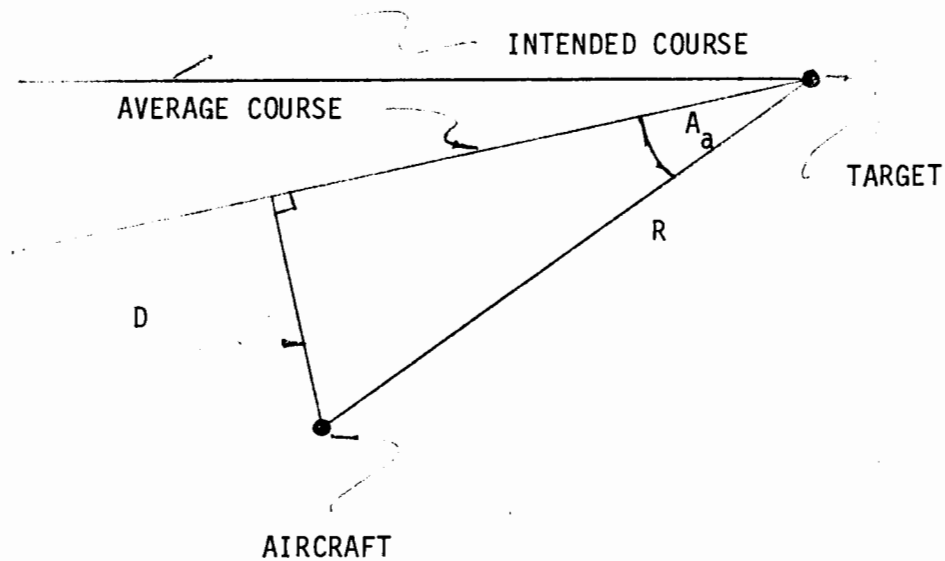


Figure A-2

Standard statistics of this angle were computed for each sample on all flights, the sample points from the offset flights, and for the sample points from the straight-in flights. These statistics may be found in Tables 8, 9, and 10. Graphs of the means with two-standard-deviation envelopes may be found in Figures 13, 14, and 15.

## EXTRACTION OF DATA-MISSED APPROACH

The missed approach segment of the flight presented very special problems in data extraction and analyzation. Two maneuvers were used in the experiment; a circular turn either left or right initiated at the missed approach point, and a 15 degree heading change, called an offset, at 1 nm followed by a circular turn initiated at the missed approach point. The pilot was allowed to choose the direction of the turn, depending on the location of obstacles in the vicinity, thus creating a mixture of left and right turns.

The coordinate system for each individual flight was rotated until the negative y-axis coincided with the intended final approach line, the positive x-axis then pointed to the left of the intended course giving a left hand coordinate system. Then the sign of each x-coordinate of each left turn was changed so that a right turn, the mirror image of the original left turn, was created. This procedure made all turns into right turns and permitted composite graphs of the circular turns and the offset turns to be made (Figures 6, 7, 8, and 9).

From the graphs, circles were determined which best fit the center of the area covered by the turns. Then, to find the average path flown precisely, the position of each flight as it crossed  $10^0$  radials emanating from the center of the best fitting circle was found. (See Figure A-3.)

MISSED APPROACH DISPERSION STATISTICS  
BASED ON SECTOR PARTITIONS ALONG "AVERAGE" PATH

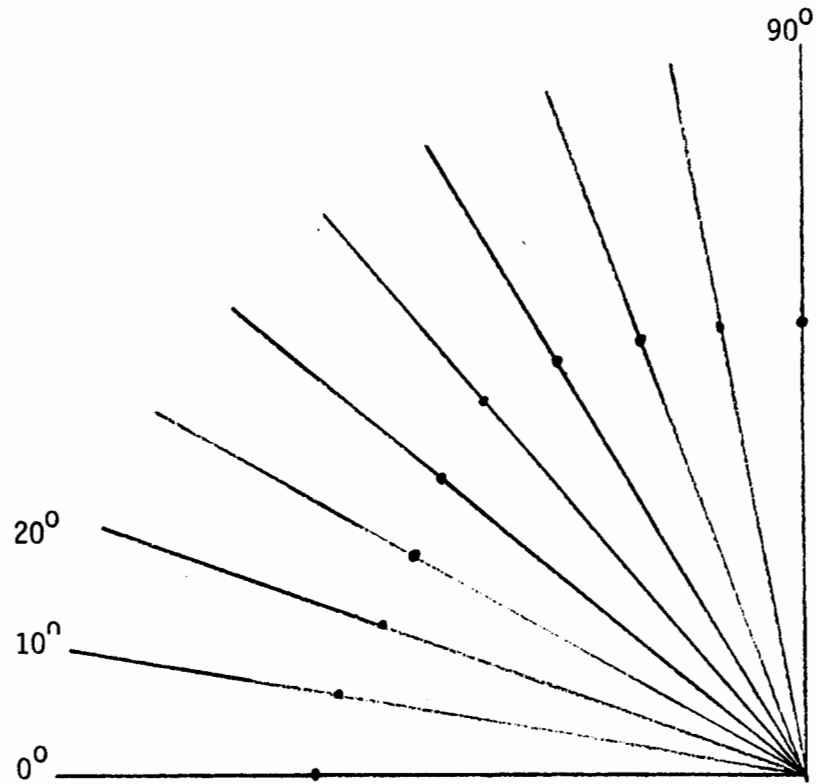


Figure A-3

#### LATERAL DISPERSION - MISSED APPROACH

This procedure produced 10 samples for the circular turns and 10 samples for the offset turns, each sample being a slice along a  $10^0$  radial of the flight paths. Within each sample the distance of each point from the center was found and standard statistics for the distance were computed. These statistics may be found in Tables 23 and 24. The average distances together with two-standard-deviation upper and lower bounds were plotted on their corresponding radials to produce graphs (Figures 22 and 23) of the average paths with two-standard-deviation envelopes.

#### DATA COLLECTION - RANGE INTERPRETATION ERROR

The crewmembers of the helicopters were provided with a contact switch so that they could place a mark on the data tape of the flight. The crew was requested to mark the data when, from observation of the radar screen, they determined that the aircraft was at specified distances or ranges from the target. (The test was designed to detect differences in the ability of the crew to determine distances when using the primary mode as opposed to the beacon mode. It was also designed to detect differences in determining distances between scales and to detect differences between offline distances and online distances.)

#### STATISTICAL ANALYSIS - RANGE INTERPRETATION ERROR

The data collected represents the true range of the aircraft from the target when the crew indicated the range of the aircraft. In order to detect differences, the data was arranged into two matrices with the rows of each being data collected from the individual flights. The first matrix was from aircraft operating in the primary mode and the other matrix was from aircraft operating in the beacon mode. The columns contained the true distances for each specified distance. That is, the first column contained the true distance when the crew endeavored to mark 1/4 nm, the second contained the true distance when the crew attempted to mark 1/2 nm. The true or specified distance was subtracted from the entries of each column. For example, 1/4 nm was subtracted from each entry of the first column and 1/2 nm was subtracted from each entry of the second column. Standard statistics were computed for each column of each matrix. The Mann-Whitney U test was used to test corresponding columns of the two matrices for differences and the Kruskal-Wallis test was used to test for differences between columns within each matrix.

#### DATA COLLECTION - FLIGHT TECHNICAL ERROR

A camera was focused upon the radar screen and photographs of the display were made at regular intervals during the final approach segment of each flight. The photographs were made most frequently during the final approach segment of each flight. Camera malfunctions caused the number of flights sampled in this manner to be smaller than the number of flights actually flown.

The position of the helicopter, as indicated by the radar, was accurately determined from each photograph and compared to the actual position of the aircraft at the time the photograph was made. This resulted in values of the Range RSE, Radar Bearing Error, Radar Position Error, and Azimuth Flight Technical Error corresponding to each photograph.

#### DATA EXTRACTION - FLIGHT TECHNICAL ERROR

In order to analyze the data, the Radar Range Error, Radar Bearing Error, Radar Position Error, and Angular Flight Technical Error of each aircraft when at 4 nm from the target on final approach was recorded to form one sample. In a similar manner, the data described above for each aircraft, was recorded when the aircraft reached 3 nm and then in decreasing 500 foot intervals to the missed approach point for the particular flight to form 33 other samples. Each sample contains all the available data from all the flights at a particular distance from the target rig.

#### STATISTICAL ANALYSIS - FLIGHT TECHNICAL ERROR

Standard statistics of each type of error were computed for each sample on all flights, the flights using the beacon mode, and the flights using the primary mode. The statistics may be found in Tables 15, 16, and 18.

The Kolmogorov-Smirnov two sample test was used to compare the Range RSE data from the flights using the beacon mode to that of the flights using the primary mode from the 4 nm, 3 nm, 2 nm, and 1 nm samples. Similarly, the other types of error were tested to determine possible differences

between the data taken from the flights using the beacon mode and the flights using the primary mode. The results of these tests may be found in Table

#### MANN-WHITNEY U TEST

The Mann Whitney U test is used to test whether two independent groups have been drawn from the same population. It is one of the most powerful nonparametric tests, and it does not require the assumptions necessary for the parametric t test.

Given a sample A and a sample B, let the null hypothesis  $H_0$  be that A and B were drawn from the same population and let the alternate hypothesis  $H_1$  be that the population from which A was drawn is stochastically larger than the population from which B was drawn. Let  $N_1$  be the number of cases in the smaller of the two groups and let  $N_2$  be the number of cases in the larger group. Arrange the numbers from the two samples into one increasing series, being careful to retain each number's identity as being from sample A or sample B.

Now focus attention upon the numbers from one of the samples; for example, from sample A. For each entry from A, count the number of elements of B which precede it in the series. Then find the sum of the numbers produced by this counting procedure. The sum is called the U statistic. Note that two different U values are possible depending on whether the A sample or the B sample was used to find U. If U and U' are the two values then

$$U = N_1 N_2 - U'$$

A small value of U corresponding to the sample A would indicate that A was probably drawn from a population stochastically smaller than B.

When  $N_1$  and  $N_2$  are smaller than 20, tables of extreme values of U found in reference 2 may be used. When U is not greater than the tabled U, the null hypothesis is rejected. If  $N_2$  is larger than 20, then the sampling distribution of U rapidly approaches the normal distribution, with

$$\text{Mean} = \frac{N_1 N_2}{2}$$

and

$$\text{Standard Deviation} = \sqrt{\frac{(N_1)(N_2)(N_1 + N_2 + 1)}{12}}$$

The significance of U may then be determined from the normal table.

#### KRUSKAL-WALLIS K-SAMPLE TEST

The Kruskal-Wallis test is a very useful and powerful test for determining whether k independent samples are from different populations. This test is also a non-parametric test which requires no assumptions about the underlying populations from which the samples are drawn.

Given k independent samples, let the null hypothesis  $H_0$  be that the K samples were drawn from the same population and let the alternate hypothesis  $H_i$  be that they were not drawn from the same population.

Arrange the numbers into one ascending series being careful to retain the identity of the sample from which number was taken. Assign a rank to each

number as follows: The smallest is given the rank of 1, the next to the smallest is given rank 2, and the largest is given rank N, where N is the total number of observations in the k samples combined. Let  $R_j$  be the sum of the ranks of the observations from the j-th sample and compute the Kruskal-Wallis statistic H as follows:

$$H = \frac{12}{N(N+1)} \sum_{j=1}^k \frac{R_j^2}{n_j} - 3(N+1)$$

where  $n_j$  is the number of observations in the j-th sample.

It can be shown that H is distributed approximately as chi-square with  $df = k-1$ . Thus the null hypothesis  $H_0$  may be rejected when H exceeds the critical value as given by a chi-square table.

#### KOLMOGOROV-SMIRNOV TWO - SAMPLE TEST

The Kolmogorov-Smirnov test is a non-parametric test used to decide whether two independent groups have been drawn from the same population. The two-tailed test is sensitive to any kind of difference in the distributions from which the samples were drawn, differences in central tendency, in dispersion, in skewness, etc.

Given a sample A and a sample B, let the null hypothesis  $H_0$  be that A and B were drawn from the same population and let the alternate hypothesis  $H_1$  be that they were not. Make a cumulative frequency distribution for each sample of observations, using the same intervals for both distributions.

Let  $S_A(X) = K_1/N_1$ , where  $K_1$  = the number of scores of A equal to or less than  $X$  and  $N_1$  = the total number of observations in sample A. Likewise, let  $S_B(X) = K_2/N_2$ . Now for each  $X$ , which the endpoint of an interval as described above, let

$$D_X = \left| S_A(X) - S_B(X) \right|.$$

The test focuses on

$$D = \text{maximum } D_X$$

for a two-tailed test. The sampling distribution of  $D$  is known and the probabilities associated with the occurrence of values as large as an observed  $D$  under the null hypothesis have been tabled. A large value of  $D$  would indicate the null hypothesis should be rejected.

#### SPEARMAN RANK CORRELATION TEST

The Spearman rank correlation test (reference 2) is a non-parametric test for correlation based on the relative rank of the two variables in question. The test was performed by arranging the angles in the two samples in two ascending series while maintaining the identification of the flight from which each angle is taken. Then if  $X_i$  is the rank of the angle for flight  $i$  in the first series and  $Y_i$  is the rank of the angle for flight  $i$  in the second series the difference  $d_i$  is given by

$$d_i = X_i - Y_i$$

If correlation was perfect, each  $d_i$  would be zero. However, since correlation is seldom perfect, the Spearman rho statistic is computed by the formula

$$\rho = 1 - \frac{6 \sum_{i=1}^N d_i^2}{N^3 - N}$$

The distribution of  $\rho$  when the two variables under study are not associated is known and is based on the number of possible permutations of the numbers in each sample. If the two series are not associated, then a large absolute value of  $\rho$  would be unlikely. Thus the null hypothesis  $H_0$  is that the two variables are unrelated in the population whereas the alternate hypothesis  $H_1$  is that they are related in the population. The null hypothesis may be rejected at the 99.9 percent level if the absolute value of  $\rho$  exceeds the critical value  $\rho_0$  given by

$$\rho_0 = 3.2905 / \sqrt{N-1}$$

where  $N$  is the size of the samples.

## APPENDIX B

The instrument approach procedure investigated in this paper is based upon the premise that the on-board radar may be used to see and avoid obstacles, fixed or dynamic, which may lie in the flight path. The purpose of this portion of the analysis is to determine if conditions may exist which would weaken that premise.

The instrument approach procedure is designed to cause the aircraft flight path to be directly into the wind resulting in a straight flight path. However, due to the lack of a fix at the downwind final approach point and the possibility of inaccurate wind information, the approach may be made with a crosswind component. If the aircraft flies a homing course to the target, the result will be a curved flight path. Thus the aircraft will be flying in a direction different from the heading of the aircraft or slightly sideways. This sideways movement and the restricted peripheral vision of the radar leads to the possibility of a blind flight path.

This portion of the paper will investigate those conditions which could result in a blind flight path and attempt to deal with the possible consequences.

## THE THEORETICAL HOMING CURVE

Assume that the pilot of an aircraft always keeps the nose of the aircraft pointed toward a target T located due west of his starting point. Let his airspeed be  $v$  knots and let the wind be blowing at the rate of  $w$  knots from the southwest quadrant. Assume that he starts from a point P, which is a distance of  $a$  nm from T. For ease of solution, choose the origin to be the point T with the positive  $y$ -axis in the direction the wind is blowing. If the wind is not from due south, the point P will not lie on the  $x$ -axis. Let  $\alpha$  be the angle TP makes with the positive  $x$ -axis. The initial conditions at  $t = 0$ , therefore, become

$$x = a \cos \alpha$$

$$y = a \sin \alpha$$

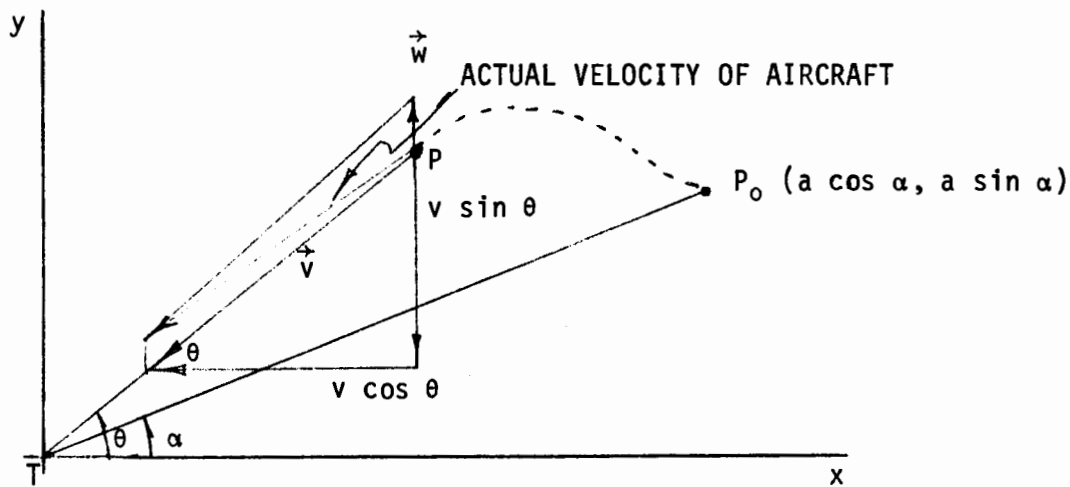


Figure B-1

Let the position of the aircraft at any time  $t$  be  $P(x,y)$ . The vector representing the airspeed of the aircraft is of magnitude  $v$  and is pointed toward T. Let  $\theta$  be the angle this vector makes with the positive  $x$ -axis. The wind vector points in the direction of the positive  $y$  axis with magnitude  $w$ . The sum of the vectors  $\vec{v}$ , and  $\vec{w}$ , which is the diagonal of

the parallelogram formed by the vectors  $\vec{v}$  and  $\vec{w}$ , represents the actual direction and magnitude of the aircraft's velocity at time  $t$ . Without the wind, the respective components of the aircraft velocity would be

$$\frac{dx}{dt} = -v \cos \theta, \quad \frac{dy}{dt} = -v \sin \theta.$$

Taking the wind's velocity into account, the  $y$ -component becomes

$$\frac{dy}{dt} = v \sin \theta + w.$$

From Figure B-1 we have

$$\sin \theta = \frac{y}{\sqrt{x^2 + y^2}}, \quad \cos \theta = \frac{x}{\sqrt{x^2 + y^2}}.$$

Substituting for  $\sin \theta$  and  $\cos \theta$ , the components of velocity become

$$\frac{dx}{dt} = \frac{-vx}{\sqrt{x^2 + y^2}}, \quad \frac{dy}{dt} = -\frac{vy}{\sqrt{x^2 + y^2}} + w.$$

Then from the chain rule

$$\frac{dy}{dx} = \frac{dy}{dt} / \frac{dx}{dt},$$

and after a rearrangement of terms we have

$$x dy = \left( y - \frac{w}{v} \sqrt{x^2 + y^2} \right) dx.$$

This equation is homogeneous with solution

$$y = \frac{1}{2} \left( Ax^{1-k} - \frac{1}{A} x^{1+k} \right),$$

where  $k = w/v$ ,

and  $A = (\tan \alpha + \sec \alpha) (a \cos \alpha)^k$ .

### BLIND FLIGHT PATH

Since the aircraft is assumed to be always pointed toward the target T and since the radar sweeps  $20^\circ$  left and right of the aircraft heading, (assuming the  $\pm 20^\circ$  sweep angle is chosen) the pilot will not be able to see some portion of the curve ahead if the angle and between TP and the tangent to the curve is more than  $20^\circ$ .

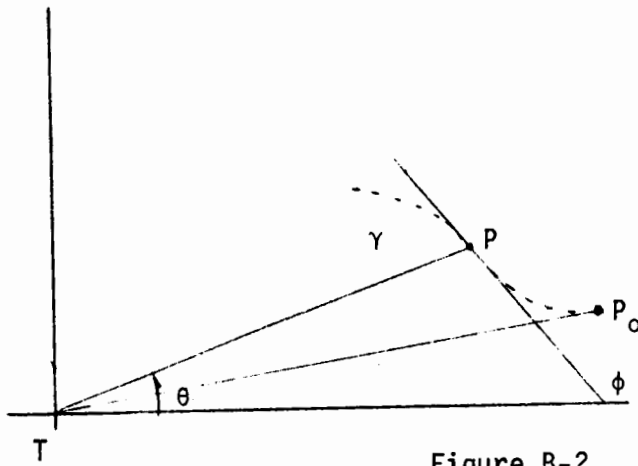


Figure B-2

Referring to Figure B-2, we have

$$\gamma = \theta + 180 - \phi,$$

so that  $\tan \gamma = \frac{\tan \theta - \tan \phi}{1 + \tan \theta \tan \phi}$ .

Since  $\tan \theta = \frac{y}{x}$  and  $\tan \phi = \frac{dy}{dx}$

it can be shown that

$$\tan \alpha = \frac{2k}{A(1-k)x^{-k} + \frac{(1+k)x^k}{A}}.$$

The radar scope will not show a portion of the path ahead if  $\gamma > 20^\circ$ .

Thus we want to find all values of  $x$  where

$$\tan \alpha > \tan 20^\circ.$$

If  $w < v$ , then  $k < 1$  so that  $1 - k > 0$ .

Also  $x > 0$  and  $A \geq 0$  since  $0 \leq \alpha < 90^\circ$ .

Hence

$$\frac{2k}{\tan 20^\circ} > A(1-k)x^{-k} + (1+k)x^k/A,$$

which implies that

$$0 > (1+k)x^{2k}/A - 2kx^k/\tan 20^\circ + A(1-k).$$

This inequality is quadratic in  $x^k$  and since the leading coefficient is positive, the solution must lie between the roots. In order to have real roots, the discriminant must be nonnegative. Therefore

$$4 k^2 / \tan^2 20^\circ - 4 (1 - k^2) \geq 0,$$

which implies that

$$k \geq \sin 20^\circ.$$

Thus a segment of the flight can be blind whenever the ratio of windspeed to airspeed is at least the  $\sin 20^\circ$ . That is, whenever

$$w/v \geq \sin 20^\circ. \quad (1)$$

From (1), given the airspeed of the helicopter, the critical windspeed which may cause a blind flight condition may be found. For example, given an airspeed of 60 knots, the aircraft may be flying blind if the windspeed is at least 60 times  $\sin 20^\circ$ ; i.e.,

$$w \geq 60 \sin 20^\circ = 20.5 \text{ knots.}$$

Thus, if the windspeed exceeds approximately one-third of the approach airspeed, then the possibility of a blind segment of the approach path exists.

When the conditions of (1) are met, the x-coordinates of the end points of the blind segment are then found from the quadratic formula to be

$$x = \left[ \frac{A}{(1 + k) \tan 20^\circ} \left( k \pm \sqrt{k^2 \sec^2 20^\circ - \tan^2 20^\circ} \right) \right]^{1/k} \quad (2)$$

Also of interest is the length of the blind segment. If  $x_1$  and  $x_2$  are the values of  $x$  given by (2), then the integral formula for arc-length,

$$s = \int_{x_1}^{x_2} \sqrt{1 + \left(\frac{dy}{dx}\right)^2} dx,$$

gives the distance the aircraft travels during the blind flight. This integral was evaluated for this study by a numerical procedure, Simpson's Rule.

It is obvious that the blind segment is not completely blind. The pilot can always see, from the radar screen, some portion of the flight path. It is not obvious just how much of the flight path is not visible when the aircraft is located at a point on the blind segment. To partially answer this question, the distance  $D$  from the aircraft located at the 5 nm point to the point of intersection of the flight path and the right edge of the radar sweep was found (Figure B-3). The point of intersection could not be found explicitly so a numerical procedure, the bisection method, was used to approximate the location to an accuracy of  $10^{-10}$  in the  $x$  direction.

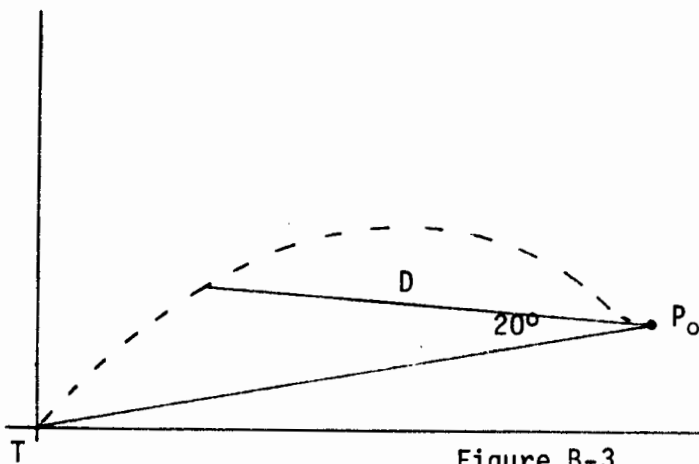


Figure B-3

The length of time during which the aircraft flies blind can be determined once the x coordinates of the end points  $x_1$  and  $x_2$ , are known. As shown earlier

$$\frac{dx}{dt} = \frac{-vx}{\sqrt{x^2 + y^2}}$$

which becomes after substitution for y,

$$\frac{dx}{dt} = \frac{-vx}{\frac{1}{2} (Ax^{1-k} + \frac{x^{1+k}}{A})}$$

The solution of this differential equation is

$$\frac{Ax^{1-k}}{1-k} + \frac{x^{k+1}}{A(k+1)} = -2vt + c.$$

Substituting  $x_1$  and  $x_2$ , where  $x_1 < x_2$  gives the time of flight t,

$$t = \frac{1}{2v} \left[ \frac{A(x_2^{1-k} - x_1^{1-k})}{(1-k) + (k+1)(x_2^{k+1} - x_1^{k+1})/A} \right]. \quad (3)$$

Since v is in knots, t is in hours. If t is multiplied by 3600, the time in seconds is obtained.

To completely model the homing path to the target, the unique problem of moving ships should also be considered. It is desirable to know if a ship could possibly travel on a collision course with the helicopter, with the flight path in full view, but be undetected because of the restricted peripheral "vision" provided by the radar. To answer this question, it

was assumed that a ship was located at a point S just outside the sweep of the radar at the 5 nm point (Figure B-4). Then the shortest distance d from S to the flight path was found. The time t required for the helicopter to fly to the collision point was also found. The speed v which the ship would have to travel to collide with the helicopter is  $v = d/t$ .

If the speed required to travel the distance d is small (up to 20 knots) then such a collision with a ship operating near the flight path would be possible.

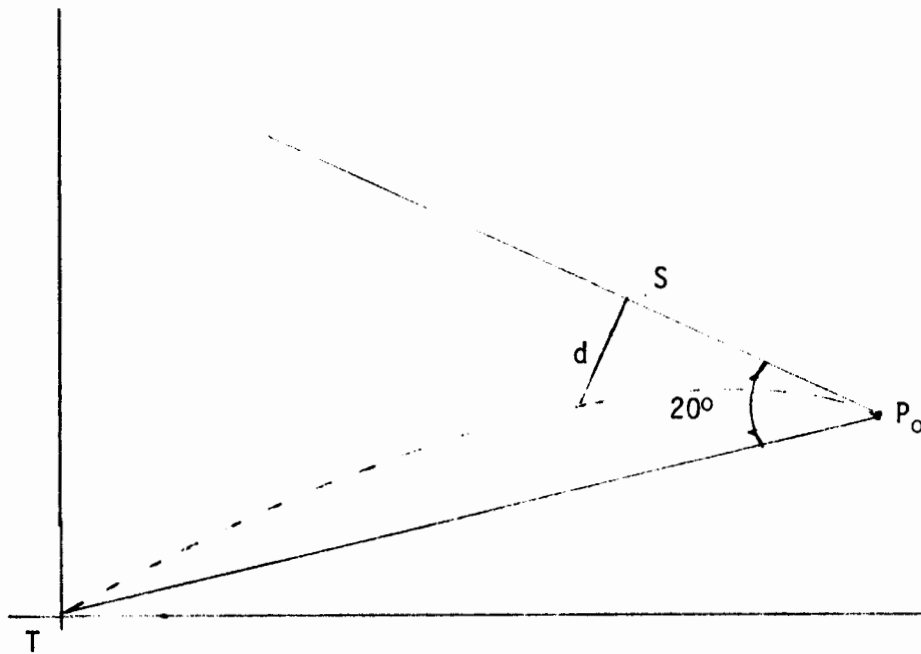


Figure B-4

### THE MISSED APPROACH CURVE

Assume the pilot of an aircraft is flying directly into the wind and decides to make a circular turn to the left. Let his airspeed be  $v$  knots and let the wind be blowing at the rate of  $w$  knots. Let the radius of the intended turn without wind be  $r$ . Choose the  $y$ -axis so that the wind blows from the direction of the positive  $y$ -axis and choose the  $x$ -axis so that the initial point of the turn is at  $(r,0)$ . Without wind, the center of the turn would be at  $(0,0)$ . After time  $t$ , the center of the turn will be located at  $C$ .

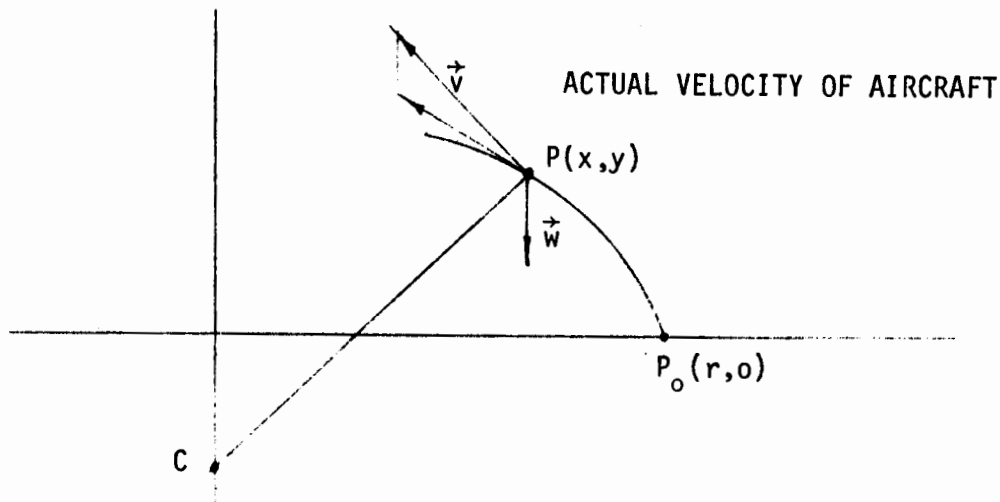


Figure B-5

Let the position of the aircraft at any time  $t$  be  $P(x,y)$ . The vector representing the airspeed of the aircraft is of magnitude  $v$  and is pointed in the direction the aircraft would have flown without wind. The wind vector is of magnitude  $w$  and is pointed in the  $-y$  direction. The sum

of the vectors  $\vec{v}$  and  $\vec{w}$  represents the actual velocity  $\vec{V}$  of the aircraft at time  $t$ .

The vector  $\vec{v}$  has the horizontal component

$$\frac{dx}{dt} = -v \sin \theta = -\frac{v \sqrt{r^2 - x^2}}{r},$$

and vertical component

$$\frac{dy}{dt} = v \cos \theta = \frac{vx}{r},$$

where  $\theta$  is the angle through which the aircraft would have flown without wind.

The vector  $\vec{V}$  will have the same horizontal component, but will have the windspeed subtracted from the vertical component. Thus for  $\vec{V}$  the horizontal and vertical components are respectively,

$$\frac{dx}{dt} = -\frac{v \sqrt{r^2 - x^2}}{r}$$

$$\text{and } \frac{dy}{dt} = \frac{vx}{r} - w$$

Then, from the chain rule,

$$\frac{dy}{dx} = -\frac{x}{\sqrt{r^2 - x^2}} + \frac{wr}{v} \frac{1}{\sqrt{r^2 - x^2}}. \quad (4)$$

Since at  $t = 0$ ,  $x = r$ , and  $y = 0$ , integration of (4) yields the equation of the curve

$$y = \sqrt{r^2 - x^2} + \frac{wr}{v} \operatorname{Arcsin} \frac{x}{r} - \frac{wr\pi}{2v} \quad (5)$$

The domain of definition of this function is  $-r \leq x \leq r$  so that it only represents a  $180^\circ$  turn.

Suppose the wind is not parallel to the line of flight, but instead makes an angle  $\alpha$  as indicated in Figure B-6. Choose the y-axis

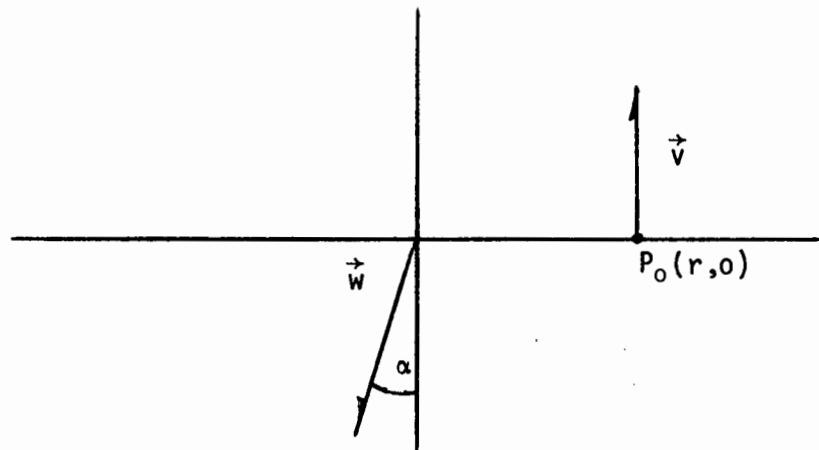


Figure B-6

so that it is parallel to the wind  $\vec{w}$  (Figure B-7).

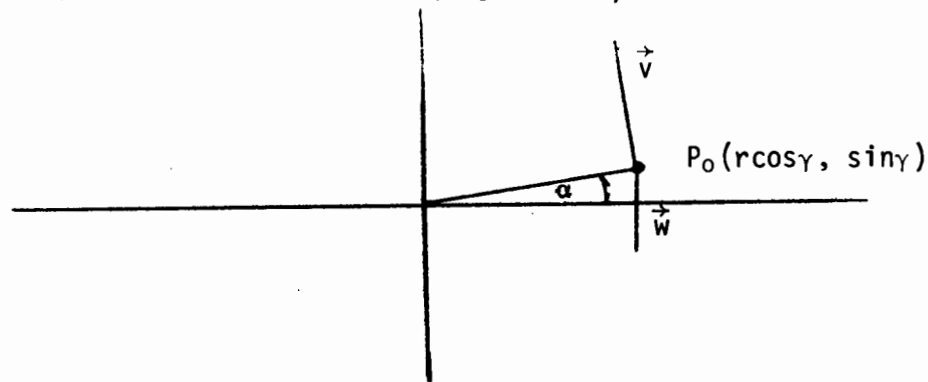


Figure B-7

The analysis is the same except for the choice of the constant of integration. At  $t = 0$ ,  $x = r \cos \alpha$ , and  $y = r \sin \alpha$ ; hence, (5) becomes

$$y = \sqrt{r^2 - x^2} + \frac{wr}{v} \operatorname{Arccsin} \frac{x}{r} + \frac{wr}{v} \left( \alpha - \frac{\pi}{2} \right).$$

The aircraft will be flying blind whenever the angle  $\gamma$  between the aircraft heading and the tangent to the curve is at least equal to half the sweep angle of the radar. The half angle of the radar will be assumed to be  $20^\circ$ . The angle  $\gamma$  may be determined from Figure B-8 to be

$$\gamma = \phi - \theta - 90^\circ,$$

where  $\phi$  is the angle, the tangent to the curve makes with the positive x-axis and  $\theta$  is the angle through which the aircraft would have turned without wind.

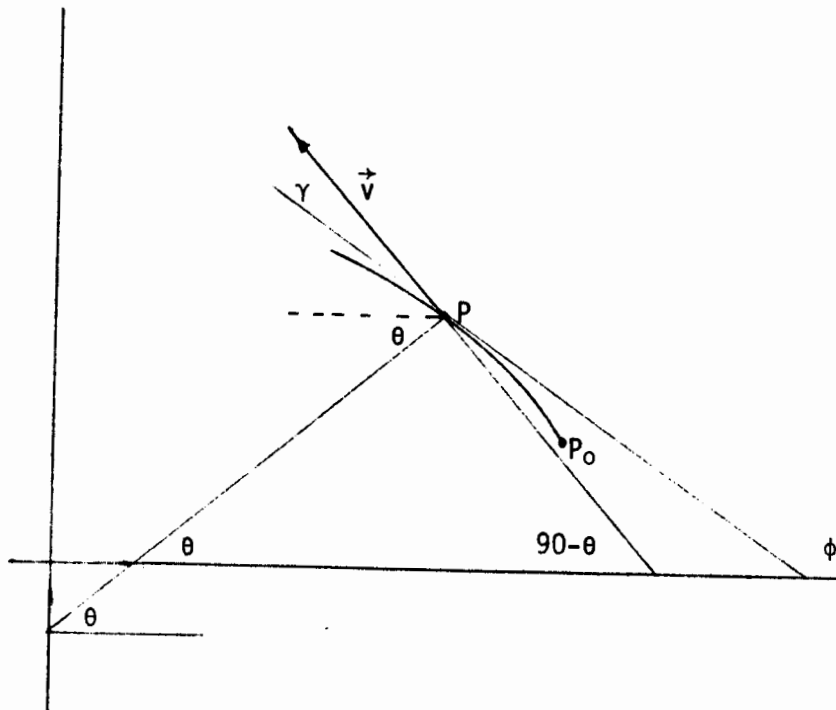


Figure B-8

If  $\gamma \geq 20^\circ$  then  $\tan \gamma \geq \tan 20^\circ$ . The  $\tan \gamma$  may be found as follows:

$$\tan \gamma = \frac{\tan \phi - \tan (\theta + 90)}{1 + \tan \phi \tan (\theta + 90)}$$

$$= \frac{\tan \phi + \cot \theta}{1 - \cot \theta \tan \phi},$$

where  $\cot \theta = \frac{x}{\sqrt{r^2 - x^2}}$

$$\tan \phi = \frac{dy}{dx} = \frac{-vx + wr}{v \sqrt{r^2 - x^2}};$$

hence, after substitution and rearrangement of terms

$$\tan \gamma = \frac{w \sqrt{r^2 - x^2}}{vr - wx}. \quad (6)$$

Since  $\tan \gamma \geq \tan 20^\circ$ , substitution of (6) yields the inequality

$$r^2 (v^2 \tan^2 20^\circ - w^2) - 2 v r w \tan^2 20^\circ x + \sec^2 20^\circ w^2 x^2 \leq 0$$

This inequality is quadratic in  $x$  and the coefficient of  $x^2$  is positive; therefore, the solution lies between the roots. The quadratic equation will have real roots only if the discriminant is non-negative. The

discriminant proves to be the same as that found for the homing curve.

It follows that a segment of the path will be blind if

$$\frac{w}{v} \geq \sin 20^\circ. \quad (7)$$

If the conditions of (7) are met then the x-coordinates of the end points of the blind segment may be found from the quadratic formula to be

$$x = \frac{r}{w} (v \sin^2 20^\circ \pm \cos 20^\circ \sqrt{w^2 - v^2 \sin^2 20^\circ}).$$

The time required to traverse the blind flight path may be found from the horizontal component of the velocity,

$$\frac{dx}{dt} = \frac{-v \sqrt{r^2 - x^2}}{r}.$$

The equation has the general solution

$$t = -\frac{r}{v} \operatorname{Arccsin} \frac{x}{r} + c.$$

If the x-coordinates of the end points of the blind flight segment are  $x_1 < x_2$  then the time required is

$$t = \frac{r}{v} \left( \operatorname{Arccsin} \frac{x_2}{r} - \operatorname{Arccsin} \frac{x_1}{r} \right).$$

Since the units of  $v$  is knots, the time will be in hours. The time in seconds may be obtained by multiplying by 3600.

It is obvious that this blind flight is different from that of the homing path in that once the initial point of the blind segment is reached, the rest of the path is completely invisible. Before this initial point is reached, only a small portion of the path may be seen. In order to find the farthest distance ahead that may be seen at the initial point, the distance from the aircraft at the beginning of the turn to the point of intersection of the curve and the left edge of the radar sweep was found.

#### CONCLUSIONS - HOMING CURVE

The mathematical model of the curve produced by homing to the target indicates that conditions can exist which could allow the helicopter to fly along a ground track not visible to the radar operator. These conditions would not be considered unusual or improbable using the  $40^\circ$  sweep. It is only necessary the wind be a crosswind with windspeed greater than approximately one-third of the helicopter airspeed. However, if the  $120^\circ$  sweep is used, the windspeed must be greater than  $\sin 60^\circ$  times the aircraft speed, or about 87 percent of the aircraft speed. The least speed which can cause a blind flight path will be called the critical speed.

It was found that the length of the blind segment is a function of the windspeed, the helicopter airspeed, and the crosswind angle. As the windspeed increases and/or the crosswind angle increase, the blind segment increases. If the windspeed and direction is held constant, then the length of the blind segment increases as the helicopter airspeed decreases.

The initial point of the homing curve was found to always be the initial point of the blind segment. The length of the blind segment can be as much as 3.5 nm, assuming an initial distance from the target of 5 nm, under potential operational wind conditions, using the  $40^{\circ}$  sweep. An airspeed of 70 knots, windspeed of 30 knots, and crosswind angle of  $45^{\circ}$  will produce a curve 3.5 nm long. At the initial point of the blind segment, it was found that the  $40^{\circ}$  radar sweep intersected the flight path 3.1 nm away. Thus, the nearest point of the flight path visible to the radar operator at the initial point of the homing curve is 3.1 nm away.

The length of the blind segment and the nearest point of the flight path visible to the radar operator on the  $40^{\circ}$  sweep at the initial point of the homing curve have been tabulated for various combinations of windspeeds, airspeeds, and crosswind angles. Some have been presented in graphical form in order to show more clearly the effects of angle and windspeed. Moderate conditions of windspeed and crosswind angle can cause long segments of the flight path to be invisible to the radar operator. It was found that windspeeds which exceed the critical windspeed by about

10 knots combined with a crosswind angle of  $20^{\circ}$  -  $30^{\circ}$  can produce a significant blind segment. The same combinations of windspeed and angle can also cause the nearest visible point of the flight path to be a significant distance away.

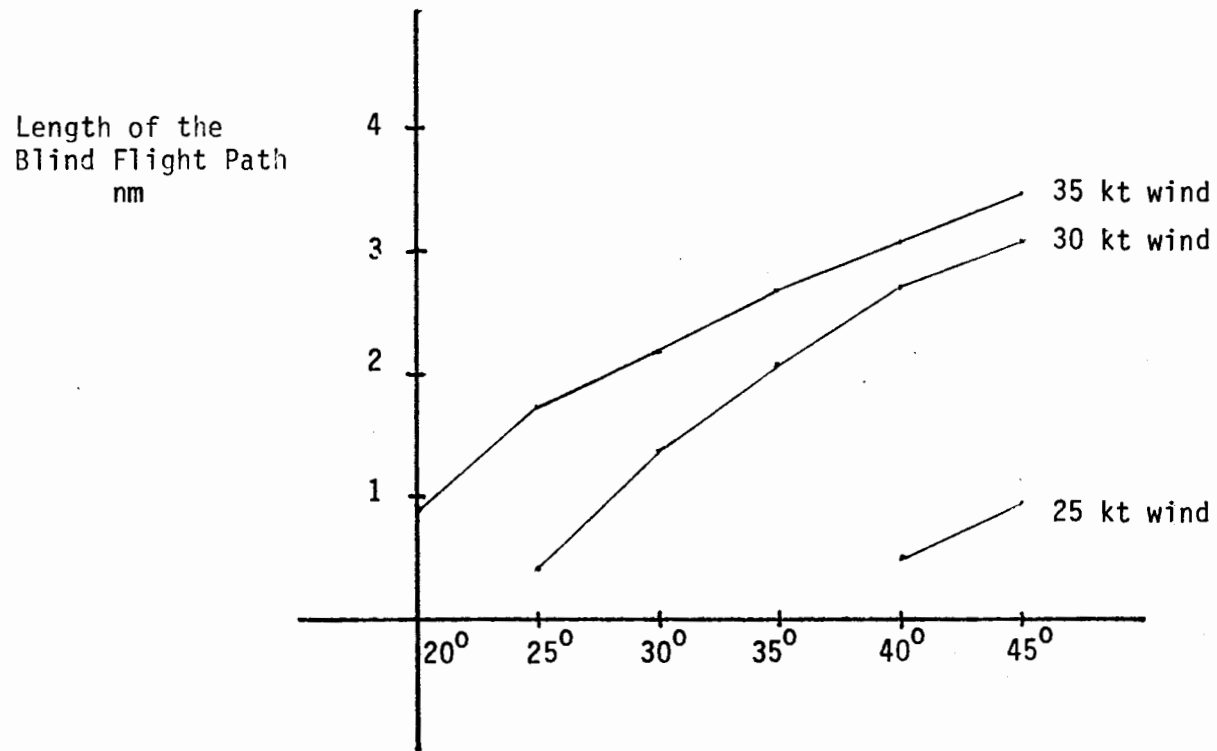
It was also found that ships could move into the path of the aircraft while remaining invisible to the radar operator. Even though the windspeed is less than the critical windspeed so that the entire flight path is visible to radar operator, ships are capable of speeds which would allow them to move behind the radar sweep and into the path of the aircraft. In Figure B-4, a ship at point S moving toward the curve would only have to have a speed of about 8 - 12 knots to stay behind the  $40^{\circ}$  radar sweep and intercept the aircraft. Table B-1 shows the maximum speed a ship would have to travel in order to be at the edge of the radar sweep when the aircraft is 5 nm from the target rig and yet intercept the aircraft at the 1/2 nm missed approach point. It was found that the ship could travel at smaller speeds and intercept the aircraft before it reached the 1/2 nm missed approach point.

In conclusion, the update rate of the  $40^{\circ}$  sweep is desirable since it allows the radar operator to more accurately determine the distance to the target; however, the restricted field of view means that conditions exist when portions of the flight path are not visible to the radar operator. It is even possible that moving ships could intercept the aircraft while remaining undetected by the radar operator.

## CONCLUSIONS - MISSED APPROACH CURVE

The mathematical model of the missed approach curve indicates that the blind flight problem is more severe than for the homing curve. The same critical windspeeds as those of the homing curve will cause a blind flight path. In the case of the homing curve, some of the flight path is always visible, but during the flight along the missed approach path, the operator can lose sight of the entire curve. Even when windspeeds are below the critical windspeed, only very short segments of the curve are visible to the operator. This, combined with radar sweep delay and tilt adjustment in the climbing turn, would indicate that the missed approach turn should be treated as a completely blind maneuver.

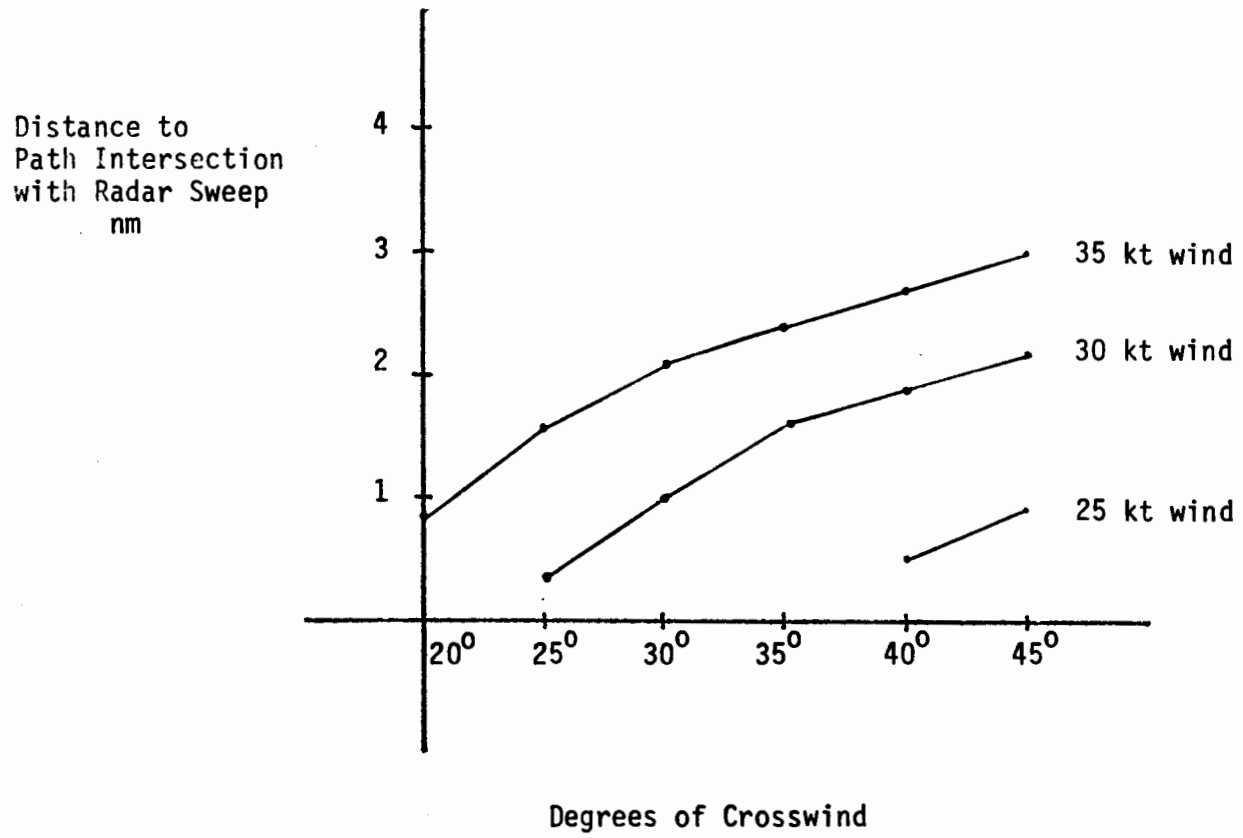
Table B-2 has been compiled to show the farthest point of the curve visible from the initial point of the curve.



Degrees of Crosswind

Airspeed 60 knots

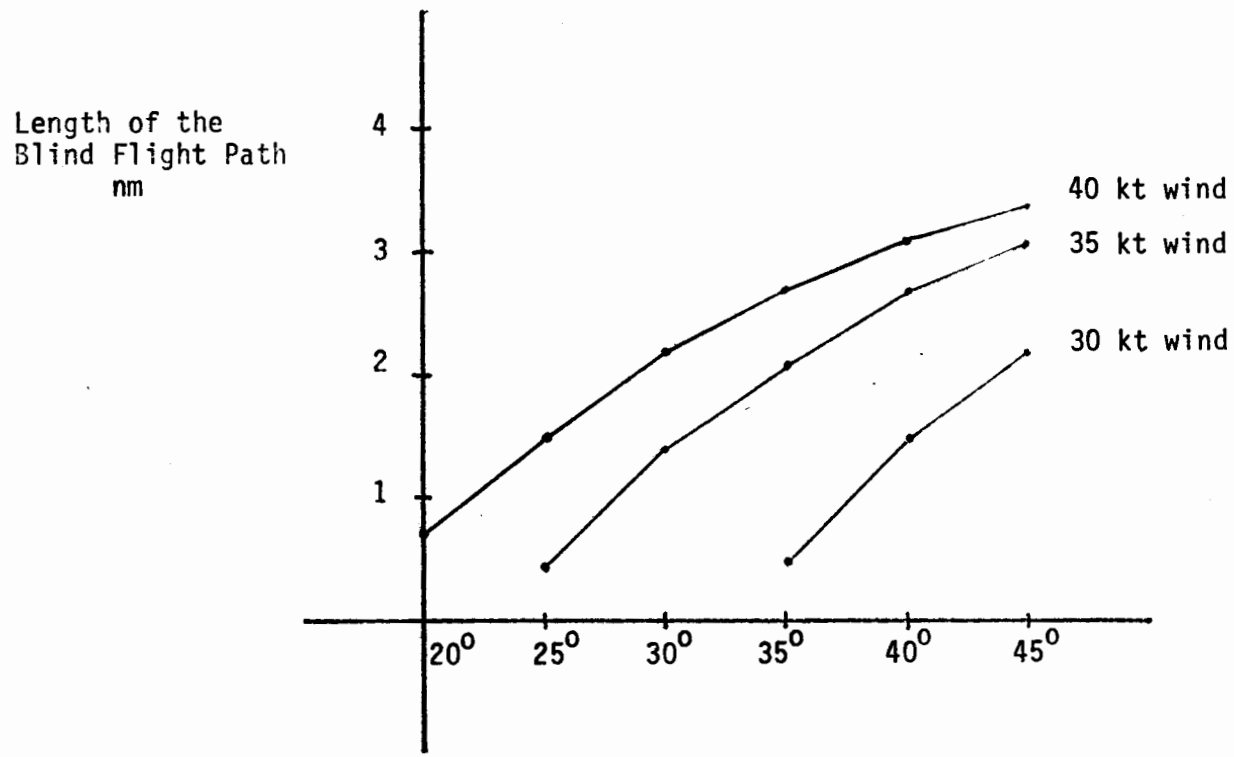
Figure B-9



Degrees of Crosswind

Airspeed 60 knots

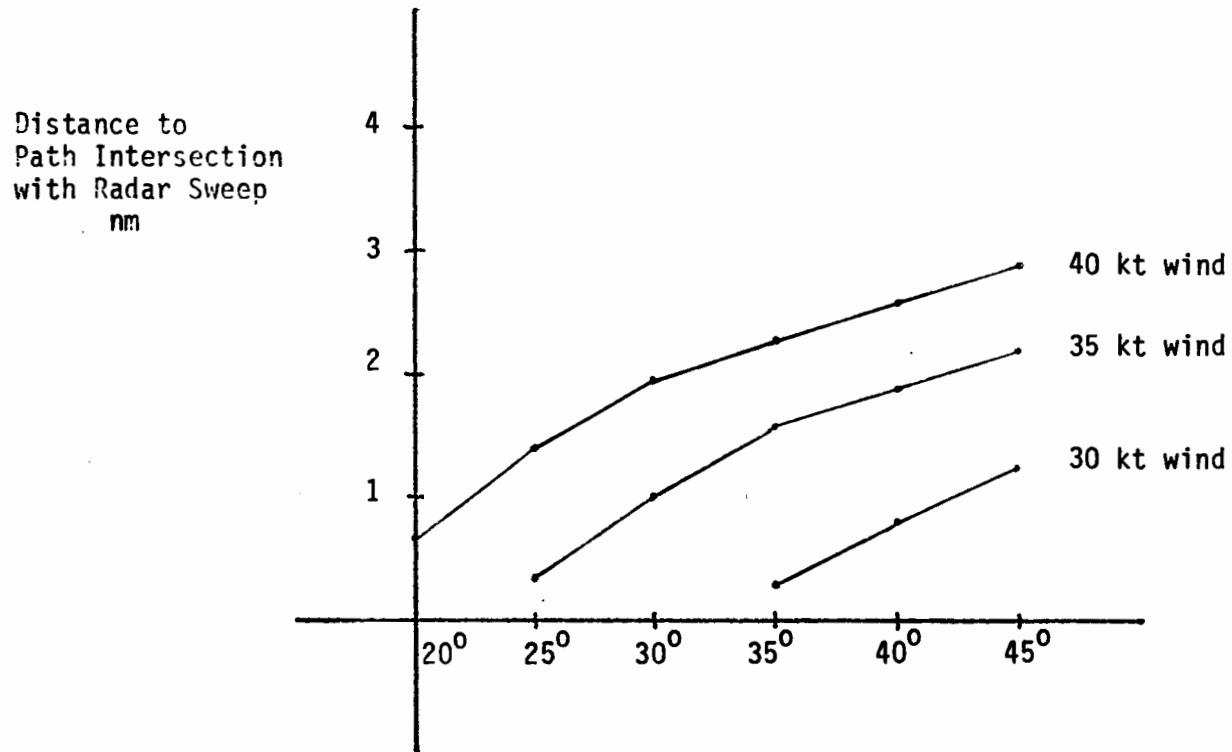
Figure B-10



Degrees of Crosswind

Airspeed 70 knots

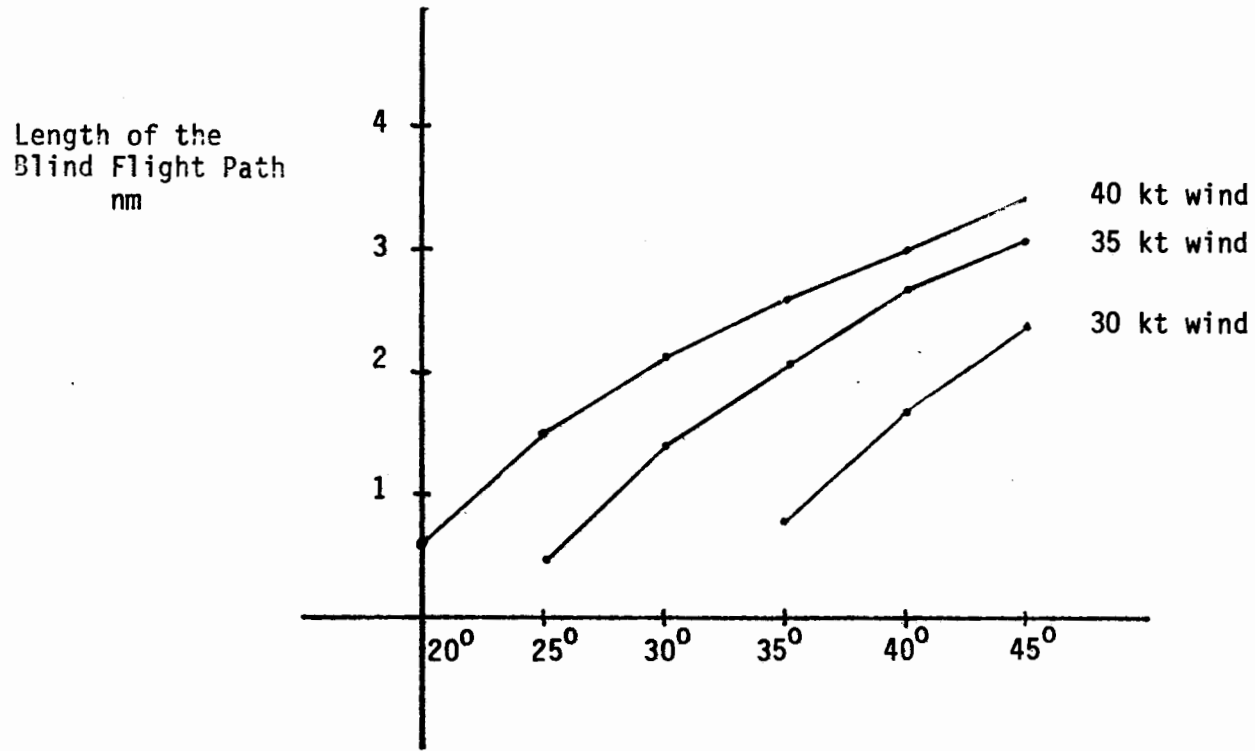
Figure B-11



Degrees of Crosswind

Airspeed 70 knots

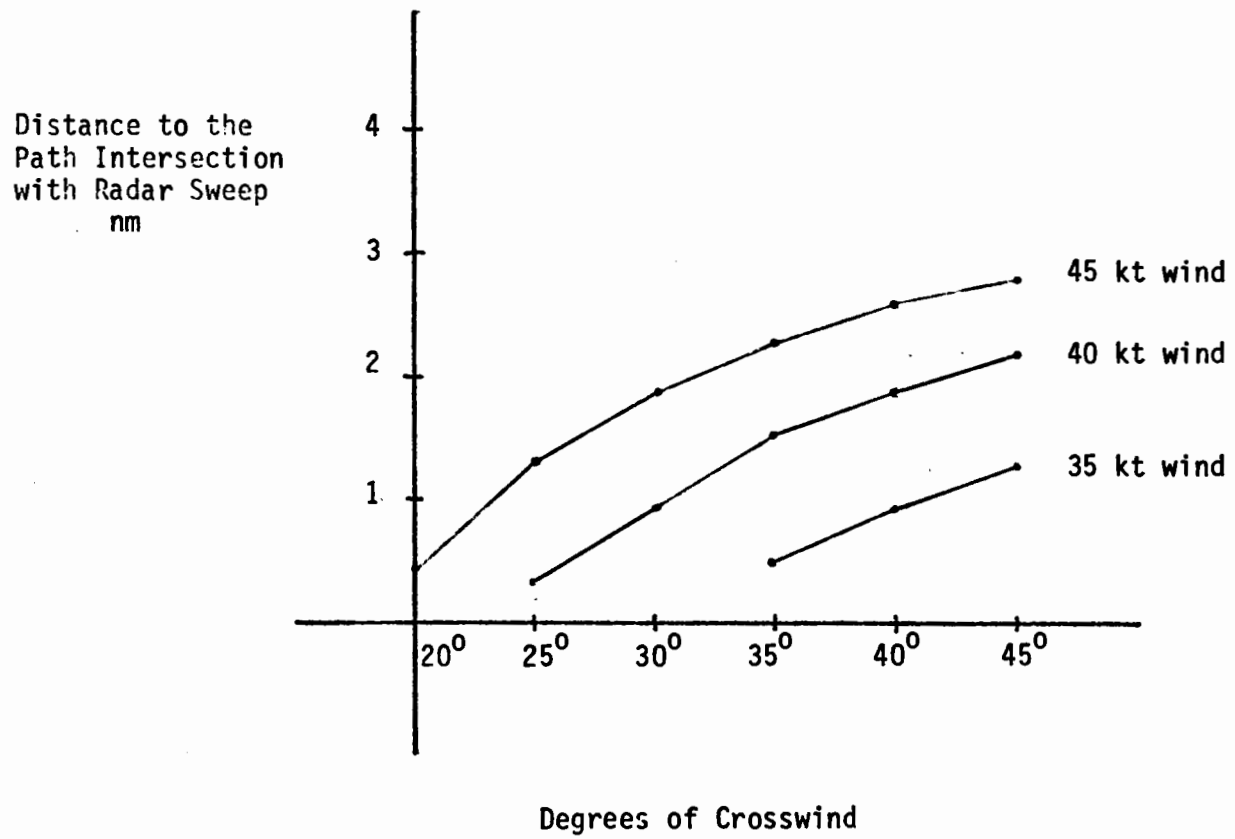
Figure B-12



Degrees of Crosswind

Airspeed 80 knots

Figure B-13



Degrees of Crosswind

Airspeed 80 knots

Figure B-14

MAXIMUM SPEED TO INTERCEPT MOVING AIRCRAFT

WINDSPEED 20 KNOTS

AIRCRAFT SPEED	LEFT CROSSWIND			
	10 <sup>0</sup>	20 <sup>0</sup>	30 <sup>0</sup>	40 <sup>0</sup>
60	13.25	12.96	12.81	12.82
70	16.63	16.31	16.14	16.14
80	20.01	19.67	19.49	19.48

Table B-1

FARTHEST POINT OF RADAR VISION  
 LEFT HAND TURN  
 40° SWEEP - 60 KNOT AIRSPEED

WINDSPEED KNOT	RIGHT CROSSWIND COMPONENT							
	0°	5°	10°	15°	20°	25°	30°	35°
0	.2	.2	.2	.2	.2	.2	.2	.2
5	.17	.17	.17	.16	.16	.16	.16	.16
10	.14	.14	.13	.13	.12	.12	.11	.11
15	.12	.11	.10	.095	.088	.082	.076	.070
20	.093	.084	.075	.065	.057	.048	.041	.033
25	.072	.061	.051	.040	.030	.020	.01	.003

Table B-2

## Bibliography

1. Duncan, A.J. Quality Control and Industrial Statistics. Homewood, Illinois: Richard D. Irwin, 1965.
2. Siegel, Sidney. Nonparametric Statistics for the Behavioral Sciences. New York: McGraw-Hill, 1956.
3. Tenenbaum, M. and Pollard, H. Ordinary Differential Equations. New York: Harper & Row, 1963.